Out beyond ideas of right doing and wrong doing, there is a field.

I'll meet you there.

(~*Rumi*)

University of Alberta

Micro-Modeling and Study of the Impact of Microstructure on the Performance of Solid Oxide Fuel Cell Electrodes

by

Ali Abbaspour Gharamaleki

A thesis submitted to the Faculty of Graduate Studies and Research
in partial fulfillment of the requirements for the degree of

Doctor of Philosophy
in
Chemical Engineering

Chemical and Materials Engineering

Fall 2010
Edmonton, Alberta

Examining Committee

Dr. Jingli luo, Chemical and Materials Engineering

Dr. Karl T. Chuang, Chemical and Materials Engineering

Dr. Krishnaswamy Nandakumar, Chemical Engineering

Dr. Amit Kumar, Mechanical Engineering

Dr. Kunal Karal, Chemical Engineering

This thesis is lovingly dedicated:

To the memory of my father, Mohemmed Jefer
Who showed me the right way with his wisdom and knowledge

To my mother, Mehbube
For her sacrifice, devotion, love and silent tears

To my lovely wife, Somayeh
Who gave life to my living

And to my brother, Jelil
Who is not just a brother for me but a father and caring friend

Abstract

As the demand for green energy and fuel cells grows, more attention is drawn towards Solid Oxide Fuel Cells (SOFCs). Random and complex structure of composite electrodes and underlying electrochemical process has not been completely unveiled yet and further study is required to acquire more understanding. Modeling in this regard plays an important role as it pinpoints key parameters in optimum design of the cell without resorting to costly and uncertain experiments which might even lead to misinterpretations due to random nature of experimental data. The aim of this work is to develop a new rigorous model to study the structure performance relationship of (SOFC) composite electrodes. The work has been conducted in two phases, a two-dimensional continuous approach and three-dimensional discrete model.

A new two-dimensional, geometrical model which captures the inhomogeneous nature of the location of electrochemical reactions based on random packing of electronic and ionic conducting particles has been developed. The results show that the concentration of oxygen inside the cathode in the two-dimensional model is not only a function of the electrode depth but also changes along the width of the electrode. Furthermore the effect of composition of the electrode on the length of three phase boundary (TPB) and total polarization resistance has been demonstrated. A parametric study of the effect of the conductivity of ionic conductor and diffusion coefficient on the performance of the electrode has been given.

To make a more realistic analysis, a three-dimensional reconstruction of (SOFC) composite electrodes was developed to evaluate the performance and further investigate the effect of microstructure on the performance of electrodes. To enhance connectivity between particles and increase the length of TPB, sintering process is mimicked by enlarging particles to certain degree. Geometrical characteristics such as length of TBP and active contact area as well as porosity can easily be calculated using the current model. Electrochemical process is simulated using resistor-network model and complete Butler-Volmer equation is used to deal with charge-transfer process on TBP. The model shows that TPBs are not uniformly distributed across the electrode and location of TPBs as well as amount of electrochemical reaction is not homogeneous. Effects of particle size, electrode thickness, particle size ratio, electron and ion conductor conductivities and rate of electrochemical reaction on overall electrochemical performance of electrode are investigated.

Acknowledgments

I appreciate the guidance and support received from my supervisors, Dr. Krishnaswamy Nandakumar and Dr. Jingli Luo. I am also very thankful to computer support team specially Mr. Bob Barton, Mr. Jack P. Gibeau and Mr. Andrew Bates who sincerely helped this research with their exceptional computer support. Dr. Maham provided all kinds of support and consultation for me during the course of this work. I am grateful to him for all the help he provided.

I am also pleased to thank my colleague friends Dr. Misha Monder, Dr. Mohammad Amiri, Dr. Mranal Jain and Dr. Chidambaranathan Veeramani who helped me with their constructive suggestions and discussions. I also would like to thank my friends Hassan, Farid, Vahid, Aslan, Yashar, Rojin, Behrang, Reza, Nilufar, Mehrdad, Ali, Roshanak, Masoud, Mitra, Siavash, Arezu, Kayvan, parastoo, Farshad and all other friends who made my life much easier, fun and joyful in Edmonton so that I could pursue this research.

Without question, the best thing that happened to me during this work was marrying Somayeh. I have the most wonderful person who has chosen to spend her life with me as my soul mate. Above all, I am especially thankful to her, who has made my life the happiest ever. Without her encouragement and inspiration, I would not be able to accomplish my thesis.

My dear father, who passed away while I was doing this research, was the greatest supporter of me. Thank you dad for standing through the years by my side. When it comes to mother, there is absolutely no word or phrase to describe her. She taught me how to be a man and to love people. In this period of separation, her prayers have always followed me. Thank you mom! I'd be lost and lonely without you. I also would like to thank the other great supporter of my life, my brother who I always respect him for being a wonderful brother and friend. I am also grateful to two wonderful women in my life, my two sisters, for their kind support all through my studies and life.

The funding for this research was provided by National Science and Engineering Research Council of Canada and the author is grateful to this organization.

Table of contents

List of tables

List of figures

Nomenclature

Symbol	Description
a_i	Activity of gaseous specie i
A_c	Interfacial area between particles, (μm^2)
A_{TPB}	Active triple phase area, ($\mu m^2.\mu m^{-3}$)
C_o	Concentration of oxygen, ($gr.cm^{-3}$)
d	Particle diameter, *(μm)*
d_{el}	Diameter of electron conductor particle, (μm)
d_{io}	Diameter of ion conductor particle, (μm)
D	Diameter of the electrode, (μm)
D_{ij}^{B}	Binary diffusion coefficient, *($cm^2.s^{-1}$)*
$D_{ij}^{B,eff}$	Effective binary diffusion coefficient, *($cm^2.s^{-1}$)*
$D_{O_2-N_2}^{B,eff}$	Effective binary diffusion coefficient of O_2 in N_2, *($cm^2.s^{-1}$)*
D_{ij}^{eff}	Effective diffusion coefficient of i in j, *($cm^2.s^{-1}$)*
$D_{O_2-N_2}^{eff}$	Effective diffusion coefficient of O_2 in N_2, *($cm^2.s^{-1}$)*
$D_{O_2}^{K,eff}$	Effective Knudsen diffusion coefficient of O_2, *($cm^2.s^{-1}$)*
E	Potential, (*Volts*)
E_0	Standard potential, (*Volts*)
E_{Op}	Open circuit voltage, (*Volts*)
E_{rev}	Reversible potential, (*Volts*)
F	Faraday's constant equal to 96485.34, ($C.mol^{-1}$)
f	Constant equal to F/R_gT, ($Volts^{-1}$)
I_{ij}	Current passing through j^{th} contact point of particle i
i	Current generated on the boundary ($A.m^{-2}$)
i_0	Exchange current density, ($A.m^{-2}$)
L	Thickness of electrode, (μm)
L_{TPB}	Length of triple phase boundary, ($\mu m.\mu m^{-3}$)
M	Molecular mass of gaseous species(mol^{-1})
N_i	Diffusive flux of species i, ($mol.\ m^{-2}$)

n	Total number of particles per unit volume
n_c	Number fraction of particles at percolation threshold
n_e	Number of electrons transferred per reaction
n_i	Number fraction of particle i in the packing
P	Total pressure, (kpa)
P_i	Partial pressure of species i, (kpa)
r	Size ratio of ion and electron conductor particles
r_c	Contact radius between two particles, (μm)
r_{el}	Radius of the electron conductor, (μm)
r_{io}	Radius of the ion conductor, (μm)
r_p	Radius of the particle, (μm)
R_b	Bond resistance, (Ω)
$R_{b,c}$	Resistance of equivalent cylinder, (Ω)
R_c	Contact resistance, (Ω)
R_{ct}	Charge transfer resistance, (Ω)
R_{el}	Bond resistance inside electron conductor particle, (Ω)
$R_{el\text{-}io}$	Overall resistance between two electron and ion conductor particles, (Ω)
R_{io}	Bond resistance inside ion conductor particle, (Ω)
R_g	Universal gas constant, ($KJ.mol^{-1}.K^{-1}$)
R_{ohm}	Ohmic resistance, (Ω)
R_p	Polarization resistance, ($\Omega.cm^2$)
R_t	Total electrode resistance, ($\Omega.cm^2$)
T	Temperature (K)
V_{i0}	Potential at the center of particle i
V_{ij}	Potential at j^{th} contact point of particle i neighbouring particle
x_i	Mole fraction of species i
Z	Total coordination number
Z_{eff}	Effective coordination number (isolated particles excluded)
Z_i	Coordination number of particle i
Z_{ii}	Average number of contacts between two i particles
Z_{im}	Average number of contacts between an i and m particles
$Z_{LSM\text{-}LSM}$	Average contacts of an LSM particle with other LSM particles

$Z_{YSZ\text{-}YSZ}$	Average contacts of an YSZ particle with other YSZ particles
$Z_{LSM\text{-}YSZ}$	Average contacts of an LSM particle with YSZ particles
$Z_{YSZ\text{-}LSM}$	Average contacts of an YSZ particle with LSM particles
eff	Effective properties
el	Electronic conductor
io	Ionic conductor

Greek letters

α	Charge transfer coefficient in Butler-Volmer equation, (=0.5)
ΔG_f	Total Gibbs free energy change, (KJ)
Δg_f	Molar Gibbs free energy change, ($KJ.mol^{-1}$)
ΔH_f	Enthalpy of formation, (KJ)
ΔV_{el}	Potential difference between two points in LSM, ($Volts$)
ΔV_{io}	Potential difference between two points in YSZ, ($Volts$)
ε	Porosity of the electrode
η	Overpotential, ($Volts$)
η_{act}	Activation overpotential, ($Volts$)
η_{conc}	Concentration overpotential, ($Volts$)
η_f	Fuel utilization efficiency
η_{ohm}	Ohmic overpotential, ($Volts$)
η_{rev}	Reversible efficiency of fuel cell
η_v	Voltage efficiency
ρ_{el}	Resistivity of electron conductor particles, ($\Omega.\mu m$)
ρ_{el}^{eff}	Effective resistivity of electron conductor particles, ($\Omega.\mu m$)
ρ_{io}	Polarization resistance, ($\Omega.\mu m$)
ρ_{io}^{eff}	Effective resistivity of ion conductor particles, ($\Omega.\mu m$)
σ	Characteristic length of atoms in Chapman-Enskog relation
σ_0	Bulk conductivity, ($S.\ m^{-1}$)
τ	Tortuosity of the cathode
ϕ_{ap}	Volume fraction of active particles
$\phi_{a,LSM}$	Volume fraction of active LSM particles
$\phi_{a,YSZ}$	Volume fraction of active YSZ particles

ϕ_{el}	Volume fraction of electron conductor particles
ϕ_{io}	Volume fraction of ion conductor particles
ϕ_{ip}	Volume fraction of isolated particles
$\phi_{i,LSM}$	Volume fraction of isolated LSM particles
$\phi_{i,YSZ}$	Volume fraction of isolated YSZ particles
ϕ_n	Number fraction of particles
Ω_D	Diffusion collision integral in Chapman-Enskog relation

Chapter 1

Introduction

1.1 Discovery of Fuel Cell

The discovery of fuel cell effect dates back to December 1838 when William Robert Grove, an English lawyer and scientist reported his observation of voltage in a cell with platinum electrodes during reaction of Oxygen and Hydrogen. Almost at the same time in January 1839 Cristian Friedrich Schoenbein a Swiss scientist, published a paper about some voltaic activities he observed as a result of temperature change in an electrolyte solutions connected with platinum electrodes to a galvanometer. Later on, on May 1843, Grove wrote his famous paper on the invention of fuel cell. He called his apparatus “Gaseous Voltaic Battery”. In fact his voltaic battery was an early copy of today’s phosphoric acid fuel cells but with sulphuric acid utilized as electrolyte. Grove and Schoenbein then exchanged ideas for many years to further nurture this first concept [1]. In 1959, Francis Thomas Bacon developed the first 5kW fuel cell. Since then, fuel cells have undergone many changes and developments.

1.2 Fuel Cells

Fuel cells are electrochemical devices that convert chemical energy in hydrogen, hydrocarbons or other fuels directly into electricity. Unlike batteries, fuel cells are designed to operate continuously by supplying reactants and their parts are not supposed to be consumed or degrade by the time of operation as is the case for batteries. High efficiency of fuel cells in comparison to heat engines and the need to produce low-pollution electricity has made the fuel cells the best candidate to power the future vehicles and to be used as future distributed power system.

1.2.1 Applications of Fuel Cells

Fuel cells have wide range of applications from stationary to portable and micro scale to large scale power plant applications [2]. In stationary large scale applications it is used as a reliable source of power for emergency power units in hospitals, banks and other organizations. Almost all car manufacturers today are working on fuel cells and many have introduced their fuel cell cars. In some big and highly populated cities, fuel cell buses are employed as clean energy conversion devices for public transportation. Mehdi *et al*. [3] describes prospective of application of two main type of fuel cells; Solid Oxide Fuel Cells (SOFC) and Polymer Electrolyte Membrane Fuel Cells (PEMFC) in aviation industry and challenges facing the industry. The first piloted 100% fuel cell powered aircraft took off just recently on June 2009[4]. Fuel cell has many applications on marine industry in fuel cell propulsion systems and to generate the power of vessels and submarines [5,6]. On small scales, micro fuel cells are used to power personal electronic devices such as cell phones, digital cameras, laptops and other portable gadgets [7,8].

1.2.2 Advantages/Disadvantages

Energy efficiency and environmentally cleanness are the most favoured advantages of fuel cells. If pure hydrogen is used as fuel, fuel cells basically

produce no emissions. Fuel cells are more energy efficient that internal combustion engines. If hydrogen fuel comes from electrolysis of water, zero greenhouse emission can be realized. With very silent operation, fuel cell power plant can be installed almost everywhere in small modular units and if more power is required, simply more modules can be added. Most of the fuel cell units have no moving parts and that makes maintenance and repair of these systems easier. Their installation and working mechanism is much simpler than internal combustions engines and less personal is required to supervise a fuel cell unit compared to similar conventional power plants.

But fuel cells have some disadvantages. Despite all efforts and advances in making low cost fuel cell and material, fuel cells are still expensive compared to conventional internal combustion engines or batteries. Hydrogen, the most favoured fuel for fuel cells is very dangerous and explosive and hard to contain. Its tiny molecules can leak and escape from thick steel cylinders and cause fire and explosion. A research indicates that leakage from commercial hydrogen storage and transportation plant can reach as high as 20% [9]. Another research indicate that if current fossil fuel technology is replaced with hydrogen, the leakage from all hydrogen sources can cause real threats and fasten the depletion of ozone layer [10]. Usually fuel cells have shorter life that other internal combustion engines. Material durability and capability to withstand high temperatures is still an issue. There are many other technical problems, difficulties and challenges that have not been resolved [11].

1.2.3 Fuel for Fuel Cells

In theory, fuel cells can consume any type of hydrocarbons to produce electricity. The most convenient and preferred fuel from both theoretical and practical aspects of fuel cell structure, is pure hydrogen which is obtained from hydrolyses of water or steam reforming of hydrocarbons. Fuel cells based on hydrocarbons and especially natural gas and methanol with internal reforming system are also common. Many researchers are trying to adopt biofuels coming

from organic wastes to use as a clean and safe source of fuel which can be used in biofuel cells [12].

1.2.4 Main Components and Structure

Fuel cell consists of three main components:

- Cathode
- Anode
- Electrolyte

The general structure of a fuel cell is shown in Fig. 1.1. Oxidation reaction occurs at anode then resultant electrons travel through the external circuit to cathode where reduction reaction takes place. Cathode and anode together are also called *electrodes* of fuel cell and in any type of fuel cell act as catalyst to speed up electrochemical reaction. They also provide a medium to conduct ions into or away from reaction interface. Moreover, micro structure of electrodes plays an important role in determining mass transfer resistances and eventually the overall performance of fuel cell [13]. Main challenges in this area are to manufacture electrodes with high three phase interface, high ionic and electronic conduction, less resistance to transfer of gaseous species, high activity at low temperatures and thermal expansion match between adjacent components [14]. Electrolyte on the other hand, acts as a conductive media to transfer ions from one side to the other side. Depending on fuel cell type and structure, electrolytes may transfer positive or negative ions. It is very important that electrolyte transfers only ions and acts as a barrier to electrons and gaseous species. Leakage of electrons and gaseous species will cause internal currents and fuel crossover, which both tend to decrease the performance of the cell and is more common in direct methanol fuel cells [15]. Depending on type of fuel cell and fuel, electrochemical reactions on electrodes will be different. This will be discussed in the section devoted to types of fuel cells.

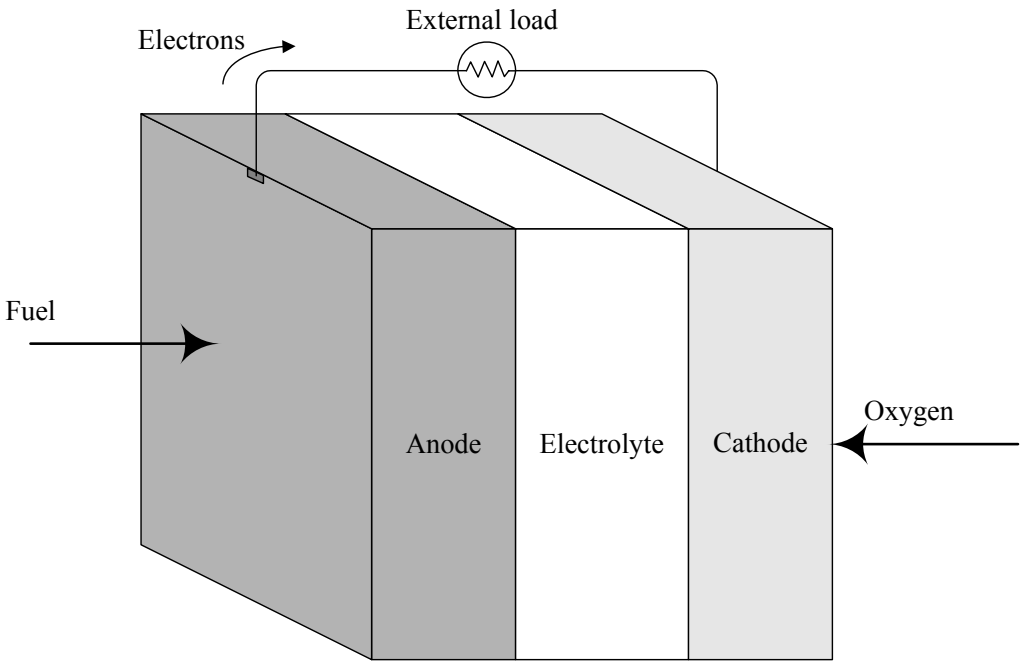

Figure 1.1 Schematic diagram of a typical fuel cell structure.

1.2.5 Types of Fuel Cells

Since their introduction, fuel cells have undergone many changes and developments. Development of fuel cell science and technology has solved older problems but new problems emerged as a result of increase in the level of expectations. Sometimes, a fundamental modification needed to overcome a difficulty and that was how different types of fuel cells were born. Temperature for example is an important factor in fuel cell research. Low temperatures are favoured from material stability point of view, while high temperatures cause higher reaction rates and therefore better cell performance. Operating temperature of fuel cell starts from as low as 80^{o}C for polymer electrolyte fuel cells to as high as 1000^{o}C in solid oxide fuel cells. Fuel cells are usually classified and named by the type of electrolyte utilized. At the same time each type of fuel cell belongs to category of high temperature or low temperature fuel cells. Fig. 1.2 shows working principles of main fuel cell types. Most types of fuel cells follow same working principles with minor differences. A brief description of common types of fuel cells is given below on the order of increasing operating temperature.

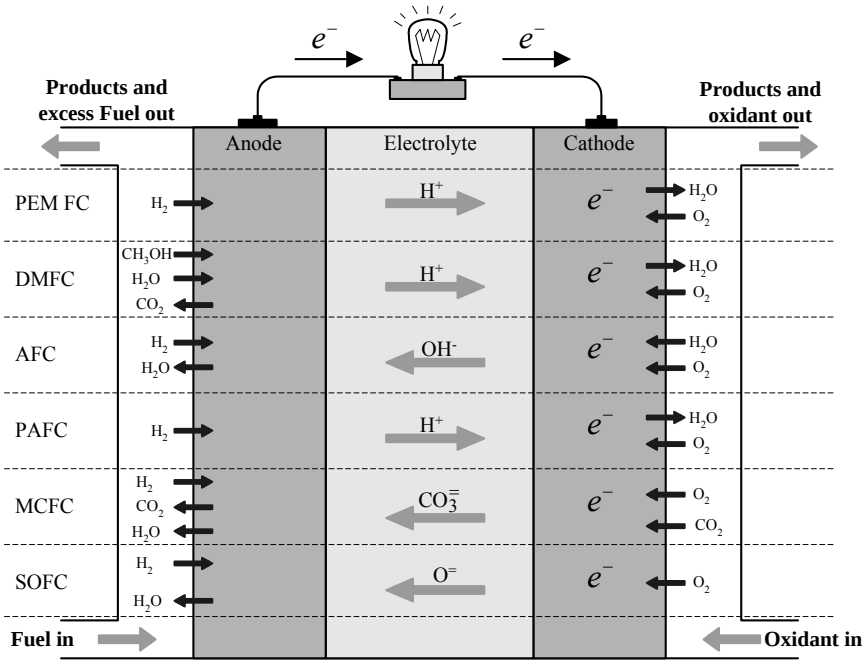

Figure 1.2 Working principles of different types of fuel cells.

1.2.5.1 Proton Exchange Membrane Fuel Cell (PEMFC)

A solid polymer membrane, saturated with water is used as electrolyte for this type of fuel cell. Electrochemical oxidation of hydrogen at the anode produces protons that are transferred to cathode through polymer electrolyte and is followed by reaction with oxide ions to produce water and heat. Polymer electrolyte membrane fuel cells operate at low temperatures of about 80^{o}C. This relatively low temperature allows short start up times for systems based on PEM fuel cells. Due to low temperatures, a noble metal catalyst such as platinum is usually used inside anode to separate protons and electrons of hydrogen. Platinum catalyst however, is very sensitive to carbon monoxide (CO) which may exist in low concentration with Hydrogen feed as a product of steam reforming of hydrocarbons and causes CO poisoning of catalyst [16] which leads to significant loss in performance of PEM fuel cells. Several techniques have been proposed to overcome CO poisoning including pre-processing of hydrogen feed to remove CO, bleeding oxidant into feed stream to convert CO into CO_2 and use of CO tolerant catalysts [17,18]. Electrolytes for PEM fuel cells mostly are based on

perfluoro sulfonated acids such as Nafion from Dupont [19]. Due to low operation temperature, PEM fuel cells need short start up times which makes them suitable for portable and transportation applications such as cars and motor bikes as well as small electronic devices.

1.2.5.2 Direct Methanol Fuel Cells (DMFC)

As shown in Fig. 1.2 direct methanol fuel cells are similar to PEM fuel cells in a sense that both types of fuel cells utilize a polymer membrane proton carrier. Unlike PEM fuel cells, DMFCs utilize methanol in the presence of water as fuel. This direct use of methanol cuts the cost of reforming to produce hydrogen and solves the difficulty of storage and transportation of hydrogen while replacing low energy density hydrogen fuel with relatively high energy density methanol. Like PEMs, direct methanol fuel cells operate at low temperatures of about $80^{o}C$ to $100^{o}C$ [20]. Main problem facing the commercial development of direct methanol fuel cells is their low efficiency as well as need for active catalysts that operate at low temperatures [21]. DMFC technology is relatively new compared to other types and fuel cells and it is expected that by development of science and technology of DMFC, these problems can be easily outweighed by the advantage of eliminating production, storage and transportation of hydrogen. DMFCs are expected to be a suitable candidate for future transportation systems and portable electronic devices.

1.2.5.3 Alkaline Fuel Cells (AFC)

Unlike polymer membrane fuel cells, alkaline fuel cells use a liquid solution as electrolyte. This solution is usually potassium hydroxide in water which conducts hydroxyl (OH^{-}) ions. Depending on the concentration of solution, alkaline fuel cells operate in wide range of temperatures from $60^{o}C$ to $250^{o}C$. High concentration of KOH requires higher temperatures.

Alkaline fuel cells are among the most developed fuel cells and they have been successfully utilized in space explorations to produce electricity and drinking

water in spacecrafts. They are easy to make, have cheap electro-catalysts and demonstrate very high efficiencies of about 70%.

The principal disadvantage of alkaline fuel cells is their sensitivity to Carbon dioxide and Carbon monoxide. CO and CO_2 usually come with Hydrogen in low concentration as products of steam reforming. CO poisons the electrodes and CO_2 reacts with KOH solution and forms K_2CO_3 [22]. Even very low concentration of CO_2 is detrimental [23].

Despite disadvantages, Alkaline fuel cell cells are cost effective and it is shown that these types of fuel cells are less costly compared to PEM fuel cells [24,25].

1.2.5.4 Phosphoric Acid Fuel Cells (PAFC)

Liquid phosphoric acid contained in silicon carbide matrix is used as electrolyte to conduct protons and platinum is used in both anode and cathode as electro-catalysts. Since ionic conductivity of phosphoric acid is low at low temperatures, operating temperature is kept high and above 150^{o}C. PAFCs are first commercial fuel cells among other types and they are mostly utilized for stationary power generation systems with first power plant installed in 70s. The world largest fuel cell power plant operated for 6 years between 1991 and 1997 was a PAFC [26].

PAFCs have long life time which is required for commercial success and because of high operating temperatures, PAFC are more tolerant to CO contained in fuel stream. The efficiency of PAFC is also high and about 37%, however; when utilized in combined heat and power (CHP) systems or cogeneration plants, they can reach efficiencies of up to 80% [26] and that is because PAFCs produce high quality steam at high temperatures.

Main disadvantage of PAFC is being bulky compared to PEM fuel cells. Moreover, high temperatures assist the evaporation of the solution and continued make up of electrolyte solution is required. Nevertheless, low cost electrolyte makes this disadvantage less important. Long warm up times and use of expensive platinum catalysts are other disadvantages of this type of fuel cell [27].

1.2.5.5 Molten Carbonate Fuel Cells (MCFC)

As the name implies, electrolyte of molten carbonate fuel cells is a melt and it is usually a mixture of two alkali carbonates. These alkali carbonates are typically potassium carbonate (K_2CO_3) and lithium carbonate (Li_2CO_3) which are contained in a chemically inert ceramic lithium aluminum oxide ($LiAlO_2$) matrix. Operation temperature of MCFC's is high and above melting point of electrolyte. That requires a temperature of about 600-1000^oC which puts MCFC on high temperature fuel cell category. [28]. Carbon dioxide reduces to carbonate ion in the presence of oxygen at the cathode. Carbonate ion then travels to anode through molten electrolyte and reacts with fuel hydrogen to produce water, carbon dioxide and electrons. Carbon dioxide is then separated and recycled to the anode.

Since the operation temperature is very high, non-precious metal catalysts can be used at anode and cathode which cuts the cost of these systems. Ni and NiO are usually enough to catalyze anode and cathode reaction. Furthermore, high operating temperature eliminates the need for external reforming of fuel to produce hydrogen thus methane or other hydrocarbons can be used directly with reforming process occurring internally at the anode. In addition, unlike most types of fuel cells, molten carbonate fuel cells are not poisoned by CO and CO_2 and in fact CO can be used as fuel for this type of fuel cell to conduct water gas shift reaction which produces hydrogen [29,30]. Some studies suggest that MCFC's can even be used for internal reforming of coal [27].

High operating temperature has its own problems. Carbonate solution is corrosive at high temperature which degrades electrodes. Furthermore, high temperature requires longer warm up times that other types of fuel cell. This suggest that due to slow response times and additional equipment to manage electrolyte and carbon dioxide, molten carbonate fuel cells are not suitable for small power supplies where power demand is changing over short periods of time. MCFC's are suitable for large electrical utility stations and distributed power generation systems [31] especially in combined heat and power generation

systems which can reach efficiencies of up to 85%. A technical review of MCFC development status and challenges is given by Selman [32].

1.2.5.6 Solid Oxide Fuel Cells (SOFC)

Unlike all other types of fuel cells, electrolyte in solid oxide fuel cell is a solid oxide. It is non porous and therefore gas species cannot pass through it. It is also non conductive to electrons while oxide ions can pass through it and migrate from cathode side all the way to the anode, however, ionic conductivity of most solid electrolyte is few orders of magnitude less than typical conductivity of metals to electrons. Usually Yttria-stabilized zirconia (YSZ) is employed as electrolyte for solid oxide fuel cells.

Solid oxide fuel cells belong to the category of medium to high temperature fuel cells and typical SOFC operates at about 800^{o}C, while there are medium temperatures SOFC which operate at lower temperatures. The main challenge in solid oxide fuel cell design which keeps the temperatures high is the ion conductivity of electrolyte and activity of electro-catalyst. Ionic conductivity of solid electrolytes is very low at low temperatures making the process of ion conduction difficult and hence impossible low temperature operations.

Solid oxide fuel cell has drawn much attention recently due to its advantages. SOFC's are very efficient; when used in CHP systems they can reach efficiencies of up to 90%. High efficiency however, is not the main advantage of solid oxide fuel cells. High temperature allows simple non-precious catalysts to be used. SOFC's can operate with wide variety of hydrocarbons as fuel. Compact structures can be realized with high power density and all solid structure gives SOFC a flexibility to be used in any type of application.

Since modeling of SOFC electrodes is the subject of current work, solid oxide fuel cells will be described in detail in section 1.3.

1.2.6 Comparison of Fuel Cell Types

Table 1.1 provides a comparison for different types of fuel cell. As for other technologies each type of fuel cell solves some problems while brings other shortcomings. There are many other detail issues about different types that have not been pointed out in here. No one claims that only a single fuel cell type suits all applications and in future we will continue to see different types of fuel cells for various applications.

Table 1.1 Comparison of different types of fuel cell technologies

Fuel Cell Type	**Electrolyte**	**Charge carrier**	**Operating temperature**	**Applications**	**Advantage**
PEMFC	Ion exchange membrane	H^+	80°C	- Portable electronics - Distributed power generation - Transportation	- Relatively small - Low temperature - Short war up times - Solid electrolyte
DMFC	Ion exchange membrane	H^+	80-100°C	- Portable electronics - Transportation - Military - Mobile systems	- Direct use of Methanol - Low temperature
AFC	Potassium hydroxide solution	OH^-	60-200°C	- Space explorations - Military use	- Cost effective - Easy to make - High performance - Wide range of electro-catalysts
PAFC	Liquid Phosphoric acid	H^+	200°C	- Distributed power generation	- Tolerant to CO and other impurities - Long life time - High efficiency in cogeneration systems - Cheap and readily available electrolyte
MCFC	Potassium and lithium carbonate melt	CO_3^{2-}	650°C	- distributed power generation - Combined heat and power	- Wide range of catalyst - Wide range of fuel - Tolerant to CO and CO_2 - Wide range of readily available catalyst
SOFC	Y_2O_3 stabilized with ZrO_2	$O^=$	600-1000°C	- distributed power generation - Utility power - Cogeneration plants - small applications	- High efficiency - All solid structure - Wide range of fuel - Wide range of catalyst

1.3 Solid Oxide Fuel Cells

1.3.1 Historical Background

The history of SOFC dates back to 1899 when Walther Nernst discovered that mixtures of zirconia and some rare earth oxides exhibit ionic conductivity at high temperatures of above 800^{o}C. About two years later, he patented his electric lamp glowers composed of 85% of zirconium oxide (ZrO_2) and 15% of yttrium oxide (Y_2O_3) or other rare earth oxides such as neodymium oxide or Scandium oxide or thorium oxide [33]. Baur and Preis in 1937 used same solid electrolyte to develop their solid oxide fuel cell and later on, Westinghouse developed his first SOFC in 1962 [29]. Since then, solid oxide fuel cells have undergone many phases of development but still Yttria stabilized Zirconia is the main electrolyte being used in the structure of SOFCs.

1.3.2 Basics of Operation and Main Components

As mentioned before, electrolyte in this type of fuel cell is solid material which conducts oxide ions ($O^{=}$). Oxygen is reduced at cathode by absorbing 2 electrons coming from external circuit. Oxide ions then travel to anode through solid electrolyte. On the anode side, hydrogen gas reacts with oxide ions to produce heat, water and electrons. Electrons produced in this process, flow to cathode through external circuit and that is how a close circuit is established and electricity is produced.

1.3.2.1 Cathode

A blend of electrolyte material such as YSZ and strontium-doped lanthanum manganite ($LaMnO_3$) or LSM is used to form cathode of high temperature solid oxide fuel cells. This is because there is a very good thermal expansion match between LSM and YSZ at temperatures above 800^{o}C [28]. High temperatures results in higher cost and material durability and compatibility problems [34].

Main barrier in bringing down the operating temperature is low activity of electrode material for electrochemical reduction of oxygen [35]. At medium temperatures (600^{o}C-800^{o}C) however, other electrode materials such as lanthanum strontium cobalt ferrite (LSCF) [36] and lanthanum strontium manganese ferrite (LSMF) are used. The use of many other less common material is also reported [7,28]. Main challenges in selecting cathode material for solid oxide fuel cells are to reduce overall polarization resistance of the electrode as well as increasing durability and compatibility.

1.3.2.2 Anode

Electrochemical oxidation of hydrogen or other fuels occur on the anode of solid oxide fuel cells. Since ions, electrons and gas species are present in this reaction, anode is a porous structure made of a cermet of YSZ and a metal. Anode material must be very stable in reducing and variable composition environment, must possess high electronic and ionic conductivity, must be highly porous and thermal expansion coefficient must match with that of the electrolyte. Selman provides thermal expansion coefficient data of various solid oxide fuel cell components [37]. These characteristics apply to cathodes too, except that reaction for cathode is different.

Several materials such as Ni, Pt, Co and Ru has been studied for this purpose and so far nickel (Ni) has been the most appropriate metal for anode material on cost grounds and having high electro-catalytic activity [38,39]. Studies have shown that addition of YSZ to Ni significantly increases three phase boundary (TPB) and reduces polarization resistance [40,41]. Furthermore it reduces thermal expansion coefficient of pure nickel to match the thermal expansion coefficient of the electrolyte [42] and avoids grain coarsening of Ni particles [43].

1.3.2.3 Electrolyte

As pointed out before, zirconia based electrolyte are first and most popular electrolytes for solid oxide fuel cells. Apart being conductive to oxide ions, SOFC

electrolytes must be stable in oxidizing and reducing environments. Furthermore they must be cost competitive to keep the manufacturing costs down. Moreover, it must have minimum electronic conductivity and must be mechanically strong and stable [44,45]. Ionic conductivity of a solid state electrolyte depends on many parameters such as microstructure, grain size, dopant concentration, impurities and processing condition [44,46]. Furthermore it is a thermally activated process where the conductivity increases with increasing temperature and partial pressure of oxygen. In fact the high temperature of SOFCs based on YSZ is the result of low ionic conductivity of this electrolyte at temperatures lower than 800^{o}C, compared to some other electrolytes [45].

Lowering the operating temperature of solid oxide fuel cell can be seen as the main goal of fuel cell research. This is equivalent to search for a good oxide ion conductor at temperatures lower that 800^{o}C gadolinia-doped ceria (GDC) or lanthanum gallate-based electrolytes such as $La_{0.8}Sr_{0.2}Ga_{0.8}Mg_{0.2}O_3$ (LSGM) have shown ion conductivities higher than YSZ at temperatures lower than 800^{o}C [47]. Stabilized bismuth oxide (Bi_2O_3) shows the highest ionic conductivity among other oxide ion conductors [45] have ionic conductivity of about 1 to 2 orders of magnitude higher than zirconia oxide at low temperatures of 500^{o}C-700^{o}C [48]. Although this high ionic conductivity offers a potential application at low temperature solid oxide fuel cells, the practical application of this material is limited due its disadvantages. Bismuth oxide based electrolytes are thermodynamically unstable in reducing condition and decomposes into bismuth metal [37]. Furthermore it is volatile at intermediate temperatures and possesses high corrosion activity [45].

1.3.2.4 Interconnects

Interconnect in solid oxide fuel cell makes electrical connection between neighbouring cells. Furthermore, interconnect protects cathode from reducing atmosphere of the anode and provides gas channels to carry fuel and oxygen to electrodes and take away reaction products.

High operating temperatures of solid oxide fuel cells and severe operating conditions eliminates most of the candidates from being considered as interconnects. Interconnect needs to be solid with no pores to avoid mixing of fuel and oxygen, must have high electronic conductivity to avoid further losses and its thermal expansion coefficient must match with other components especially anode and cathode. Furthermore, it must be stable and inert in the reducing environment of anode and oxidizing environment of cathode [20,49,50]. Ceramic interconnects such as $LaCrO_3$ and $YCrO_3$ doped with a rare earth element such as Ca, Mg to improve conductivity, have been extensively used in high temperature SOFCs [37]. Although they have good conductivity and thermal compatibility, they are difficult to fabricate and expensive. Lowering fuel cell operating temperature makes it possible to use cheaper and easy to make metals and metal alloys as interconnect. Metals are highly sensitive to oxidation at high temperatures. At temperatures around 800^{o}C nickel based alloys can be used with confidence and when the temperatures are well below 800^{o}C even ferritic steels can be used[20,49,51].

1.3.3 Thermodynamics

1.3.3.1 Open Circuit Voltage

Open Circuit Voltage (OCV) is the maximum voltage available between two electrodes of fuel cell and it happens when there is no external load. In a solid oxide fuel cell and similar fuel cells the following reaction of reduction of oxygen takes place on the cathode side:

$$\tfrac{1}{2}O_2 + 2\bar{e} \rightarrow 2O^{=} \qquad (1.1)$$

Oxide ions produced in this way are transferred to the cathode through electrolyte. The reaction on the anode side:

$$H_2 + O^{=} \rightarrow H_2O + 2\bar{e} \qquad (1.2)$$

These two cathodic and anodic reactions result in overall reaction of Hydrogen oxidation inside the fuel cell to give water and heat:

$$H_2 + \tfrac{1}{2}O_2 \rightarrow H_2O \tag{1.3}$$

The change in Gibbs free energy of formation (ΔG_f or Δg_f in molar base) is the maximum amount of external work that can be extracted from this reaction in a reversible process. That is:

$$\Delta g_f = \text{External work} \tag{1.4}$$

But the external work which is electrical work is the product of current and voltage:

$$\text{External electrical work} = EI = E \times (-2Ne) = -2FE \tag{1.5}$$

And therefore:

$$\Delta g_f = \text{-}2FE \Rightarrow E = \frac{-\Delta g_f}{2F} \tag{1.6}$$

In this equation 2 stands for 2 moles of electron which is being transferred for one mole of Hydrogen. E is reversible open circuit voltage. Just like Δg_f, open circuit voltage depends on temperature as well as pressure (or concentration). Based on Eq. 1.3, it is shown in thermodynamic literature that:

$$\Delta g_f = \Delta g_f^0 - R_g T \ln\left(\frac{a_{H_2}.a_{O_2}^{1/2}}{a_{H_2O}}\right) \tag{1.7}$$

Where Δg_f^0 represents the change in Gibbs free energy at standard pressure and a is the activity of species. By dividing both sides of Eq. 1.7 with *-2EF* and assuming water and hydrogen as well oxygen act like an ideal gas and noting that standard pressure is 1 bar, Eq. 1.7 simplifies to Nernst equation for reaction 1.3:

$$E = E^0 - \frac{R_g T}{2F} \ln\left(\frac{P_{H_2}.P_{O_2}^{1/2}}{P_{H_2O}}\right) \tag{1.8}$$

Where E is the open circuit voltage or Nernst voltage of hydrogen cell at given temperature and pressure. This is the maximum voltage observed if the fuel cell process is reversible. In reality this process is not reversible and some of the energy is converted to heat thereby, bringing fuel cell voltage to values less than the value indicated in Eq. 1.8.

1.3.3.2 Fuel Cell Efficiency

Like efficiency for Carnot cycle, fuel cell reversible efficiency is defined as:

$$\eta_{rev} = \frac{\text{Maximum Electrical Work Output}}{\text{Total Energy Input}} \tag{1.9}$$

In the case of a fuel cell, maximum electrical work that can be extracted from a reversible fuel cell is equal to ΔG_f, while total energy input is the energy that would be released if the fuel was burnt, that is ΔH_f and therefore:

$$\eta_{rev} = \frac{\Delta G_f}{\Delta H_f} \tag{1.10}$$

Since two values namely High Heating Value (*HHV*) and Low Heating Value (*LHV*) for ΔH_f is available based on the state of products, it is customary to mention *LHV* or *HHV* while referring to η_{rev}.

η_{rev} is the maximum efficiency that can be achieved from a fuel cell and it is only one component of real fuel cell efficiency indicators. When fuel cell is connected to external load, potential observed (operational voltage) is less than the potential indicated in Eq. 1.8. This is due to irreversible processes occurring in cell components. *Voltage efficiency* is then defined as the ratio of operating voltage and open circuit voltage:

$$\eta_v = \frac{E_{Op}}{E_{rev}} \tag{1.11}$$

Mechanisms contributing to this loss will be discussed in next section. Another component of fuel cell efficiency is *fuel utilization efficiency*. It originates from

that fact that not all the fuel entered to fuel cell is consumed in the reaction and some of the fuel leaves the cell with product gases. Fuel utilization efficiency then defined as:

$$\eta_f = \frac{\text{Mass of the fuel consumed in the cell}}{\text{Total mass of fuel entered the cell}} \tag{1.12}$$

Therefore overall fuel cell efficiency is defined as the product of efficiencies mentioned above:

$$\eta = \eta_{rev}\eta_v\eta_f \tag{1.13}$$

1.3.3.3 Actual Performance of the Cell and Polarization

Fuel cell reversible efficiency represented by Eq. 1.10 is the maximum achievable performance under reversible condition. In reality however, when the fuel cell is working (current is drawn), observed potential is less that reversible potential. This drop in potential as represented by Eq. 1.11 is due to irreversibilities occurring inside the cell components. Fig. 1.3 shows a typical fuel cell performance. This figure shows three different regions for voltage drop also known as *polarization*.

Activation polarization is caused by low electrochemical reaction kinetics. Slower electrochemical reactions are associated with larger activation losses and faster initial potential drop. Since temperature is in the favour of most electrochemical reactions, high temperature fuel cells are usually characterized with lower initial voltage drop [52].

Electrode kinetics or rate of current generation inside the electrode is usually expressed by Butler-Volmer equation:

$$i = i_0\left\{e^{\frac{\alpha n_e F \eta_{act}}{R_g T}} - e^{\frac{-(1-\alpha) n_e F \eta_{act}}{R_g T}}\right\} \tag{1.14}$$

Where n_e is the number of electrons transferred per reaction and α is a kinetic parameter and is called *transfer coefficient* and its value is usually set to 0.5 for fuel cell kinetic studies. For α=0.5 Eq. 1.14 takes the simplified form of:

$$i = i_0 \left\{ e^{\frac{n_e F \eta_{act}}{R_g T}} - e^{\frac{-n_e F \eta_{act}}{R_g T}} \right\} \tag{1.15}$$

It is evident that under high activation polarization or high current density, the second term in Eq. 1.15 becomes very small compared to the first term and can be neglected. Then Eq. 1.15 will be simplified to Eq. 1.16 which is called *Tafel* equation:

$$\eta_{act} = \frac{R_g T}{n_e F} \ln\left(\frac{i}{i_0}\right) \tag{1.16}$$

Although Tafel equation was first derived from experimental results [20], the derivation above proves its theoretical bases.

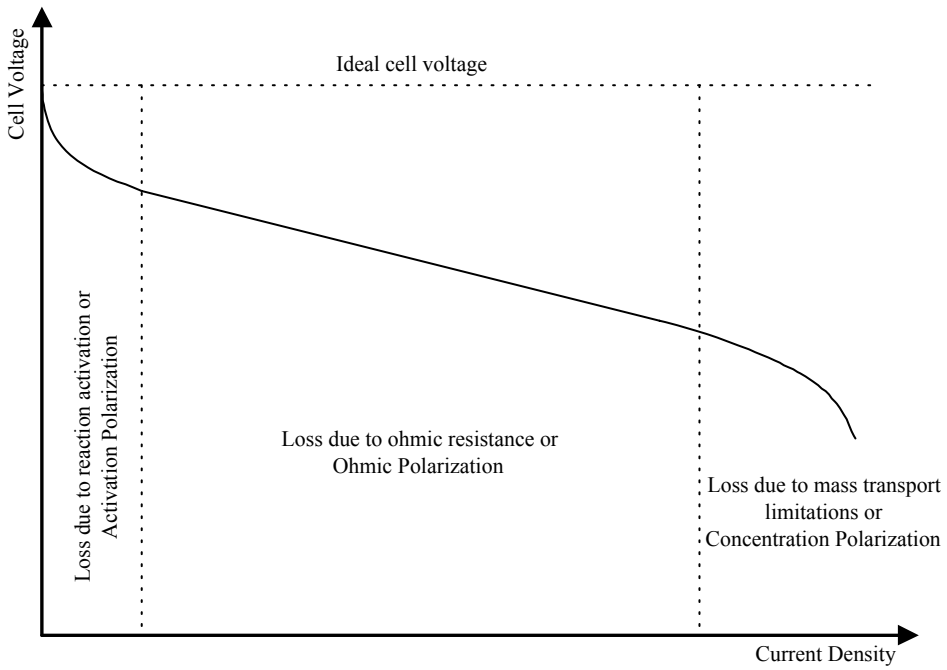

Figure 1.3 Typical performance curve for a working fuel cell.

Under low current densities, the exponentials in Eq. 1.15 become much smaller than unity and therefore can be expanded into Taylor series. After simplifying:

$$\eta_{act} = \frac{R_g T}{n_e F i_0} i \tag{1.17}$$

Eq. 1.17 is comparable with Ohm's law ($V=IR$), and hence reaction resistance or charge-transfer resistance is derived as:

$$R_{ct} = \frac{R_g T}{n_e F i_0} \tag{1.18}$$

Since implementing Eq. 1.15 in composite electrode modeling introduces nonlinearity to system of equations and this nonlinearity increases complexity of solution process and solution time, most of the modellers try to avoid it by using Eqs. 1.17 and 1.18.

Middle region in Fig. 1.3 represents the loss due to ohmic resistance of cell components and is called *ohmic polarization*. Main contribution to ohmic resistance comes from electrolyte or ion conductor material, which is YSZ in most cases. Conductivity of YSZ is about 10 $S.m^{-1}$ at 1000^{o}C [53] which is very low compared to conductivities for anode and cathode material [54]. Ohmic resistance is a linear resistance and follows Ohm's law:

$$\eta_{Ohm} = iR_{ohm} \tag{1.18}$$

At high current densities, when the rate of consumption of reactants is high, electrode media is unable to maintain the initial concentration of reactants and a concentration gradient is formed between the bulk of the fluid in fuel channel and reaction surface deep inside the electrode. This causes another voltage drop known as *Concentration polarization.* Concentration polarization can be calculated using Nernst equation for both anode and cathode sides. For anode, at open circuit conditions (no concentration polarization):

$$E_a^{i=0} = E_a^0 - \frac{R_g T}{2F} \ln\left(\frac{P_{H_2O}^B}{P_{H_2}^B}\right) \tag{1.19}$$

At operating condition when current i is drawn from the cell surface concentration of gaseous species is different from bulk concentrations and therefore:

$$E_a^i = E_a^0 - \frac{R_g T}{2F} \ln\left(\frac{P_{H_2O}^s}{P_{H_2}^s}\right) \tag{1.20}$$

Where $P_{H_2O}^B$ and $P_{H_2}^B$ are bulk concentrations of water and Hydrogen while $P_{H_2O}^s$ and $P_{H_2}^s$ are concentration at reaction surface. Subtracting Eq. 1.19 from 1.20 results in:

$$\eta_{conc,a} = \frac{R_g T}{2F} \ln\left(\frac{P_{H_2}^s P_{H_2O}^B}{P_{H_2}^B P_{H_2O}^s}\right) \tag{1.21}$$

Same discussion applies for cathode concentration polarization and the final result is:

$$\eta_{conc,c} = \frac{R_g T}{4F} \ln\left(\frac{P_{O_2}^s}{P_{O_2}^B}\right) \tag{1.22}$$

To find concentrations at reaction surface, an appropriate mass transfer model must be used [55]. This process is further discussed in chapter 3 where Stefan-Maxwell mass transfer equation is linked to electrochemical reaction equation and Ohm's law to solve for whole domain.

1.4 Summary

This introductory chapter was aimed to give the reader a brief introduction about fuel cells, their structure, types and applications and basic thermodynamic of fuel cell processes. Basic principles introduced here will be applied all over the thesis and hence is the conceptual framework of the thesis. Due to importance of solid oxide fuel cells and its relative advantage over other types, it is crucial to build a deep and solid understanding of SOFC structure and operation principles and then step further towards better understanding of the structure of this type of

fuel cell. Therefore concepts introduced here must be considered as minimum to understand fuel cell operations and reader is encouraged to consult references introduced here and other references for further information on detail of any subject covered above.

1.5 Thesis Objectives

Main objective of this thesis is to build a better understanding of the microstructure of solid oxide fuel cell composite electrodes and to develop a tool to model the behaviour of composite electrodes. Understanding the relationship between the microstructure of the electrodes and overall performance of solid oxide fuel cells is of crucial importance in design and development of high performance SOFCs. Although lot of work has been done so far to model the behaviour of composite electrodes, neither of those seem to resolve the complexity behind composite structures and further work needs to be done. Nevertheless, this thesis does not claim to unveil all the mystery about SOFC composite electrodes but can be regarded as a fruitful effort to shed more light on the subject which gives better understanding of the topic and more comfort and certainty in design of composite electrodes.

1.6 Thesis Outline

In addition to the current chapter which covered an understanding of fuel cells in general and specifically solid oxide fuel cells, this thesis consists of 5 more chapters which follow a step by step approach to fulfill the final objective.

Chapter 2 is a comprehensive literature review of modeling work directed to composite electrodes. It summarizes and classifies experimental observations of composite electrode behaviour and tries to redefine composite electrodes based on the experimental findings and characteristics. Different modeling approaches for composite electrodes modeling are then reviewed and a systematic classification of composite electrode modeling along with capabilities and shortcomings of each modeling approach is offered. Each model is evaluated based on its ability to

cover various experimental observations. Main modeling categories discussed in this chapter include thin film models, continuum models, discrete random packing models and models based on 3D reconstruction of composite electrode structures. Advantages and disadvantages of each model are discussed along with examples of studies.

Chapter 3 involves two dimensional modeling of composite electrodes. It represents a new approach to electrode modeling in a way that a continuous geometry is reconstructed based on the information from discrete packing of electron and ion conductor particles. The continuous geometry is then resolved based on using a commercial finite element software to give current, potential and concentration profiles inside the electrode as well as getting an estimate about polarization resistance and available active sites.

The work presented in chapter 4 is a first step in transition to three dimensional modeling. Composite electrodes are modeled as random packing of electron and ion conducting particles and geometrical characteristics such as porosity, length and area of three phase boundary, coordination numbers and percolation thresholds are obtained for random packing of particles. The effect of electrode composition (relative amount of electron and ion conductor particles), particle size, electrode thickness, particle size ratio and other geometrical properties on the length of three phase boundary is discussed.

In chapter 5, three dimensional modeling is completed by modeling electrochemical process using discrete resistor-network model. Despite other studies; this model uses complete Butler-Volmer equation for electrochemical reaction at three phase boundary and solves a large system of linear and nonlinear equations to obtain current and potential distribution at the center and contact points of each particle and calculates total current and overpotential. The effect of electrode composition, particle size, electrode thickness, exchange current density and particles size ratio along with other parameters on total polarization resistance of the electrode is calculated and discussed.

The main objective of chapter 6 which is the concluding chapter of this thesis is to summarize the work and to validate model predicted quantities with experimentally observed values. Reliable and consistent experimental data are hard to find for most of the modeling parameters. Sometimes experimental observations seem to contradict each other. This issue is further discussed in this chapter and experimental clues are presented to back the validity of model predictions. Suggestions are made based on model findings to improve the performance of composite electrodes and further research opportunities are discussed.

References

[1] U. Bossel, The Birth of the Fuel Cell, European Fuel Cell Forum, Switzerland, (2000).

[2] K. Adamson, Stationary Fuel Cells, Elsevier, Oxford UK (2007) 77.

[3] I. S. Mehdi, J. Trela, K. Fleckner, and A. Pattekar, Procedings of 9th International Symposium on Solid Oxide Fuel Cells, SOFC IX, PV 2005-07 (2005) 249.

[4] Staff Writers, Fuel Cells Bull. 2009-9 (2009) 3.

[5] G. Weaver and S. Barrett, Fuel Cells Bull. 2003-1 (2003) 11.

[6] Staff Writers, Fuel Cells Bull. 2007-10 (2007) 4.

[7] B. Suddhasatwa, Recent Trends in Fuel Cell Science and Technology, Springer, New York, 2007.

[8] V. P. McConnell, Fuel Cells Bull. 2009-6 (2009) 12.

[9] S. A. Sherif, N. Zeytinoglu, and T. N. Veziroglu, Int. J. Hydrogen Energy 22 (1997) 683.

[10] T. K. Tromp, R. Shia, M. Allen, J. M. Eiler, and Y. L. Yung, Science 300 (2003) 1740.

[11] H. Neef, Energy 34 (2009) 327.

[12] J. V. Volponi, B. A. Simmons, A. Walker, and D. Ingersoll, Meeting Abstracts, The Electrochemical Society, San Antonio, TX, United states (2004) 673.

[13] J. J. Hwang and P. Y. Chen, Int. J. Heat Mass Tran. 49 (2006) 2315.

[14] C. Lin, T. Chen, Y. Chyou, and L. Chiang, J. Power Sources 164 (2007) 238.

[15] S. Song, W. Zhou, W. Li, G. Sun, Q. Xin, S. Kontou, and P. Tsiakaras, Ionics 10 (2004) 458.

[16] J. J. Baschuk and X. Li, Int. J. Energy Res. 25 (2001) 695.

[17] T. Ioroi, K. Yasuda, Z. Siroma, N. Fujiwara, and Y. Miyazaki, J. Electrochem. Soc. 150 (2003) A1225.

[18] W. A. Adams, J. Blair, K. R. Bullock, and C. L. Gardner, J. Power Sources 145 (2005) 55.

[19] J. S. Lee, N. D. Quan, J. M. Hwang, S. D. Lee, H. Kim, H. Lee, and H. S. Kim, J. Ind. Eng. Chem. 12 (2006) 175.

[20] J. Larminie, Fuel Cell Systems Explained, John Wiley, United Kingdom, 2003.

[21] T. Schultz, S. Zhou, and K. Sundmacher, Chem. Eng. Technol. 24 (2001) 1223.

[22] M. Cifrain and K. V. Kordesch, J. Power Sources 127 (2004) 234.

[23] E. Gülzow and M. Schulze, J. Power Sources 127 (2004) 243.

[24] M. Ni, Energy Explor. Exploit. 23 (2005) 207.

[25] E. Gülzow, J. Power Sources 61 (1996) 99.

[26] N. Sammes, R. Bove, and K. Stahl, Curr. Opin. Solid State Mater. Sci. 8 (2004) 372.

[27] M. M. Mench, Fuel Cell Engines, John Wiley & Sons, USA, 2008.

[28] I. EG&G Technical Services, Fuel Cell Handbook, US Department of Energy, Morgantown, West Virginia, 2004.

[29] G. Hoogers, Fuel Cell Technology Handbook, CRC Press, New York, 2002.

[30] G. Lindbergh, M. Olivry, and M. Sparr, J. Electrochem. Soc. 148 (2001) 411.

[31] M. C. Williams, J. P. Strakey, and S. C. Singhal, J. Power Sources 131 (2004) 79.

[32] J. R. Selman, J. Power Sources 160 (2006) 852.

[33] W. Nernst, Material for Electric-Lamp Glowers, U.S. Patent 685730,1901.

[34] Z. Shao and S. M. Haile, Nature 431 (2004) 170.

[35] N. P. Brandon, S. Skinner, and B. C. H. Steele, Annu. Rev. Mater. Res. 33 (2003) 183.

[36] B. Fan and X. Liu, Solid State Ionics 180 (2009) 973.

[37] N. Q. Minh, J. Am. Ceram. Soc. 76 (1993) 563.

[38] S. P. Jiang and S. P. S. Badwal, J. Electrochem. Soc. 144 (1997) 3777.

[39] T. Setoguchi, K. Okamoto, K. Eguchi, and H. Arai, J. Electrochem. Soc. 139 (1992) 2875.

[40] B. De Boer, M. Gonzalez, H. J. M. Bouwmeester, and H. Verweij, Solid State Ionics 127 (2000) 269.

[41] A. Bieberle and L. J. Gauckler, Solid State Ionics 135 (2000) 337.

[42] M. Mori, T. Yamamoto, H. Itoh, H. Inaba, and H. Tagawa, J. Electrochem. Soc. 145 (1998) 1374.

[43] S. P. Jiang, J. Electrochem. Soc. 148 (2001) 887.

[44] J. B. Goodenough, Annu. Rev. Mater. Res. 33 (2003) 91.

[45] V. V. Kharton, F. M. B. Marques, and A. Atkinson, Solid State Ionics 174 (2004) 135.

[46] B. C. H. Steele, Solid State Ionics 129 (2000) 95.

[47] S. Hui, J. Roller, S. Yick, X. Zhang, C. Deces-Petit, Y. Xie, R. Maric, and D. Ghosh, J. Power Sources 172 (2007) 493.

[48] M. Miyayama, T. Nishi, and H. Yanagida, J. Mater. Sci. 22 (1987) 2624.

[49] P. Piccardo, R. Amendola, S. Fontana, S. Chevalier, G. Caboches, and P. Gannon, J. Appl. Electrochem. 39 (2009) 545.

[50] K. Kendall, Int. Mater. Rev. 50 (2005) 257.

[51] Y. Matsuzaki and I. Yasuda, J. Electrochem. Soc. 148 (2001) A126.

[52] S. C. Singhal and K. Kendall, High Temperature Solid Oxide Fuel Cells: Fundamentals, Design and Application, Elsevier, United Kingdom, 2003.

[53] S. Nagata, A. Momma, T. Kato, and Y. Kasuga, J. Power Sources 101 (2001) 60.

[54] Y. Ji, J. A. Kilner, and M. F. Carolan, Solid State Ionics 176 (2005) 937.

[55] S. H. Chan, K. A. Khor, and Z. T. Xia, J. Power Sources 93 (2001) 130.

Chapter 2

Review of Fuel Cell Electrode Modeling Work

2.1 Introduction

Solid oxide fuel cell composite electrodes are usually composed of a physical mixture of electron and ion conductor particles. Mixture of Ni (catalyst and electron conductor) and YSZ (ion conductor) initially were used in anode to create mechanical stability and reduce thermal expansion coefficient of pure nickel to match with YSZ [1,2]. Moreover, presence of YSZ avoids grain coarsening of Ni particles during sintering process [3]. Due to extreme operating conditions of solid oxide fuel cells, electrode materials need to meet various requirements to have acceptable performance inside the fuel cell. These requirements are both from practicality and performance point of view and have been pointed out by several researchers in the area [4-8]. Thermal, chemical and mechanical stability as well as low polarization resistance (R_p) are among the most important requirements of solid oxide fuel cell electrodes.

Although obtaining better mechanical properties was the main force behind the development of composite electrodes, soon it was discovered that addition of YSZ to the structure of the electrode has even more advantage in reducing the resistance to electrochemical reaction by extending the reaction into the bulk of the electrode and increasing the length of three phase boundary (L_{TPB}) [8-16]. For example Kenjo *et al.* observed that addition of 50 wt.% YSZ to LSM decreases R_p by about 5 times [10]. They ascribed this effect mainly to the extended TPBs inside the electrode by presence of YSZ. Ostergard *et al.* used spray coated LSM-YSZ air cathodes to investigate the effect of the structure on the performance of the electrodes [13]. It was found that addition of 20 wt.% YSZ to LSM decreases R_p from 2.7 $\Omega.cm^2$ to 0.65 $\Omega.cm^2$. Shizhong *et al.* reported even more radical observation and found out that by addition of 40 wt.% YSZ, oxygen ion transfer becomes the only rate determining. This implies that addition of YSZ creates enough sites for charge-transfer process and reaction resistance becomes very small compared to charge-transfer resistance [16] .

The effect of L_{TPB} on the performance of electrode has been widely studied and there is a strong agreement that increasing L_{TPB} will lead to better electrode performance [12,15,17-19]. Mizusaki *et al.* used $La_{0.6}Ca_{0.4}MnO_3$ electrodes painted on YSZ and found out that current generation or reaction rate was proportional to L_{TPB} [17]. In the case of Ni-YSZ and Pt-YSZ anodes, the reaction mechanisms were different but there was a close relationship between reaction rate and L_{TPB} [12]. Juhl *et al.* observed extra active site inside composite cathodes and presented a model to calculate active thickness of the electrode. They discovered that at high temperatures electrode performance is not sensitive to the thickness while the performance improves with thickness at low temperatures until mass transfer effects become important [10,15]. Fleig [20] and Smith *et al.* [19] reported a power low relationship between R_p and L_{TPB} for LSM cathodes painted on YSZ while Bierberle *et al.* observed that R_p decreases linearly with increasing L_{TPB} for their Ni-YSZ cermet anodes [18].

2.2 Basic Electrode Processes

Three kinds of species contribute to the electrochemical reaction inside fuel cell electrodes which are electrons, ions and gas phase molecules. Accordingly, electrode must provide means for these species to meet at some point and react. Following processes take place in a single cell of hydrogen based solid oxide fuel cell with composite electrodes:

a. Transport of oxygen through percolated pores to the reaction site inside cathode and transport of electrons from current collector to reaction sites through percolated chain of electron conductors (such as LSM)
b. Electrochemical reaction of oxygen and electrons at the reaction site to produce oxide ions
c. Transport of oxide ions from reaction site to electrolyte surface through percolated chain of ion conductors (such as YSZ)
d. Movement of oxide ions inside electrolyte towards anode-electrolyte surface
e. Transport of oxide ions from electrolyte surface to reaction sites inside anode through percolated chain of ion conductor (such as YSZ) and transport of hydrogen from electrode surface to reaction sites through percolated pores inside anode
f. Electrochemical reaction of hydrogen and oxide ions to produce electrons and water molecules
g. Transport of electrons to anode current collector through percolated chains of electron conductors (such as Ni) and transport of water to electrode surface through percolated pores

These processes are shown schematically in Fig. 2.1. From this point of view cathode and anode processes are very similar and same phenomena apply for both.

Naming the clusters in Fig. 2.1 is based on the nomenclature given by Costamagna *et al.* [21]. Clusters marked “A” are those electrolyte material

clusters that start from electrolyte surface and extend all the way to the surface of electrode. These clusters are able to carry ions to or from the electrolyte. Cluster "B" group are short chains that are only connected to electrolyte surface. These clusters are also able to carry ions. Cluster "C" group however; are the group of electrolyte materials that are not connected to electrolyte and hence are not able to carry ions. These particles do not contribute to electrochemical reaction and are considered isolated particles. Same concept applies to electrode particles too and "A", "B" and "C" clusters can be defined for electron conductor particles.

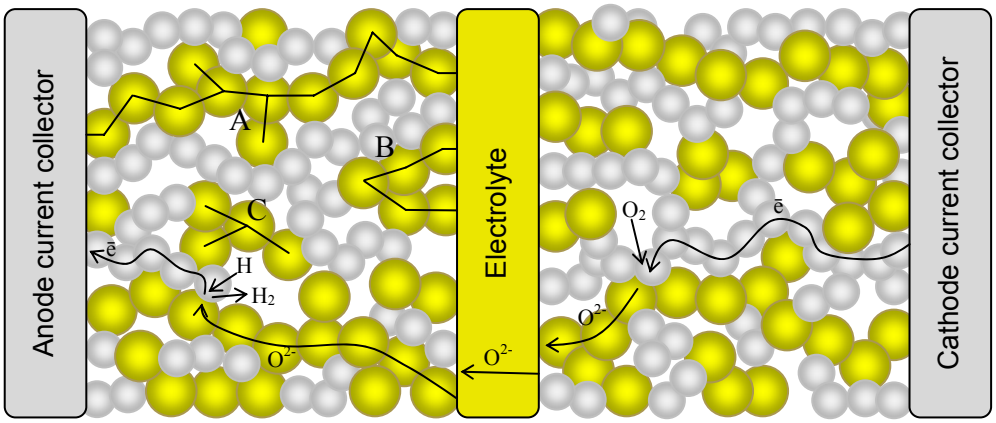

Figure 2.1 Schematic representation of solid oxide fuel cell with composite electrodes. A indicates percolating clusters, B indicates short connected clusters and C indicates isolated clusters

From the discussion above and the definition of TPB, it can be concluded that only contact between "A" or "B" cluster of one material (ion conductor for example) with "A" or "B" cluster of the other material (electron conductor) can create TPB (provided that pores exist to carry gas phase species).

2.3 Experimental Observations

It has been long time since Tedmon *et al.* investigated three different types of material for solid oxide fuel cells and concluded that "*Fully satisfactory air electrode for high temperature zirconia fuel cells is still lacking*" [4]. Although it might be general consensus that a "*fully satisfactory*" electrode has not been developed yet, there has been tremendous progress in the area of solid oxide fuel

cell and electrode design. Composite electrodes have been developed and the effect of addition of YSZ into the structure of solid oxide fuel cells has been discussed by many authors [8-11,13,14].

Numerous work have been devoted to the effect of electrode composition on the conductivity behaviour and overall polarization performance of composite electrodes [9,10,13,22-40]. All works indicate that conductivity, TPB, polarization as well as overall performance of solid oxide fuel cell depend strongly on the microstructure and morphology of the electrodes.

Dees *et al.* prepared samples of Ni-YSZ anodes and observed an abrupt increase of conductivity when vol.% of Ni in the cermet reached 30% [22]. The conductivity after this point remained constant. Other researchers observed more or less the same phenomena [31,32,37-40]. In the case of Clemmer *et al.* [31,40] sudden increase in conductivity fell between 20 and 40 vol.% of Ni with different samples. Beside other differences, samples with smaller particle size seemed to show sudden increase in less amounts of Ni. In the case of Yin *et al.* however, this sudden increase was less obvious [32]. For three samples of 3:7, 4:6 and 5:5 vol.% Ni-SDC ($Ce_{0.8}Sm_{0.2}O_{1.9}$) at 700°C, conductivity increases from about 160 $S.cm^{-1}$ for 3:7 sample to about 330 $S.cm^{-1}$ for 5:5 sample [32]. The conductivity of mixtures of Ni and metal aluminates ($Ni\text{-}MAl_2O_4$) were examined by Kwak *et al.* [35]. This research showed that the conductivity not only is affected by the amount and distribution of Ni [41] but also depends on the type of the metal used in aluminate structure and while sudden increase in conductivity occurs at 40 wt.% Ni for Ni-$NiAl_2O_4$, sample of Ni-$FeAl_2O_4$ anode does not show any conductivity below 60 wt.% Ni. Muecke *et al.* [37] studied the conductivity of nanocrystalline Nickel oxide-gadolinia doped ceria (*Ni-CGO* or *Nio-*$Ce_{0.8}Gd_{0.2}O_{1.9-x}$). They reported abrupt increase in conductivity at about 40 vol.% which is slightly more than the values reported by Yin *et al*. [32]. Their results showed that decreasing the temperature and grain size results in higher electrical conductivity of composite [37]. In addition to percolation theory which will be discussed later, the work of Lee *et al.* [28] also clarifies the conductivity behaviour of composite electrodes. By increasing Ni content of composite

electrode Ni-Ni contiguity increases which is accompanied by increase in conductivity of the electrode [28].

It can be seen from some of the works on the area that the structure of composite electrodes is highly random and disordered [10,13,23,42]. Although it is demonstrated that current production inside the electrode does not happen uniformly [43] and density of TPBs also is not uniform [44], a uniform structure in terms of distribution of ion and electron conductor clusters can be realized by analysing images of composite electrodes [39,40].

Unlike ohmic polarization which has the characteristics of sudden decrease with increasing the content of electron conductor, due to percolation effects of both phases polarization resistance acts differently and shows a minimum at intermediate compositions [10,13,23-25,27,28,30,34,36,45-47]. Polarization resistance is mostly referred as total electrode resistance less ohmic resistance which is considered to be a constant:

$$R_p = R_t - R_{ohm} \tag{2.1}$$

Although this is an accepted definition especially for experimental data, sometimes polarization resistance is referred as total resistance of the cell [29]. In this thesis when losses inside the electrode are considered, polarization usually refers to total resistance or total polarization of the electrode unless otherwise specified.

While only percolation of electron conductor (LSM for cathode) particles determine the conductivity of the electrode, several factors such LSM-LSM contiguity, LSM-YSZ contiguity [24,25] and mass transfer as well as physical and chemical properties of the components compete for polarization resistance [48].

Kenjo and Nishiya [10] obtained reciprocal polarization resistance for cathodes made of different weight ratios of YSZ to LSM. Despite their conclusion and although the observation showed a maximum for reciprocal polarization resistance at YSZ to LSM wt ratio of 1, due to lack of enough data points, one cannot conclude that the maximum falls exactly at weight ratio of 1. Other people

observed almost the same trend of a clear minimum at electron conductor volume or weight fraction around 40-50% [30]. Kim *et al.* [24,25] reported minimum polarization resistance of about 0.05 $\Omega.cm^2$ at 40 wt.% of YSZ. For their experiments size ratio of ion conductor and electron conductor particles (d_{io}/d_{el}) in the initial powder was 0.25.

Other experimental observation governs the effect of electrode thickness on the performance of electrode [9,10,14,26,49-53]. Experimental results show a sudden decrease in polarization resistance with increasing the thickness of the electrode and then polarization resistance remains constant. This sudden decrease and then leveling off of polarization resistance is more obvious in some works [14,51,52] and less obvious in the other cases [9,10,26,49,53] but is characteristic of composite electrodes. While most of the researchers use polarization resistance versus thickness data, Drescher *et al.* [50] plotted data of methane conversion at the anode, versus anode thickness and showed how methane conversion increases with increasing anode thickness and then remains constant.

Based on the abovementioned experimental observations, the following characteristic behavior can be summarized for solid oxide fuel cell composite electrode:

a. A random and highly disordered structure based on the images from electrodes [10,13,23,42,47,54-56].

b. Strong dependence of electrode conductivity to composition at low values of electron conductor volume fraction and sudden increase of conductivity with volume fraction until a critical volume fraction (ϕ_c) is reached. After this point conductivity remains almost constant and increases with a very slow pace [9,10,13,22-40,45].

c. Strong dependence of total polarization resistance on electrode composition. For the case of electron and ion conductors of the same size, polarization resistance assumes a wide range minimum at intermediate compositions and is high at very low or very high amounts of electron conductor. Another feature which seems to be common in most

experimental data is that portion of the polarization curve which contains ϕ_{el} values less than optimum ϕ_{el}, is much sharper than the other portion [10,13,23-25,27,28,30,34,36,46,47].

d. Polarization resistance decreases abruptly with increasing electrode thickness and then remains constant suggesting that there must be an optimum amount of electrode thickness beyond which the electrode performance does not improve and it might even deteriorate further as a result of hindering effect of diffusion and mass transfer resistance. At high values of ϕ_{el} there is a weak dependence between thickness and polarization resistance [9,10,14,26,49-53].

e. Dependence of polarization resistance on the particle size of electrode constituents. Coarse particles tend to show more polarization resistance than fine particles [25,57].

f. Effect of size ratio of ion and electron conductor particles on the conductivity and polarization behavior of composite electrode. While d_{io}/d_{el} equal to unity gives minimum polarization resistance close to intermediate ϕ_{el} values, minimum polarization resistance tends to shift to lower ϕ_{el} values for higher values of ratio d_{io}/d_{el} [23,34,57]

g. Dependence of impedance spectra of the cell to microstructure structure of the electrode [54].

An acceptable electrode model needs to verify all or at least most of the abovementioned experimental observations so that it can be relied upon. In some cases however the observations mentioned above are not easily noticeable. For example while the effect of particle size on electrode conductivity has been emphasized by some authors as discussed before, the conductivity data reported by Dees *et al*. [22] for particles of different size does not indicate a noticeable difference especially when Ni content is lower (higher YSZ content). The sporadic nature of experimental data in solid oxide fuel cell science and technology is further discussed on chapter 6.

2.4 Composite Electrode Models

Although there has not been a universally accepted agreement on classification of methods developed to simulate composite electrodes [21,29,54,58,59], those models may be best described based on their nature in four groups:

i) Thin film or pore models,

ii) Continuum porous electrode models,

iii) Discrete random packing models,

iv) Three dimensional reconstruction of composite electrode.

Except for the thin film model which has limited applicability, other models have gained attraction and popularity and are being used for composite electrode modeling. Although thin film model is also a continuum model, due to its fundamental differences with continuum porous electrode models, it is grouped and discussed in a separate category. 3D reconstruction of composite electrode mentioned above is not a model by itself and provides topological information about electrode structure and needs to be used with and appropriate numerical method to perform a complete simulation of transport phenomena and electrochemical reaction.

2.4.1 Thin Film Model

Thin film model was initially developed to analyze the electrode performance of liquid electrolyte fuel cells [60]. It was used to model molten carbonate [61] and alkaline [62,63] fuel cells. In this model as illustrated in Fig. 2.2 it is assumed that the porous electrode (electro-catalyst) pores are covered with a very thin continuous film of electrolyte. The electrolyte film is believed to be very thin so that gaseous reactants can pass through it without significant loss and therefore there is no concentration polarization loss considered in this model [63].

Later on Kenjo *et al*. adopted this model for solid oxide fuel cell cathodes [9,10]. Electro-catalyst is assumed to be a hollow circular channels starting from

current collector and extending all the way to electrolyte and covered with a continuous film of electrolyte [9,60].

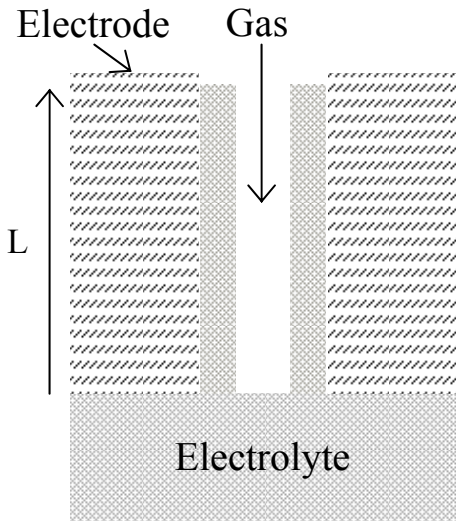

Figure 2.2 Illustration of thin film theory.

By writing Ohm's law to a differential width of electrolyte, one can get polarization resistance as a function of electrode depth [9]:

$$R_p = \sqrt{\rho k}\coth\sqrt{\frac{\rho L^2}{k}} \tag{2.1}$$

Where ρ is the resistivity of the electrolyte, k is a constant to be determined by experiment and L is the electrode thickness. Although the relationship between current and overpotential in charge-transfer process is usually expressed by nonlinear Butler-Volmer equation, this approach assumes a linear relationship and k in Eq. 2.1 is partly dependent on the kinetics of electrochemical as well as the geometry of the porous electrode. In case of very thin electrodes, that is $\rho L^2 << k$, it is clear from equation above that R_p depends only on k and L and maybe approximated as:

$$R_p = \frac{k}{L} \tag{2.2}$$

And on the other extreme, where the electrode is very thick or $\rho L^2 >> k$:

$$R_p = \sqrt{\rho k} \tag{2.3}$$

And therefore for thin electrodes, polarization is proportional to reciprocal of electrode thickness while for thick electrode it tends to be a constant value. Fig. 2.3 shows a plot of R_p as a function of electrode thickness. One noticeable problem with this model is that when $L \rightarrow 0$, R_p tends to go to infinity. One way to overcome this problem is to add a thin layer of electrolyte to pore bottoms. This thin layer adds a thickness independent term to R_p expression as discussed by Tanner *et al*. [64].

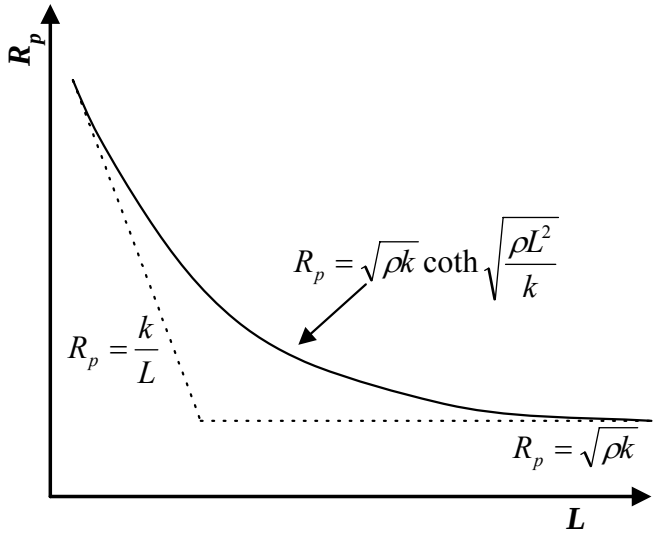

Figure 2.3 Thickness dependence of polarization in thin film theory.

The thickness dependent behavior of R_p as expressed by Eq. 2.1 and shown in Fig. 2.3 justifies experimental observation (*d*) to some extent. Regarding the effect of ϕ on polarization resistance in observation (*d*) or in general effect of ϕ, particle size and particle size ratio in observations (*b, c, e, f, g*), thin film model cannot make any comment. Observation (*a*) and issues with percolation and coordination of the particles are also clearly ignored by modeling disordered and random media of the electrode with ordered channels. Calculating empirical parameter *k* is difficult as it covers geometrical and kinetics effects and hence very sensitive to operating condition. Despite shortcomings mentioned above, thin

film model can give useful qualitative information about polarization resistance and current distribution inside the electrode [9].

In another attempt to apply thin film model to SOFC electrodes, Tanner *et al*. [64] considered electrolyte covered with electro catalyst layer and performed more detailed one dimensional and two dimensional analyses. Their model has the same limitation of being developed for linear electrochemical reaction kinetics. Due to the fact that they isolated kinetic and geometrical parameters, their model is capable of qualitative prediction of the effect of reaction kinetics on thickness-polarization relationship. The other advantage of their approach as stated before is finite value for R_p while $L \rightarrow 0$. Their view poses the same limitations with regards to experimental observations.

There are other variants of the model such as meniscus, agglomerate and filmed agglomerate and flooded pore model [61,65-70] which have been developed and used extensively in liquid electrolyte electrodes and are of little or no importance in SOFC electrode simulations.

2.4.2 Continuum Porous Electrode Models

Continuum porous electrode methods are based on percolation theory [71] and particle coordination number [72]. Like random packing models, this approach assumes that composite SOFC electrodes are formed by random mixture of electron and ion conductors but unlike those models electrode media is treated as a continuous homogeneous media for electron and ion transfer as well as electrochemical reaction [21,73,74]. Effective properties of the media such as electron and ion conductivities as well as density of triple phase boundaries are then calculated by means of percolation theory.

2.4.2.1 Description of the Model

The model is based on applying Ohm's law for transport of electrons and ions as well as equation for current generation on TPBs [21,73,74] :

$$\nabla V_{el} = -\rho_{el}^{eff}\vec{i}_{el}$$
$$\nabla V_{io} = -\rho_{io}^{eff}\vec{i}_{io} \quad (2.4)$$
$$\nabla.\vec{i}_{io} = -\nabla.\vec{i}_{el} = A_{TPB}i$$

Where ρ^{eff} values are effective resistivity of electron and ion conductors, A_{TPB} is density of electrochemically active area and i is the rate of current transfer between electron and ion conductor phases at TPB which is basically rate of electrochemical reaction. Although linear Butler-Volmer equation was used by early contributors to the model [21,73,74] , it was a matter of simplicity and there is no intrinsic limitation on the model to apply complete nonlinear equation. A complete nonlinear Butler-Volmer was used later on by Chan *et al.* [75-77] and Xia *et al*. [51] as well as other researchers. Some even put one step forward and considered current generation as a general function of overpotential and used their own detailed multistep mechanisms [29,78].

As far as mass transfer concerns, although the work done by Sunde [21,73,74] and Costamagna *et al.* [21,73,74] neglects effects of mass transfer and diffusion resistance, other contributors have implemented polarizations caused by mass transfer and diffusion effects in their models using different diffusion models such as Fick's law [51,75-77,77-81], Stefan Maxwell model or more complete dusty gas model [29,82-88]. Fick's law is simple, easy to implement and gives analytical results for concentration polarization in SOFC electrodes and therefore it is computationally inexpensive. Dusty gas model on the other hand, needs numerical solution and therefore computationally is more demanding but at the same time gives more accurate results especially if the media contains small size pores [89]. Pacheco *et al.* compared Fick's law, Stefan-Maxwell model and dusty gas model and concluded that dusty gas model is more accurate [90]. The formulation of dusty gas model is based on Stefan-Maxwell approach with addition of a term to account for Knudsen diffusion effects [91,92]. Hussain *et al.* showed that dusty gas model can be written in general form of Stefan-Maxwell equation if an effective diffusivity is defined to include the effects of Knudsen diffusion as well as molecular diffusion [82].

Although there is no limitation in Eq. 2.4 to be used in three dimensions, most of the work on electrode simulation based on continuum porous electrode models are carried out in one dimension which is the direction perpendicular to the electrolyte or current collector [21,73,74]. In fact if electrolyte and current collector are flat and parallel plates, extension of Eq. 2.4 into three dimensions has no advantage because the inside morphology of the electrode is assumed to be uniform with no variations in transverse directions. The case that may make two or three dimensional analysis necessary is the existence of concentration gradient at electrode surface or utilization of a current collector which covers parts and not all of electrode. This might happen in large scale fuel cell simulations.

2.4.2.2 Effective Properties and Percolation Theory

Percolation theory [71] along with coordination number model [72] is used to calculate properties of porous media such as L_{TPB} and A_{TPB} as well as effective conductivities [21]. Percolation theory calculates the probability that a connected chain of electron or ion conductor forms continuous clusters that starts at one end of electrode (electrolyte surface) and extends all the way to the other end (current collector) which with reference to Fig. 2.1 are "A" type clusters. In a binary mixture of spherical *i* and *m* type particles, Z_i the coordination number of particle *i* is defined as number of contact points that this particle has with other particles both *i* and *m* type:

$$Z_i = Z_{ii} + Z_{im} \tag{2.5}$$

Z, the overall average number of contacts of particles is then the number average of coordination numbers of *i* and *m* particles [72]. *Z* is believed to be 6 for a binary random packing of spherical particles. It is discussed that the average number of contacts in excess of minimum required to obtain stability is proportional to the surface area of the particles [72,93]. Assuming *r* is the ratio of the size of *m* and *i* particles, Bouvard and Lange [72] stated that:

$$\frac{Z_m - 3}{Z_i - 3} = r^2 \tag{2.6}$$

Where 3 indicates the minimum number of contact points to assure mechanical stability of the particle. Using Eq. 2.6 and assumptions stated above, Bouvard and Lange calculated Z_i and Z_m [72] :

$$\begin{aligned} Z_i &= 3 + \frac{Z - 3}{n_i + (1 - n_i)r^2} \\ Z_m &= 3 + \frac{(Z - 3)r^2}{n_i + (1 - n_i)r^2} \end{aligned} \tag{2.7}$$

Where n_i is number fraction of i particles. Since in SOFC composite electrode study contacts between electrode (i) and electrolyte (m) particles or Z_{im} is as important as Z, Z_i and Z_m, costamagna *et al.* [21] considered the following relation given by Bouvard and Lange to calculate Z_{im}:

$$Z_{im} = n_m \frac{Z_i Z_m}{Z} \tag{2.8}$$

Contact area between electron and ion conductor particles is proportional to the surface area of smaller particle. Costamagna *et al.* [21] then calculated A_{TPB} based on the work of Suzuki *et al.* [93]:

$$A_{TPB} = K r_i^2 n n_i Z_{im} p_i p_m \tag{2.9}$$

Consequently L_{TPB} can be calculated as:

$$L_{TPB} = K' r_i n n_i Z_{im} p_i p_m \tag{2.10}$$

K and K' are proportionality constants and are considered to be tuning parameters. Costamagna *et al.* considered contact angle between two particles to be 15^o and calculated K [21]. Sunde argued that in contact between electron and ion conductor resulting from sintering, length of three phase boundary line is almost three times the particle radius [94]. Based on that, Ali *et al.* used 10% enlargement of particles after packing is created, to obtain enough contact area [44]. This issue will be further discussed on chapters 4 and 5.

p_i and p_m in Eqs. 2.9 and 2.10 are the probability that electron and ion conductor particles form percolating clusters ("A" clusters in Fig. 2.1). Based on the work of Kuo *et al.* [95] (Z_{ii}=1.764 at percolation threshold), Chan *et al.* [75] modified the model proposed by Bouvard and Lange [72] to calculate p_i and p_m:

$$p_j = \left(1 - \left(\frac{4.236 - Z_{jj}}{2.472}\right)^{2.5}\right)^{0.4}, \quad j = i,\ m \tag{2.11}$$

This equation is valid in the range $1.764 < Z_{jj} < 4.236$ which corresponds to the percolation probabilities of 0 and 1. Volume fraction corresponding to percolation threshold is equal to 0.294 for particles of the same size [95,96]. Effective conductivity of the media can also be calculated using percolation theory. Based on percolation theory and Costamagna *et al.* [21,71]:

$$\sigma_j^{eff} = \frac{1}{\rho_j^{eff}} = K''\sigma_0\left(n_j - n_c\right)^2, \quad j = i, m \tag{2.12}$$

Where σ_0 is the bulk conductivity of pure material and like K and K', K'' depends on the contact angle between two particles of the same type. n_c is the number fraction of i or m type particle at percolation threshold.

2.4.2.3 Evaluation of the Model

Percolation theory provides necessary information for continuum porous electrode model to develop an understanding of SOFC composite electrodes. Most of the experimental observations of composite electrode behaviour is predicted through continuum porous electrode model and can be justified in the light of percolation theory and coordination number model. Although random and disordered structure of composite electrode (observations *a* and *g*) is not recognized in the model itself, effective parameters calculated by percolation theory take into account the random nature of the media. The reader should keep in mind however; that even effective properties obtained from percolation theory are average properties and do not reflect random nature of composite electrode as they vary from point to point inside the electrode.

Observations (*b*) through (*f*) can all be discussed and justified on the basis of percolation theory which is core to continuum porous electrode model. Sudden increase in conductivity at certain composition reported in observation (*b*) is consistent with results of Kuo *et al.* [95] and Bouvard and Lange [72] that at a binary mixture of spherical particles of the same size sudden increase in the number of percolating clusters is observed after a critical volume fraction of 0.294 is reached. Modeling results of Costamagna *et al.* [21] and Chen *et al.* [29] are consistent with experimental work done in observations (*b*) and (*f*) as long as it is used inside percolation threshold and beyond this region the model cannot be used and hence is incapable of making any comment. Other reported simulations based on this model have also proved to give consistent results with most of the experimental observations [26,29,51,75,78,81,84,97]. As far as observation (*d*), the effect of thickness is considered, model shows a competition effect of electrochemical reaction kinetics and mass transfer resistance. For the realizations of the model that do not take into consideration the effect of mass transfer limitations or mass transfer is believed to have minor effects [29], polarization resistance decreases abruptly with thickness initially and then remains almost constant no matter what the thickness is beyond that point [21,29]. On the other hand, when mass transfer is important, an optimum thickness is realized [81]. Chan *et al.* showed that while for low current densities after minimum overpotential is reached there is no increase in electrode overpotential with increasing electrode thickness, at high current densities overpotential tends to increase for thick electrodes [78]. Apparently this is due to the mass transfer resistance caused by increased consumption of oxygen at high current densities which limits the reach of oxygen to triple phase boundaries deep inside the cathode [78]. Same approach is true for the effect of particle size on polarization resistance, experimental observation (*e*). While for particle sizes over about 0.1 μm, polarization resistance increases with increasing particles size, for particle size below 0.1 μm increase in particle size results in lower polarizations [51,75,78,81,98]. Since the size of pores for gas diffusion inside composite electrodes is almost the same size as particles [99], pores create very high mass

transfer resistance when the particles are very small (<0.1 μm) and concentration polarization is dominant. For large particle sizes however, activation polarization is dominant and hence increasing particle size increases total polarization resistance.

Continuum porous electrode model is only valid inside percolation region of electron and ion conductor particles. Outside this region the model cannot make any comment about the behaviour of porous electrode. Furthermore since the model takes into consideration only electrode spanning clusters ("A" type clusters), the results of A_{TPB} and L_{TPB} may be underestimated. For intermediate values of electrode composition inside percolation threshold this error maybe ignored [21] but care must be practiced while working around percolation threshold as the amount of short chains forming triple phase spots is still high around percolation threshold [44].

2.4.3 Discrete Random Packing Models

It is assumed in discrete random packing models that composite electrodes of solid oxide fuel cells can be modeled as random packing of electron and ion conductor particles which in most cases are treated as spheres, electrically connected to each other through necks [44,73,94,100,101]. Electron and ion conductor particles (spheres) are packed either in ordered simple cubic lattice [94,102-105] or in random structure [44,73,106-108]. Some researchers have used particles of the same size in their analysis [94,102,103,104] while others had the freedom of having two different sizes for ion and electron conducting particles [44,73,106]. Kenney *et al.* [108] recently reported their electrode simulation based on polydisperse particles. Unlike mono-sized case in which all particles of the same type are of the same size, their simulation includes size distribution for each phase and the result show that introducing polydisperse particles results in slightly lower A_{TPB} values compared to the case of mono-sized particles with the size equal to mean size of polydisperse particles [108]. This effect however; is much less than the effect of particle size itself and given the fact that creating a model composite electrode based on polydisperse particles is computationally much

more demanding than the mono-sized case, one may opt to the case of mono-sized particles rather than creating a packing with polydisperse particles.

Although the method is best suited for three dimensional analysis of the electrode and most research is carried out in three dimensional modeling, there are reports of the use of the method in two dimensions where circles are used instead of spheres [43,105]. As it will be shown in chapter 3, percolation simulations of two components (LSM and YSZ particles) in two dimensions produces reasonable results that are capable of giving a qualitative description of the behaviour of composite electrodes [43,109]. However; when it comes to percolation of three components (LSM, YSZ and pores) 2D model does not seem to give even close to real predictions since percolation threshold of each component in 2D square lattice is around 60 vol.% [110]. That is why 2D results reported by Martinez *et al.* for active TPB of composite electrodes is in contrast with most of experimental and simulation results [105].

2.4.3.1 Description of the Model

Once the packing of particles is created in the computer, the structure of the packing is analysed and it is determined whether particles are connected to their corresponding base or not [44]. To have three phase boundary; ion and electron conductor particles in contact must also be connected to electrode or current collector and besides pores must exist. Only percolation of electron and ion conductor particles is considered in most of the models based on percolation of particles and pore percolation is presumed at all sites. This is true even for continuum models discussed before [21,76]. No matter whether diffusion limitations and mass transfer was considered [76] or mass transfer issue was completely ignored [21], to calculate the length of triple phase boundary only percolation of electron and ion conductor was considered. In contrast to the work of others [44,94], Abel *et al.* treated pores the same way they treated electron and ion conductors and assumed that two connected electron and ion conductor particles form a three phase boundary only if there is at least one percolating pore

hole in their neighbourhood. This of course led to lower triple phase prediction and different percolation thresholds for solid part [102]. This additional constraint on triple phase boundary seems unnecessary as significant amount of pores already exist among solid particles and Kenney *et al.* [108] showed that for porosities above 25% more than 99% of pores belonged to percolating cluster of pores. Furthermore it is widely discussed that mass transfer resistance can be ignored for porosities above about 25% [54,111] . Kenney *et al.* [108] also showed that further increasing porosity above 30% will decrease the triple phase boundary. Based on this discussion, the approach of Abel *et al.* [102] in considering three percolating phases and introducing percolating pores (other than the pores already exist) tends to underestimate three phase boundary. Since the porosity of electrode may drop significantly after numerical sintering, the introduction of pore former particles during packing process is necessary. These particles must be removed afterwards to keep the porosity at the desired level sufficient to assure insignificant mass transfer limitations. This approach is exercised in chapters 4 and 5 [44,94] .

Numerical sintering process applied in discrete resistor network model is almost the same process that was discussed before for continuum models. Sintering is responsible for creating enough contact between particles, either the same type or different types and is discussed in more detail in the literature. It is a complicated process discussed in much detail in the literature [112-115]. Implementing detailed sintering mechanism for each single contact area between particles inside an electrode is computationally costly and there is not much benefit in doing so. In most cases as discussed before, the overlap or contact angle between two particles in contact shown in Fig. 2.4 is treated as an adjusting parameter rather than considering detailed sintering mechanism [21,76]. The argument of taking l_{TPB} three times the size of the particle first introduced by Sunde [94] leads to a contact angle of about 29^{o} which is almost twice the value used by Costamagna *et al.* [21]. Schneider *et al.* [106] however; based their overlap criteria on the porosity and calculated the overlap to achieve 25% porosity which based on their system for particles of the same size corresponds to contact

angle of about 30° if neck growth process is not considered, otherwise it will be a large value of 45°. Since 25% is the minimum amount of porosity reported in literature to obtain negligible amount of mass transfer resistance and since neck growth will further lower the porosity, it seems that larger porosities around 30% must be taken to avoid overestimation of triple phase boundary. It seems that the approximation by Sunde besides its simplicity appears to give more reasonable results [94].

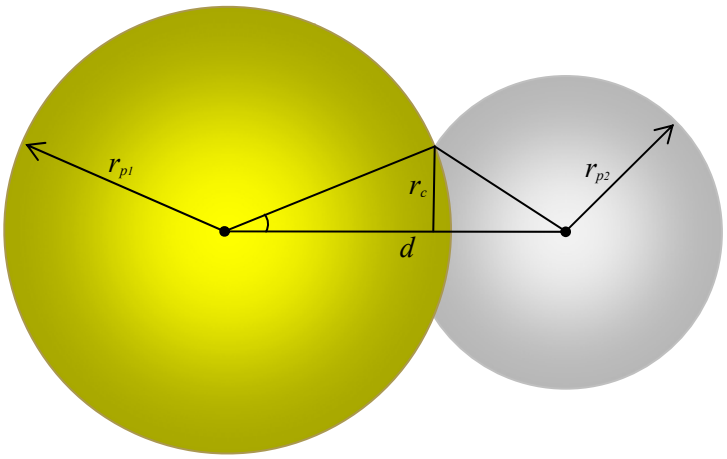

Figure 2.4 Overlap between two particles in contact.

Resistor-network model is then constructed with a similar approach shown in Fig. 2.5. Based on the argument by Feng *et al.* [116], Sunde [73,101] assumed that a neck of diameter equal to $2r_c$ will have electrical conductivity equal to a cylinder of the same diameter and length equal to $2r_c$. Based on this, electrical resistance between similar particles can be calculated as:

$$R_{ij} = \frac{\rho_i L}{A} = \frac{\rho_i (2r_c)}{\pi r_c^2} = \frac{2\rho_i}{\pi r_c} = \frac{4\rho_i}{L_{ij}} \tag{2.12}$$

L_{ij} is the contact perimeter of two similar particles. For a triple phase boundary as shown in Fig. 2.5, total resistance will be equal to [101]:

$$R_{el-io} = \frac{R_{el}}{2} + \frac{R_{io}}{2} + R_{ct} \tag{2.13}$$

Where R_{ct} is charge-transfer resistance at triple phase boundary. For particles of different size and random packing of particles in which each contact may have different contact area and contact angle, all bound resistances must be computed separately as shown in Fig. 2.5 [44]:

$$R_{io-io} = R_{io,i} + R_{io,j} \tag{2.14}$$

$$R_{el-el} = R_{el,i} + R_{el,j} \tag{2.15}$$

$$R_{el-io} = R_{el,i} + R_{el,j} + R_{ct,ij} \tag{2.16}$$

Eq. 2.16 holds when contact between electron and ion conductor particle is triple phase boundary. Otherwise at least one of the particles is isolated particle and as shown in Fig. 2.5 there is no resistance associated with that specific contact point.

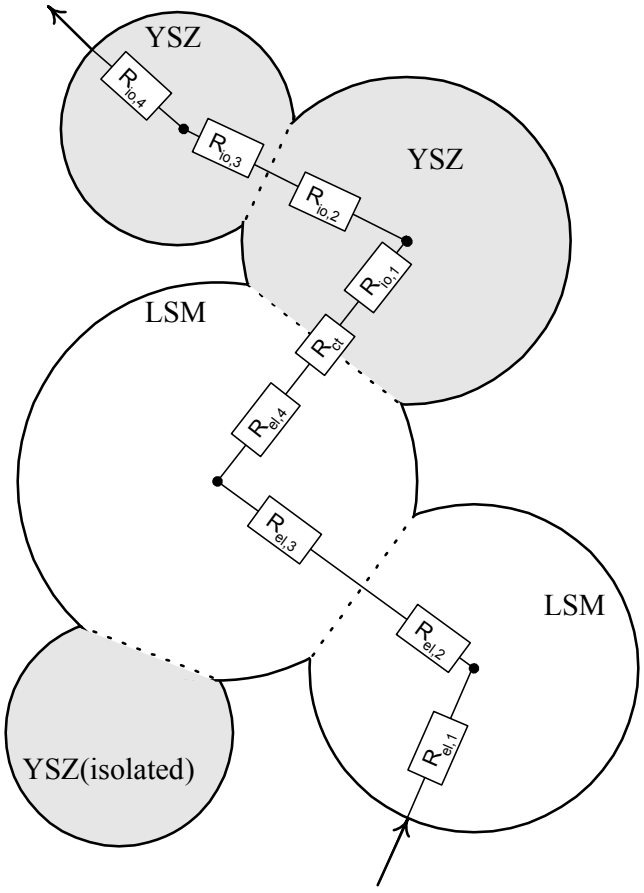

Figure 2.5 Illustration of resistor-network model for overlapping particles.

Also it should be kept in mind that Eq. 2.16 is written for a linear charge-transfer resistance, $R_{ct,ij}$. To our best knowledge, there is no record of using complete nonlinear form of Butler-Volmer equation for charge-transfer process in the literature and all the work is based on simplified linear form [94,106]. Only in the current work demonstrated in chapter 5 of the thesis nonlinear form has been introduced which is believed to give more reliable results due to nonlinear nature of charge-transfer process. In this case, Eq. 2.16 does not hold in the current format and nonlinear form of charge-transfer equation containing ionic and electronic potentials at either sides of contact region must be utilized along with separate declaration of Ohm's law for $R_{el,i}$ and $R_{io,j}$ for bound resistances on electron and ion conductor particles, respectively.

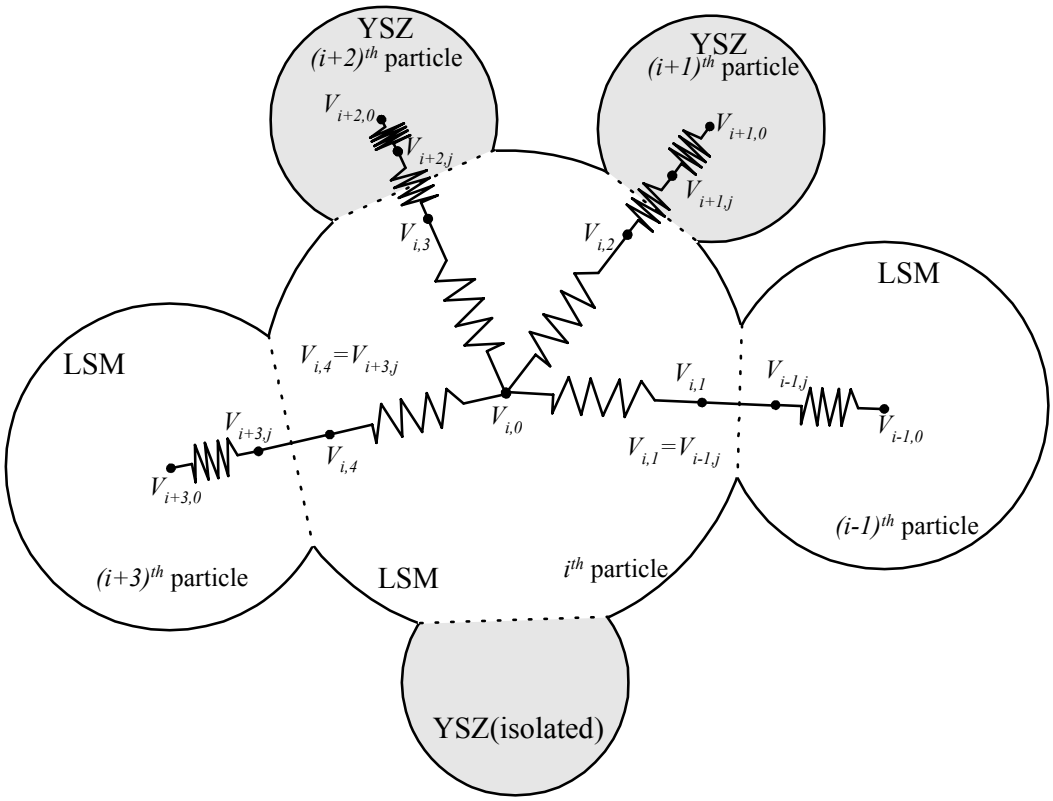

Figure 2.6 Building resistor network model for particles of different size. There is no resistance associated with isolated particles.

And finally Ohm's law for voltage and Kirchhoff's law for conservation of electric charge, help to bring network into equation form:

$$V_{i0} - V_{ij} = I_{ij} R_{ij} \quad , \quad j = 1...\text{n} \tag{2.17}$$

$$\sum_{j=1}^{n} I_{ij} = 0 \tag{2.18}$$

Where n represents the coordination number of i^{th} particle, V_{i0} is the potential at the center of i^{th} particle. Fig. 2.6 shows the notation used. All these equations are assembled together to build the system of linear or nonlinear equations and the system is solved using the appropriate method.

2.4.3.2 Evaluation of the Model

Due to its advantages and capabilities in giving a very good and consistent explanation of experimental data, this model has been chosen for further development in this thesis. Its characteristics and advantages will be further demonstrated in coming chapters especially in chapters 4, 5 and 6 of the thesis.

Among three models discussed so far, this model maybe the best to describe the highly random structure observed in the real composite electrode seen in experimental observation (a). Sunde [54,94] made a comparison of conductivity data from the model with experimental data of Dees *et al*. [22] and showed how the model satisfies experimental observation (b). In fact as it will be seen in conclusion chapter of the thesis, the model predicts experimental data of conductivity for whole range of electrode composition with very good precision. In fact it is the best model to describe conductivity and polarization data (observations b through f) as it will be shown in other chapters of this thesis. Although continuum models based and percolation theory provided a good explanation of experimental conductivity and polarization data, they do not go beyond percolation theory and therefore their explanation is incomplete. As far as observation g goes, Sunde showed that the model is capable of reflecting structural variations in impedance data and can be used for impedance spectroscopy studies as well [54].

Further merits of this model will be discussed and developed in this thesis. Since this model is based on very fundamental understanding of composite

electrode structure and no assumptions is made on the arrangement and order of particles, it gives a better picture of composite electrode structure and characteristics.

2.4.4 Three Dimensional Reconstruction of Electrode

Complex, random and highly disordered structure of SOFC composite electrodes makes it very difficult and unreliable to find properties such as L_{TPB} through indirect and electrochemical methods. Imaging techniques on the other hand give a direct picture of electrode structure and can help to directly calculate the media properties. Simwonis *et al.* [117] analyzed digital images from polished surfaces of Ni/YSZ anode to investigate Ni coarsening during fuel cell operation. By investigating online images from the cross-section of working anode they showed that after 4000 hours of operation, Ni particle size was increased by more than 25% resulting in almost 37% decrease in distinguishable Ni particle number. The problem with imaging techniques such as digital photography, SEM as BSE is that Ni and YSZ phases are not readily distinguishable and preprocessing and image analysis techniques are required to obtain clear pictures of Ni and YSZ phases along with pores [117-119]. Lee *et al.* [118,120] used SEM and BSE 2D images to investigate microstructure of anode. By using image processing software they were able to distinguish Ni, YSZ and pore phase and create elemental map of the electrode and calculate contiguity of different phases. In their analysis however, they used quantitative stereological theory [117] to transform 2D data into 3D information such as porosity, contiguity and surface area [118]. Energy Dispersive X-ray Spectroscopy (EDS) also can be employed for elemental mapping of electrodes [121].

Although 2D images can give lot of information about the microstructure of electrodes, these information are often qualitative and mathematical models needed to transform the data into 3D structures. 3D structure reconstruction on the other hand can give more reliable information about the topology of structures. Kral and Spanos [122] and Bansal *et al.* [123] reviewed the history and application of imaging 3D imaging techniques in materials science. In their study,

the application of Focused Ion Beam (FIB) sputtering ability in conjunction with SEM imaging technique is considered to etch away and obtain sequential 2D images of a multilayer Si–Si/Ge and Al_2Cu samples and interpolating 2D images to reconstruct 3D structures with 10 *nm* resolutions [123]. A discussion on the spatial resolution of SEM and BSE imaging is given by Merli *et al.* [124].

Wilson *et al.* [55] are maybe the first to resolve the 3D structure and triple phase boundary of SOFC electrode. They used FIB to remove thin 50 *nm* sections of Ni-YSZ anode followed by SEM imaging. By stacking 2D images, a 3D structure of the electrode with all three phase (Ni, YSZ and pores) was obtained and analysed. For an anode with starting powder of NiO:YSZ = 47.61:52.39 volume percent, they calculated final volume of pores, Ni and YSZ and concluded that almost all the porosity of 19.5% comes from initial NiO and final volume percent of Ni is only 25.9% leaving volume of YSZ almost untouched at 54.6 vol.%. They obtained total triple phase boundary length of about $4.28\mu m.\mu m^{-3}$. About 63% of this total length is connected and contribute to electrochemical reactions [55]. This figure is lower compared to the values obtained by Shearing *et al.* [125] who did a modified FIB-SEM 3D reconstruction on Ni-YSZ anode and reported value of about $10\mu m.\mu m^{-3}$ for the length of which 53.9% percolated. This discrepancy in the data maybe justified with having different fabrication techniques, different starting powder composition and the fact that particle size distribution of initial powders might be different. Moreover, porosity of about 10% in the case of Shearing *et al.* is very low suggesting that porosities has been sacrificed to gain more triple phase boundary [108] and most of triple phase locations will have poor access to percolating pores [125]. The main disagreement between two investigations, however; lies in the relative amount of each phase after and before sintering. While Wilson *et al*. [55] observed 41% volume reduction of initial NiO in converting to Ni in the final structure which emerges in the form of pores, the results of Shearing *et al.* indicate about 20% volume increase in transition from NiO to Ni [125]. Furthermore YSZ volume percentage reported by Shearing *et al*. has dropped to 50% of initial value which is in contrast to the conclusion made by Wilson *et al.* that YSZ volume remains constant.

Wilson repeated their experiments for other compositions of same starting powder and obtained the same trend of constant YSZ volume and decrease in Ni phase volume [126] . Furthermore, the results of Wilson *et al.* is more consistent with results obtained by discrete models based on random packing of particles [44,108]. By calculating polarization resistance and counting L_{TPB} from FIB-SEM based reconstruction method, they showed that polarization resistance is minimized for NiO:YSZ=50:50 wt.% of starting powder in which L_{TPB} is minimum [126]. They also showed that for the same composition of starting powder, 100% of YSZ is contiguous while 86% of Ni phase and 96% of pore phase belonged to percolating clusters [55]. Smith *et al.* [19] conducted a detailed study on the effect of processing conditions on microstructure and performance of SOFC simple LSM cathodes using EIS and FIB-SEM. By measuring L_{TPB} and comparing with EIS data and proposing equivalent electrical networks, they concluded that both charge-transfer resistance and adsorption polarization resistances follow power law relationships with L_{TPB} [19]. Same group considered the effect of sintering temperature on the microstructure of LSCF cathode and showed that while porosity and pore diameter increases with increasing sintering temperature, L_{TPB} reaches maximum at intermediate temperature [127] .

Porosity results of Wilson *et al.* [55] mentioned about is in close agreement with the results of Izzo *et al.* [128] using X-ray Computed Tomography (XCT) which shows that for an Ni-YSZ anode more than 98% of pores are connected. Higher percentage of connected volume in the case of Izzo *et al*. can be ascribed to higher porosity of 30% compared to almost 20% of Wilson *et al*. [55]. Despite FIB-SEM, XCT is a non-destructive method to obtain 3D images of fuel cell electrodes using X-ray microscope [128-131]. 2D images are obtained by rotating sample in front of X-ray beam and then analysed in the computer to obtain precise 3D morphology. XCT is a fast and non-destructive technique but due to its nature, the method can only be used to distinguish solid and pore phases. On the other hand the result of XCT analysis will be one solid phase (Ni+YSZ) and a pore phase. Therefore this method at the current state of development cannot be used to track TPBs and Ni or YSZ contiguities. Izzo *et al.* [128] and Chiu *et al.* [131] as

well as [132] combined the structure obtained by this method and Lattice Boltzmann Model (LBM)[133] to simulate mass transfer inside the pores. In their simulations however, they limited TPB to electrode/electrolyte interface due to inability of the method to recognize Ni and YSZ phases. This assumption in fact is equivalent to reducing composite structure of the electrode to a simple case of Ni pasted on dense YSZ.

Although imaging methods and especially the work done by Wilson *et al.* [55] and Shearing *et al.* [125] have opened a new and exciting horizon to better understanding of solid oxide fuel cell electrodes; this technique is still in its infancy period. This technique is capable of modeling detail operation of electrode and produce experimental observations from (*a*) to (*g*) only if it is coupled with an advanced numerical simulation methods. It is clear that the random structure of the electrode is fully appreciated by this method (observation *a*). From the work of Gostovic *et al*. [127] and Smith *et al.* [19] mentioned above, one may conclude that a relationship between polarization resistance and L_{TPB} has already been established by this method, it must be noted however, this is not an independent achievement of the method and polarization resistance was obtain by experiment.

Finally, it must be noted that imaging technique is only responsible to build the structure and provide information about different phases and hence we do not call it a model. Performing real simulation on this structure is a separate issue which due to very random and complex nature of the structure has not been conducted yet. If completed with pore level transport and reaction scheme, 3D imaging can give the most accurate data of electrode operation, which still remains a challenge. Whether this level of complexity is required for fuel cell development or not, is another issue.

2.5 Concluding Remarks

From SOFC composite electrode modeling methods described above, it is clear that thin film theory is a very simple model that cannot explain most of the real

behaviour of composite electrodes. Continuum methods on the other hand are powerful tools to predict polarization and conductivity behaviour of composite electrodes. They are relatively simple and easier to implement compared to discrete random packing models. These models are well suited for use by commercial CFD (computational fluid dynamics) programs and are low cost computationally. However; the electrode in these models is treated as a homogeneous media which in fact is not correct. Furthermore, since effective properties are calculated based on percolation of only ion and electron conductor particles, calculation of L_{TPB} is independent of porosity which is not necessarily correct [108]. In fact porosity is introduced as an independent input to calculate quantities such as effective diffusivity [76] while the correlation between porosity and L_{TPB} is ignored.

Discrete models based on random packing of particles have the advantage of taking the randomness and complexity of electrode into account. This method describes all the experimental observations and shows good agreement with laboratory data. The problem with this method is the difficulty of implementing mass transfer resistances and diffusion effects. Although it was discussed before that for the typical porosities of the electrode diffusion effects can be ignored, the problem of coupling mass transfer equations with charge-transfer and electrochemical reaction still remains a challenge. Lattice Boltzmann model [133] seems to be a promising approach as opposed to conventional convection-diffusion models.

And finally creating random 3D structure through imaging techniques such as FIB-SEM is a new start and challenge to better understand composite electrodes. Although the method is now mostly used to determine geometrical parameters, it is a promising technique that will disclose mysteries around composite electrode structure.

References

[1] F. Tietz, Ionics 5 (1999) 129.

[2] M. Mori, T. Yamamoto, H. Itoh, H. Inaba, and H. Tagawa, J. Electrochem. Soc. 145 (1998) 1374.

[3] S. P. Jiang, J. Electrochem. Soc. 148 (2001) 887.

[4] C. Tedmon Jr, H. S. Spacil, and S. P. Mitoff, J. Electrochem. Soc. 116 (1969) 1170.

[5] B. C. H. Steele, J. Power Sources 49 (1994) 1.

[6] N. Q. Minh, J. Am. Ceram. Soc. 76 (1993) 563.

[7] P. J. San and H. C. Siew, J. Mater. Sci. 39 (2004) 4405.

[8] M. Mogensen, S. Primdahl, M. J. Jorgensen, and C. Bagger, J. Electroceram. 5 (2000) 141.

[9] T. Kenjo, S. Osawa, and K. Fujikawa, J. Electrochem. Soc. 138 (1991) 349.

[10] T. Kenjo and M. Nishiya, Solid State Ionics 57 (1992) 295.

[11] T. Kawada, N. Sakai, H. Yokokawa, M. Dokiya, M. Mori, and T. Iwata, Solid State Ionics 40-41 (1990) 402.

[12] J. Mizusaki, H. Tagawa, T. Saito, J. Electrochem. Soc. 141 (1994) 2129.

[13] M. J. L. Ostergard, C. Clausen, C. Bagger, and M. Mogensen, Electrochim. Acta 40 (1995) 1971.

[14] M. Mogensen and S. Skaarup, Solid State Ionics 86-88 (1996) 1151.

[15] M. Juhl, S. Primdahl, C. Manon, and M. Mogensen, J. Power Sources 61 (1996) 173.

[16] W. Shizhong, J. Yi, Z. Yahong, Y. Jingwang, and L. Wenzhao, Solid State Ionics 113-115 (1998) 291.

[17] J. Mizusaki, H. Tagawa, K. Tsuneyoshi, and A. Sawata, J. Electrochem. Soc. 138 (1991) 1867.

[18] A. Bieberle and L. J. Gauckler, Solid State Ionics 135 (2000) 337.

[19] J. R. Smith, A. Chen, D. Gostovic, D. Hickey, D. Kundinger, K. L. Duncan, R. T. DeHoff, K. S. Jones, and E. D. Wachsman, Solid State Ionics 180 (2009) 90.

[20] J. Fleig, Annu. Rev. Mater. Res. 33 (2003) 361.

[21] P. Costamagna, P. Costa, and V. Antonucci, Electrochim. Acta 43 (1998) 375.

[22] D. W. Dees, T. D. Claar, T. E. Easler, D. C. Fee, and F. C. Mrazek, J. Electrochem. Soc. 134 (1987) 2141.

[23] C. Lee, C. Lee, H. Lee, and S. M. Oh, Solid State Ionics 98 (1997) 39.

[24] J. Kim, G. Kim, J. Moon, Y. Park, W. Lee, K. Kobayashi, M. Nagai, and C. Kim, Solid State Ionics 143 (2001) 379.

[25] J. Kim, G. Kim, J. Moon, H. Lee, K. Lee, and C. Kim, Solid State Ionics 133 (2000) 67.

[26] A. V. Virkar, J. Chen, C. W. Tanner, and J. Kim, Solid State Ionics 131 (2000) 189.

[27] P. Costamagna, M. Panizza, G. Cerisola, and A. Barbucci, Electrochim. Acta 47 (2002) 1079.

[28] J. -H. Lee, H. Moon, H. -W. Lee, J. Kim, J. -D. Kim, and K. -H. Yoon, Solid State Ionics 148 (2002) 15.

[29] X. J. Chen, S. H. Chan, and K. A. Khor, Electrochim. Acta 49 (2004) 1851.

[30] E. Perry Murray and S. A. Barnett, Solid State Ionics 143 (2001) 265.

[31] R. M. C. Clemmer and S. F. Corbin, Solid State Ionics 166 (2004) 251.

[32] Y. Yin, W. Zhu, C. Xia, and G. Meng, J. Power Sources 132 (2004) 36.

[33] J. L. M. Rupp and L. J. Gauckler, Solid State Ionics 177 (2006) 2513.

[34] M. Camaratta and E. Wachsman, J. Electrochem. Soc. 155 (2008) B135.

[35] B. H. Kwak, H. K. Youn, and J. S. Chung, J. Power Sources 185 (2008) 633.

[36] J. Li, S. Wang, Z. Wang, R. Liu, T. Wen, and Z. Wen, J. Power Sources 179 (2008) 474.

[37] U. P. Muecke, S. Graf, U. Rhyner, and L. J. Gauckler, Acta Mater. 56 (2008) 677.

[38] S. F. Corbin, R. M. C. Clemmer, and Q. Yang, J. Am. Ceram. Soc. 92 (2009) 331.

[39] M. Mukhopadhyay, J. Mukhopadhyay, A. D. Sharma, and R. N. Basu, Mater. Sci. Eng., B 163 (2009) 120.

[40] R. M. C. Clemmer and S. F. Corbin, Solid State Ionics 180 (2009) 721.

[41] J. H. Yu, G. W. Park, S. Lee, and S. K. Woo, J. Power Sources 163 (2007) 926.

[42] T. Kawada, N. Sakai, H. Yokokawa, M. Dokiya, M. Mori, and T. Iwata, J. Electrochem. Soc. 137 (1990) 3042.

[43] A. Abbaspour, K. Nandakumar, J. Luo, and K. T. Chuang, J. Power Sources 161 (2006) 965.

[44] A. Ali, X. Wen, K. Nandakumar, J. Luo, and K. T. Chuang, J. Power Sources 185 (2008) 961.

[45] V. Dusastre and J. A. Kilner, Solid State Ionics 126 (1999) 163.

[46] D. Ding, W. Zhu, J. Gao, and C. Xia, J. Power Sources 179 (2008) 177.

[47] J. R. Wilson and S. A. Barnett, Electrochem. Solid-State Lett. 11 (2008) B181.

[48] S. B. Adler, Chem. Rev. 104 (2004) 4791.

[49] E. P. Murray, T. Tsai, and S. A. Barnett, Solid State Ionics 110 (1998) 235.

[50] I. Drescher, W. Lehnert, and J. Meusinger, Electrochim. Acta 43 (1998) 3059.

[51] Z. T. Xia, S. H. Chan, and K. A. Khor, Electrochem. Solid-State Lett. 7 (2004) A63.

[52] W. Gong, S. Gopalan, and U. Pal, J. Mater. Eng. Perform. 13 (2004) 274.

[53] A. Barbucci, M. Carpanese, A. P. Reverberi, G. Cerisola, M. Blanes, P. L. Cabot, M. Viviani, A. Bertei, and C. Nicolella, J. Appl. Electrochem. 38 (2008) 939.

[54] S. Sunde, J. Electroceram. 5 (2000) 153.

[55] J. R. Wilson, W. Kobsiriphat, R. Mendoza, H. Chen, J. M. Hiller, D. J. Miller, K. Thornton, P. W. Voorhees, S. B. Adler, and S. A. Barnett, Nat. Mater. 5 (2006) 541.

[56] J. R. Wilson, A. T. Duong, M. Gameiro, H. Chen, K. Thornton, D. R. Mumm, and S. A. Barnett, Electrochem. Commun. 11 (2009) 1052.

[57] T. Suzuki, Z. Hasan, Y. Funahashi, T. Yamaguchi, Y. Fujishiro, and M. Awano, Science 325 (2009) 852.

[58] M. Cannarozzo, A. D. Borghi, and P. Costamagna, J. Appl. Electrochem. 38 (2008) 1011.

[59] A. M. Gokhale, S. Zhang, and M. Liu, J. Power Sources 194 (2009) 303.

[60] S. Srinivasan and H. D. Hurwitz, Electrochim. Acta 12 (1967) 495.

[61] C. Y. Yuh and J. R. Selman, J. Electrochem. Soc. 131 (1984) 2062.

[62] K. Mund, G. Richter, and F. von Sturm, J. Electrochem. Soc. 124 (1977) 1.

[63] T. Kenjo, J. Electrochem. Soc. 132 (1985) 383.

[64] C. W. Tanner, K. Fung, and A. V. Virkar, J. Electrochem. Soc. 144 (1997) 21.

[65] A. Borucka and J. N. Agar, Electrochim. Acta 11 (1966) 603.

[66] D. N. Bennion and C. W. Tobias, J. Electrochem. Soc. 113 (1966) 593.

[67] J. Giner and C. Hunter, J. Electrochem. Soc. 116 (1969) 1124.

[68] S. C. Yang, M. B. Cutlip, and P. Stonehart, Electrochim. Acta 35 (1990) 869.

[69] M. Viitanen and M. J. Lampinen, J. Power Sources 32 (1990) 207.

[70] M. B. Cutlip, S. C. Yang, and P. Stonehart, Electrochim. Acta 36 (1991) 547.

[71] D. Stauffer and A. Aharony, Introduction to Percolation Theory, CRC, London, 1994.

[72] D. Bouvard and F. F. Lange, Acta Metall. Mater. 39 (1991) 3083.

[73] S. Sunde, J. Electrochem. Soc. 143 (1996) 1930.

[74] P. Costamagna, P. Costa, and E. Arato, Electrochim. Acta 43 (1998) 967.

[75] S. H. Chan and Z. T. Xia, J. Electrochem. Soc. 148 (2001) A388.

[76] S. H. Chan, K. A. Khor, and Z. T. Xia, J. Power Sources 93 (2001) 130.

[77] S. H. Chan and Z. T. Xia, J. Appl. Electrochem. 32 (2002) 339.

[78] S. H. Chan, X. J. Chen, and K. A. Khor, J. Electrochem. Soc. 151 (2004) A164.

[79] J. Kim, A. V. Virkar, K. Fung, K. Mehta, and S. C. Singhal, J. Electrochem. Soc. 146 (1999) 69.

[80] A. V. Virkar, J. Chen, C. W. Tanner, and J. Kim, Solid State Ionics 131 (2000) 189.

[81] M. Cannarozzo, S. Grosso, G. Agnew, A. Del Borghi, and P. Costamagna, J. Fuel Cell Sci. Technol. 4 (2007) 99.

[82] M. M. Hussain, X. Li, and I. Dincer, Int. J. Energy Res. 29 (2005) 1083.

[83] D. H. Jeon, J. H. Nam, and C. Kim, J. Electrochem. Soc. 153 (2006) A406.

[84] J. H. Nam and D. H. Jeon, Electrochim. Acta 51 (2006) 3446.

[85] M. Ni, M. K. H. Leung, and D. Y. C. Leung, J. Power Sources, 168 (2007) 369.

[86] L. Pisani and G. Murgia, J. Electrochem. Soc. 154 (2007) B793.

[87] Y. Shi, N. Cai, C. Li, C. Bao, E. Croiset, J. Qian, Q. Hu, and S. Wang, J. Electrochem. Soc. 155 (2008) B270.

[88] H. Zhu and R. J. Kee, J. Electrochem. Soc. 155 (2008) B715.

[89] E. A. Mason and A. P. Malinauskas, Gas Transport in Porous Media: The Dusty-Gas Model, Elsevier, New York, 1983.

[90] E. Hernández-Pacheco, D. Singh, P. N. Hutton, N. Patel, and M. D. Mann, J. Power Sources 138 (2004) 174.

[91] R. Taylor and R. Krishna, Multicomponent mass transfer, Wiley Series in Chemical Engineering, New York, 1993.

[92] R. Suwanwarangkul, E. Croiset, M. W. Fowler, P. L. Douglas, E. Entchev, and M. A. Douglas, J. Power Sources 122 (2003) 9.

[93] M. Suzuki and T. Oshima, Powder Technol. 35 (1983) 159.

[94] S. Sunde, J. Electrochem. Soc. 142 (1995) L50.

[95] C. Kuo and P. K. Gupta, Acta Metall. Mater. 43 (1995) 397.

[96] L. Oger, J. P. Troadec, D. Bideau, J. A. Dodds, and M. J. Powell, Powder Technol. 46 (1986) 133.

[97] P. Costamagna, M. Panizza, G. Cerisola, and A. Barbucci, Electrochim. Acta 47 (2002) 1079.

[98] Y. Shi and N. Cai, Tsinghua Sci. Technol. 11 (2006) 701.

[99] M. Brown, S. Primdahl, and M. Mogensen, J. Electrochem. Soc. 147 (2000) 475.

[100] S. Sunde, J. Electrochem. Soc. 143 (1996) 1123.

[101] S. Sunde, J. Electroceram. 5 (2000) 153.

[102] J. Abel, A. A. Kornyshev, and W. Lehnert, J. Electrochem. Soc. 144 (1997) 4253.

[103] D. H. Jeon, J. H. Nam, and C. Kim, J. Power Sources 139 (2005) 21.

[104] Y. Ji, K. Yuan, and J. N. Chung, J. Power Sources, 165 (2007) 774.

[105] A. S. Martinez and J. Brouwer, Electrochim. Acta 53 (2008) 3597.

[106] L. C. R. Schneider, C. L. Martin, Y. Bultel, D. Bouvard, and E. Siebert, Electrochim. Acta, 52 (2006) 314.

[107] L. C. R. Schneider, C. L. Martin, Y. Bultel, L. Dessemond, and D. Bouvard, Electrochim. Acta, 52 (2007) 3190.

[108] B. Kenney, M. Valdmanis, C. Baker, J. G. Pharoah, and K. Karan, J. Power Sources 189 (2009) 1051.

[109] H. G. Ballesteros, L. A. Fernandez, V. Martin-Mayor, A. M. Sudupe, G. Parisi, and J. J. Ruiz-Lorenzo, J. Phys. A: Math. Gen. 32 (1999) 1.

[110] M. E. J. Newman and R. M. Ziff, Phys. Rev. Lett. 85 (2000) 4104.

[111] B. Kenney and K. Karan, Solid State Ionics, 178 (2007) 297.

[112] R. L. Coble, J. Amer. Ceram. Soc. 41 (1958) 55.

[113] C. L. Martin, D. Bouvard, and S. Shima, J. Mech. Phys. Solids 51 (2003) 667.

[114] C. L. Martin, L. C. R. Schneider, L. Olmos, and D. Bouvard, Scr. Mater. 55 (2006) 425.

[115] E. A. Olevsky, Mater. Sci. Eng. R, 23 (1998) 41.

[116] S. Feng, B. I. Halperin, and P. N. Sen, Phys. Rev. B 35 (1987) 197.

[117] D. Simwonis, F. Tietz, and D. Stöver, Solid State Ionics 132 (2000) 241.

[118] K. -R. Lee, S. H. Choi, J. Kim, H. -W. Lee, and J. -H. Lee, J. Power Sources 140 (2005) 226.

[119] K. Thydén, Y. L. Liu, and J. B. Bilde-Sørensen, Solid State Ionics 178 (2008) 1984.

[120] J. -H. Lee, H. Moon, H. -W. Lee, J. Kim, J. -D. Kim, and K. -H. Yoon, Solid State Ionics 148 (2002) 15.

[121] A. Lanzini, P. Leone, and P. Asinari, J. Power Sources 194 (2009) 408.

[122] M. V. Kral, M. A. Mangan, G. Spanos, and R. O. Rosenberg, Mater. Charact. 45 (2000) 17.

[123] R. K. Bansal, A. Kubis, R. Hull, and J. Fitz-Gerald, J. Vac. Sci. Technol. B 24 (2006) 554.

[124] P. G. Merli, A. Migliori, M. Nacucchi, and M. Vittori Antisari, Ultramicroscopy 65 (1996) 23.

[125] P. R. Shearing, J. Golbert, R. J. Chater, and N. P. Brandon, Chem. Eng. Sci. 64 (2009) 3928.

[126] J. R. Wilson and S. A. Barnett, Electrochem. Solid-State Lett. 11 (2008) B181.

[127] D. Gostovic, J. R. Smith, D. P. Kundinger, K. S. Jones, and E. D. Wachsman, Electrochem. Solid-State Lett. 10 (2007) B214.

[128] J. Izzo John R., A. S. Joshi, K. N. Grew, W. K. S. Chiu, A. Tkachuk, S. H. Wang, and W. Yun, J. Electrochem. Soc. 155 (2008) B504.

[129] S. Griesser, G. Buchinger, T. Raab, D. P. Claassen, and D. Meissner, J. Fuel Cell Sci. Technol. 4 (2007) 84.

[130] S. H. Lau, W. K. S. Chiu, F. Garzon, H. Chang, A. Tkachuk, M. Feser, and W. Yun, J. Phys. Conf. Ser. 152 (2009) 012059.

[131] W. K. S. Chiu, A. S. Joshi, and K. N. Grew, Eur. Phys. J. Special Topics 171 (2009) 159.

[132] A. S. Joshi, K. N. Grew, A. A. Peracchio, and W. K. S. Chiu, J. Power Sources 164 (2007) 631.

[133] S. Chen and G. D. Doolen, Annu. Rev. Fluid Mech. 30 (1998) 329.

Chapter 3

Two-Dimensional Continuous Modeling

3.1 Introduction

The focus of this chapter is two dimensional modeling of solid oxide fuel cell composite electrodes and to develop a better understanding of composite electrode performance using packing of particles in two dimensions. Although this simplification of real three dimensional structures into two dimensions might seem too simplifying, it will be seen that it is a useful tool in predicting some basic behaviour of composite electrodes. Numerous works has been conducted in the past to study the effect of material and preparation methods on microstructure and performance of SOFC electrodes [1-4]. Although a wide variety of materials have been proposed and examined, lanthanum strontium manganate or LSM is considered to be the most promising electron conductor along with yttria-stabilized zirconia (YSZ) as an ion conductor. Apart from relatively high electronic conductivity and low ionic conductivity, LSM has good electro-catalytic properties for the reduction process that takes place in the cathode and its thermal expansion coefficient is very close to that of YSZ, which makes this pair a popular combination for use in composite electrodes [5-7].

Many parameters influence the performance of SOFC composite cathodes. Among those are size of electronic and ionic conductor particles, composition of the cathode, porosity and electrode thickness. Although some experimental work has been done to determine the effect of those parameters [4,8,9], broader study of SOFC cathodes through detailed simulation to obtain an optimized structure seems to be necessary.

Few models have been proposed by the previous researchers to describe the SOFC cathode operation. Despite minor differences in interpretation of reaction kinetics, most of these models rely on the homogeneity of composite electrode media for the electrochemical reaction and transport of ion, electron and material within the electrode [10-12].

Costamagna *et al*. [10] considered whole contact area between electronic and ionic conductors to be active for the electrochemical reaction and calculated the active area using percolation theory and particle coordination number. They showed that simultaneous electronic and ionic conductivity inside the electrode is not likely to happen for particles of the same size when concentration of one of the species is less than about 30 vol.% and depending on the relative size of ionic and electronic particles they obtained the minimum polarization resistances for the compositions of the electrode around 40 vol.% Chan *et al*. [13] proposed a new kinetic model for electrochemical reaction and showed that polarization resistance assumes a relatively constant value over the wide composition range of about 37-63 vol.% of YSZ. They showed that the electronic current generation is much higher near the electrode-electrolyte interface and attributed this observation to the low ionic conductivity of YSZ [11].

Sunde [14] on the other hand used Monte Carlo method to show that while changing the conductivity of electron conductor particles does not have a pronounce effect on cell performance, increasing or decreasing the ionic conductivity and kinetic constants may have large impact on polarization resistance. Best performance has been found to fall within 40-60 vol.% of electron conducting particles.

3.2 Model Development

Electrochemical reaction in a fuel cell composite electrode occurs at the contact area between electronic and ionic conducting particles. Furthermore, the electronic conductor (LSM) must be connected contiguously between its contact with ionic conductor (YSZ) and the current collector through chains of other electronic conductors to be able to transfer the electron to the reaction point and similarly the ionic conductor must be connected to the electrolyte to conduct ions. To complete the process, open pores must be present to provide reactants for the reaction and to carry away the products of the electrochemical reaction. These conditions make the active site or active three-phase boundary a very specific place in a sense that not all three-phase contact regions are active. Furthermore it will be shown that the distribution of three phase boundaries is not homogeneous throughout the electrode as assumed by continuous models based on percolation theory and coordination number. This non homogeneous distribution affects the electrode behaviour and should be considered in electrode design as will be shown in next chapters of this works.

An ideal structure might be a co-continuous morphology that is commonly used in the polymer composite literature wherein every point within a phase is topologically connected to every other point within the same phase. Otherwise islands of one phase that are not connected to others are inactive and do not participate in the electrochemical processes. Realization of such morphologies depends on the fabrication processes and it is not commonly found in SOFC composite electrodes.

Fig. 3.1a illustrates the initial configuration from which the model emerges. Model electrode is a random packing of LSM (grey) and YSZ (yellow) particles packed in random order. Top layer is pure LSM representing current collector while bottom layer represents electrolyte being pure YSZ. Figs. 3.1 and 3.2 are simplified electrodes and prepared for illustration purpose only. Real models from which the data are extracted are much higher in LSM and YSZ population.

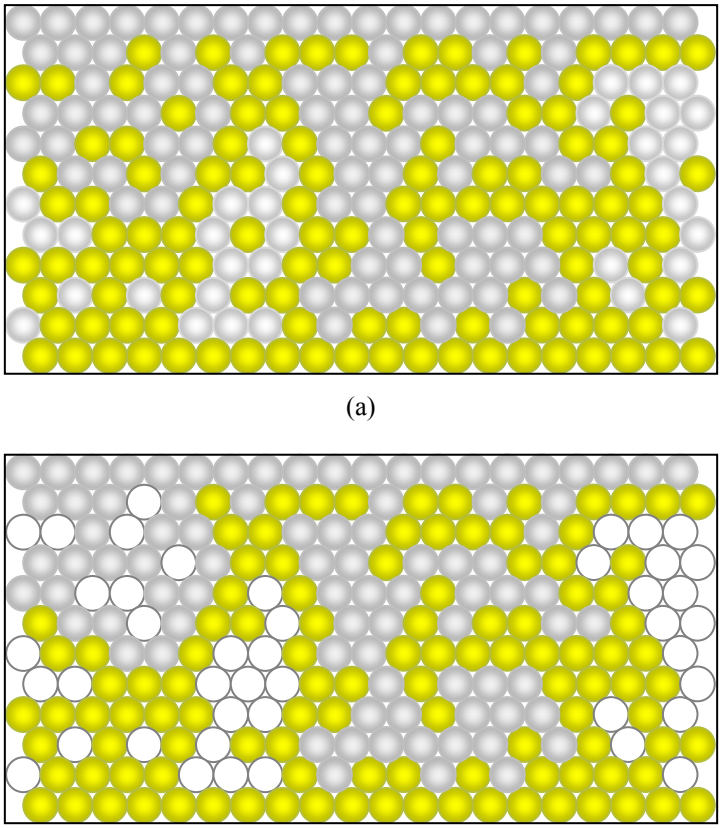

(a)

(b)

Figure 3.1 Simplified random packing of electron (grey coloured) and ion (yellow coloured) conductor particles. Top layer accounts for electrode current collector while bottom layer represents electrolyte. a) Initial random structure and b) Isolated particles are identified.

After the random packing of predetermined composition (here 50/50 vol.%) of Fig. 3.1a was created, the particles are scanned to determine whether or not they are isolated particles. This is done by assuming bottom and top layers to be electrolyte and current collector respectively and then specifying the status of other particles with respect to those layers. Starting from the top layer it is determined whether LSM particles are connected to top most layer or not and same is done for YSZ particles starting from the bottom layer. After this is stage, the code searches among connected particles to determine whether or not they contribute to a TPB. All the information in this regard is stored inside particle objects. Fig. 3.1b shows isolated LSM or YSZ particles in white colour surrounded by either YSZ or LSM particles respectively. No matter if the isolated particles are LSM or YSZ, they are treated the same way; they do not contribute

to electron or ion transfer neither they contribute to electrochemical reaction. These particles are considered a loss for the system and the purpose of the electrode design must be to minimize the amount of isolated particles in the electrode structure. Isolated particles however contribute to mass transfer in the electrode as they contain same structure and morphology as other connected clusters. After isolated particles are tagged, the program looks to determine the role of other particles in the electrode. If a particle is not isolated, it is either only conductive or both conductive and electrochemically active.

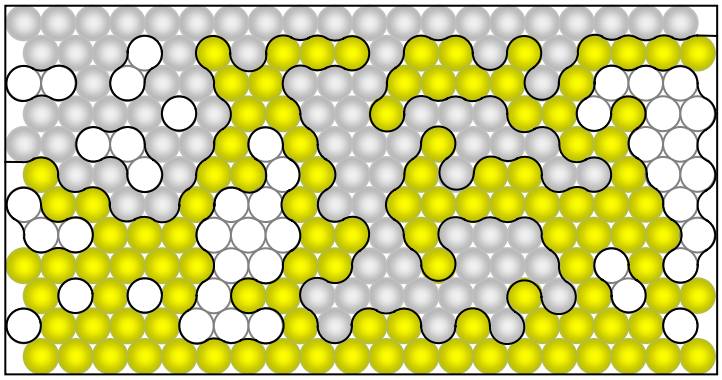

(a)

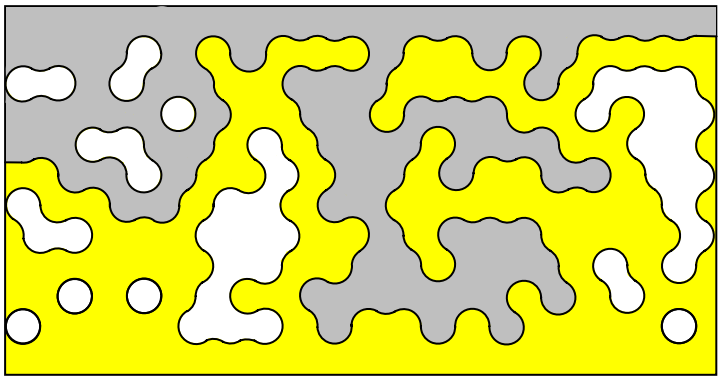

(b)

Figure 3.2 Packing of Fig. 3.1 when a) active, conductive and isolated particles are identified and active line is drawn and b) when the packing is transformed into a continuous geometry. Active line always starts from one side of the electrode and extends to the other side.

From the concept of three phase boundary, a LSM particle is electrochemically active if it is connected to the current collector and it is in contact with an YSZ particle which is connected to the electrolyte and furthermore open pores exist to

carry gaseous reactants to or from the reaction point. In this current model only contiguity of electron and ion conductor particles is considered to determine the availability of an active TPB and pores are assumed to exist wherever they are needed. Although this might seem an oversimplification of the problem, it is shown that for typical electrodes with enough porosity all sites can be assumed to have adequate access to gaseous reactants [15,16]. Fig. 3.2a shows the model electrode after electrochemically active LSM and YSZ particles are determined. By careful inspection of Fig. 3.2a it can be seen that all three phase boundaries can be connected into a continuous line without breaking other phases. Connecting all electrochemically active TPBs a reactive line can be constructed for this 2D model of the cathode. This line is shown in Fig. 3.2a starting from left hand side of the electrode and extending to the right hand side. The length of this line which is a measure of the available sites for the reaction is a function of composition of electrode. It is believed that the size ratio of the particles also has great impact on the length of this line [10,13]. The current two dimensional model is not capable of examining particle size ratio and this feature will be further discussed and examined on the next chapters of this work.

All particles below active line of Fig. 3.2a are either connected YSZ particles or isolated clusters and all particles above are either connected LSM particles or isolated clusters. Therefore active line of Fig. 3.2a divides model electrode into two regions or domains. Upper region is pure electron conductor (LSM) and lower region is pure ion conductor (YSZ). Only particles falling on either side of active line are electrochemically active. Another implication of this structure is that while whole electrode contributes equally to mass transfer of gaseous species, upper domain transfers electrons and lower domain transfers ions too. Note although being a reasonable approximation, in this model mass transfer resistance is not ignored but regions are assumed to have equal access to open pores. The same assumption is applied in continuum models based on percolation theory. While only percolation of only electron and ion conductors are considered in calculating three phase area, mass transfer and diffusion equations are imposed to solve for total polarization [10,13]. Therefore the terms “Equal access to open

pores" and "negligible mass transfer resistance" are two different concepts and should not me mixed up.

This discrete structure can be resolved using resistor network model for different overpotentials to obtain current and potential at each individual particle. Resistor network approach is applied to three dimensional structures and will be demonstrated later. For this case of simplified two dimensional structures however, an innovative approach is applied. This approach involves transformation of two dimensional discrete structure of Fig. 3.2a into continuous model of Fig. 3.2b. This continuous model is aimed to be meshed and solved on COMSOL® which is commercial finite element software. To do this transformation a MATLAB® code has been be developed to extract packing information and create COMSOL® geometry object that can be recognized with COMSOL®. This geometry object when visualized in COMSOL® looks like Fig. 3.2b. The geometry of Fig. 3.2b consists of three COMSOL® subdomains and relevant boundaries. Physical properties of yellow coloured subdomain are set to physical properties of YSZ and grey coloured one to LSM. Whole domain has unique morphological properties such as porosity, tortuosity and diffusion properties. Active line is set to have boundary condition of source or sink to gaseous species and current.

To summarize, the development of the model consists of the following steps:

1- Creating a random matrix of electronic and ionic conductor particles with prescribed composition similar to Fig. 3.1a.

2- Identifying the role of each particle in the packing according to Fig. 3.1b. Whether a particle is reactive, conductive or isolated.

3- Transforming the data to a geometrical form similar to Fig. 3.2. LSM, YSZ and isolated phases are identified and separated.

4- Model the transport and reaction processes in each domain using any multiphysics solver which in this case COMSOL® is used.

3.3 Governing Equations and Boundary Conditions

3.3.1 Governing Equations

Ohm's law governs the electron and ion transfer inside electronic and ionic conductors along with the charge balance equation:

$$\nabla V_{el} = \rho_{el}^{eff} i_{el} \tag{3.1}$$

$$\nabla V_{io} = \rho_{io}^{eff} i_{io} \tag{3.2}$$

$$i_{el} = -i_{io} = i \text{ (in the active boundary)} \tag{3.3}$$

Where V is voltage, ρ^{eff} is the effective resistivity and i is the current density. Subscripts *io* and *el* represent ionic and electronic conductors respectively. Symbol i denotes the transfer current density of the cathode which is an indication of the rate of electrochemical reaction taking place along the active line and is expressed by the classical Butler-Volmer equation:

$$i = i_0 \left[\frac{C_O}{C_O^*} e^{-\alpha f \eta} - e^{(1-\alpha) f \eta} \right] \tag{3.4}$$

Where i_0 is the exchange current density, C_o is oxygen concentration and C_o^* is the equilibrium oxygen concentration. Table 3.1 summarizes the value of i_0 and other most important constant parameters used in this model. Over-potential η in this equation is defined in general as:

$$\eta = E - E_0 = \left(V_{io} - V_{el}\right) - E_0 \tag{3.5}$$

And E_0 which is equilibrium potential of the electrode and is calculated from well known Nernst equation. For the purpose of this thesis which deals with cathode and also since in Eq. 3.4 only over-potential defines the amount of current, E_0 is set to zero.

Effective porous media resistivity for electronic and ionic sub-domain is calculated from pure material resistivity by the following equation: [10,13]

$$\rho_k^{eff} = \frac{\rho_k}{1-\varepsilon} \tag{3.6}$$

Subscript k refers the electronic or ionic conductor and ε is the porosity which is set to average value of 34.66% [17].

Table 3.1 Values of constants used in the model

Parameter	value	Reference
ρ_{el}	7.817×10^{-5} $\Omega.m$	[20]
ρ_{io}	0.442 $\Omega.m$	[20]
i_0	2000 $A.m^{-2}$	[15]
T	1073 K	
ε	34.66 %	[17]
τ	15.6	[17]
$D_{O_2}^{k,eff}$	0.624 $cm^2.s^{-1}$	[17]
$D_{O_2-N_2}^{B}$	1.336 $cm^2.s^{-1}$	Eq. 3.9

The diffusion flux through the cathode can be determined using the well-known Stefan-Maxwell equation [18]:

$$-c\nabla x_i = \sum_{j=1,i\neq j}^{n} \frac{1}{D_{ij}^{eff}}\left(x_j N_i - x_i N_j\right) \tag{3.7}$$

Where c is the total concentration of the gas mixture, x denotes the mole fraction of each species contributing to the gas mixture and N_i is the diffusive flux of specie i. D_{ij}^{eff} denotes the overall effective binary diffusion coefficient and carries both effects of ordinary binary diffusion coefficient and Knudsen diffusion coefficient [15]:

$$\frac{1}{D_{O_2-N_2}^{eff}} = \frac{1}{D_{O_2-N_2}^{B,eff}} + \frac{1}{D_{O_2}^{K,eff}} \tag{3.8}$$

Binary diffusion coefficient can be calculated using kinetic theory by Chapman-Enskog relation [18]:

$$D_{ij}^{B} = 0.0018583 T^{3/2} \frac{\sqrt{(M_1 + M_2)/(M_1 M_2)}}{P \sigma_{12} \Omega_D} \tag{3.9}$$

In this equation T is temperature in K, M_1 and M_2 are molecular weights of oxygen and nitrogen and σ_{12} is collision diameter in angstroms which is equal to arithmetic average of oxygen and nitrogen diameters equal to 3.557 angstroms [19]. Collision integral, Ω_D is a dimensionless parameter and is set to unity [19].

Knudsen diffusion coefficient is a function of molecular velocity and radius of the pores. In this work experimental values reported by Zhao *et al*. [17] have been used.

Finally to calculate effective binary diffusion coefficients for the porous media from the values obtained using Eq. 3.8, the following equation based on Cussler [19] has been used:

$$D_{ij}^{B,eff} = \frac{\varepsilon}{\tau} D_{ij}^{B} \tag{3.10}$$

Tortuosity τ of the porous media is set to 15.6 [17]

3.3.2 Boundary Conditions

The following concentration and voltage boundary conditions apply to this simulation. Mole fraction of oxygen is assumed to be o.21 at electrode surface and electrolyte is assumed to be impermeable to any gas flow which also is the case for real electrodes.

Electrolyte surface: V_{io}=-200 mv, $\frac{\partial x}{\partial t} = 0$

Current collector surface: V_{el}=0 mv, $x_{O_2} = 0.21$

Where t denotes position vector in direction perpendicular to electrolyte surface and is zero at electrolyte surface.

3.4 Results and Discussion

3.4.1 Current Generation and Concentration Profiles

Fig. 3.3 shows the results obtained from the model for a cathode composed of about 2000 particles in a mixture of 50 vol.% of both LSM and YSZ. Applied over-potential to the electrode is 0.2 volts. It can be seen in Fig. 3.3a that the concentration of reactant oxygen is not uniform along the cell width. Instead it changes depending on the density of electrochemically active points and the minimum concentration occurs near the electrode-electrolyte interface at regions of high active three phase boundary. Fig. 3.3b shows the variation of current generation or the rate of electrochemical reaction along active boundary. This figure shows that although the concentration of oxygen is lower near the cathode-electrolyte interface, the reaction rate is higher in this region. This can be attributed to the lower ionic conductivity of YSZ. Since the ionic conductivity of YSZ is much smaller than the electronic conductivity of LSM the reaction tends to occur near the electrolyte to face smaller ionic resistance. This result is consistent with the results published by Chan *et al*. [11] who reported the same phenomena for the anode. Although this trend holds for the practical range of the value of parameters, simulation showed that one cannot always expect higher reaction rates near the electrode-electrolyte interface. In fact apart from activation polarization or resistance, concentration and ohmic resistances are both important in determining the rate of electrochemical reaction. If by any means oxygen supply to the reaction sites deep inside the electrode decreases it would result in electrode starvation at that points and the trend will be altered. This can happen when the porosity of electrode is not enough to transport the oxygen to reaction sites resulting in low effective diffusivity and thereby starvation of the cell near the electrode-electrolyte interface. Although it is not the case for LSM-YSZ, high electro-catalyst activity resulting in high exchange current density can also result in the alteration of the abovementioned trend.

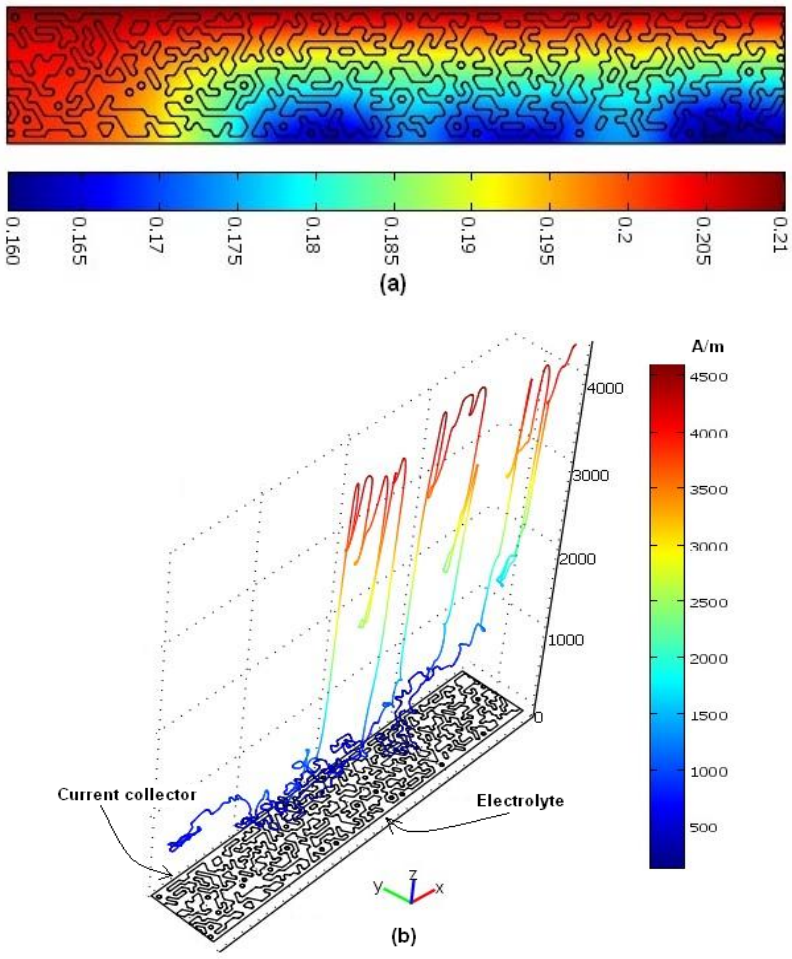

Figure 3.3 a) Mole fraction of oxygen inside the SOFC cathode obtained by the model. Upper boundary is current collector; lower boundary is cathode-electrolyte interface. Mole fraction of oxygen on the current collector side is set to 0.21. b) Amount of current generation along the active boundary. Current generation is higher at points closer to electrolyte surface.

3.4.2 Length of Active Line

Fig. 3.4 shows the dimensionless length of active line, l (length of active line per unit electrode width) as a function of LSM volume fraction. Since ϕ_{el} of 0 or 1 corresponds to simple layer of YSZ adjacent to a layer of LSM, those values have not been included in Fig. 3.4. As pointed out by most of the authors [10,13] the length of active line or the active area assumes its maximum value when the electrode is made up of equal amounts of electronic and ionic conductors of the same size.

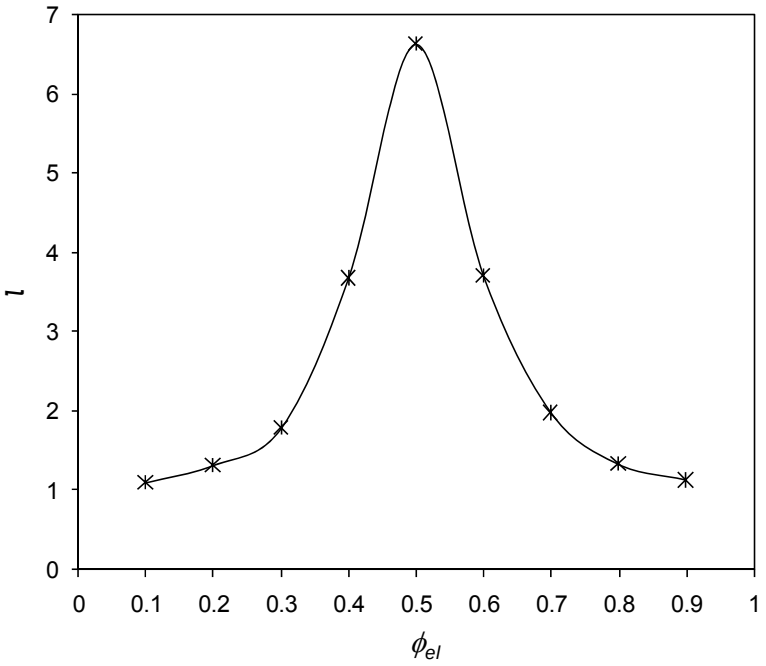

Figure 3.4 Effect of composition on the length of active line. Length of active line is defined as the length of the curve dividing two yellow and grey phases in Fig. 3.2b divided by the base length of rectangle

3.4.3 Overall Polarization Resistance

The effect of electrode composition on the overall electrode resistance is shown in Fig. 3.5 Overall polarization resistance is defined as:

$$R_p = \frac{d\eta}{dI} \tag{3.11}$$

I is the total current density passing through the electrode. In calculating this and other polarization curves, circles of Figs. 3.1 and 3.2 are assumed to be cylinders of unit length perpendicular to the page thus giving the electrode, unit depth or width. As it can be seen the polarization resistance for the cell is minimum somewhere around 50-60 volume percent of the electron conductor. Although the length of active line is maximum at exactly 50% and the variations are symmetric according to Fig. 3.4, for polarization it is not symmetric and minimum resistance does not happen in the same composition. Even though activation polarization is minimized for the maximum length of active line (50%), total polarization resistance depends on some other factors such as diffusion and ohmic resistance which tend to affect it. While the length of active area is only a function of the geometry of the electrode, the polarization resistance depends not only on the geometry but also on other parameters such as conductivities, diffusivity and electrode porosity. That is why different researchers obtained slightly different optimum composition of the electrode depending on the operating condition and parameters of their simulations or experiments while everybody agrees that the maximum active line or area occurs when equal amounts of LSM and YSZ particles of the same size are used.

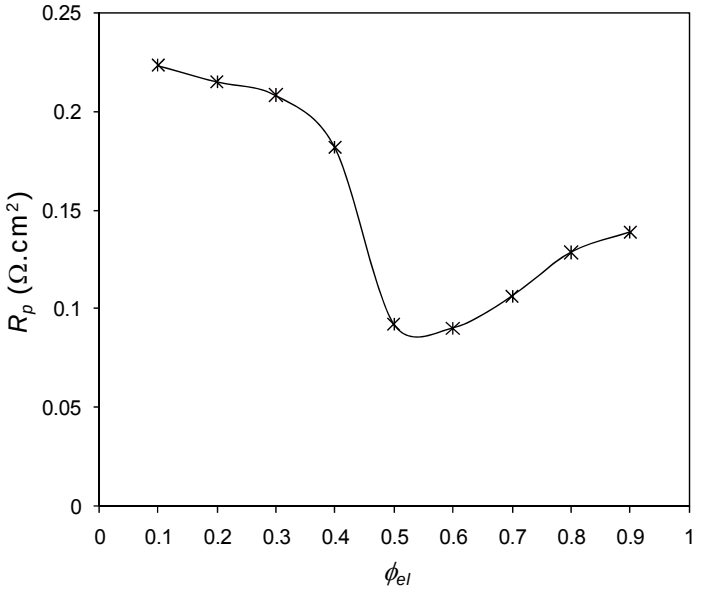

Figure 3.5 Effect of composition on the overall polarization resistance of the electrode.

Kenjo *et al*. [8] and Haanappel *et al*. [21] reported the best performance for the electrode for the weight ratio of LSM and YSZ equal to 1. While the first group did not mention the size of the particles, second group used 1 μm LSM particles. On the other hand, Ostergard *et al*. [4] and Kim *et al*. [9] obtained the minimum polarization resistance in their experiments when YSZ content was around 40%. Juhl *et al*. [22] reported the same results. On the simulation side also there are differences between reported data. While Costamagna *et al*. [10] report the minimum polarization resistance at about 37% of electronic conductor, Sunde [23] and Chan *et al*. [12] believe that for a wide range of electrode composition of about 40-60% the polarization resistance remains constant at its minimum value.

3.4.4 Concentration and Ohmic Polarizations

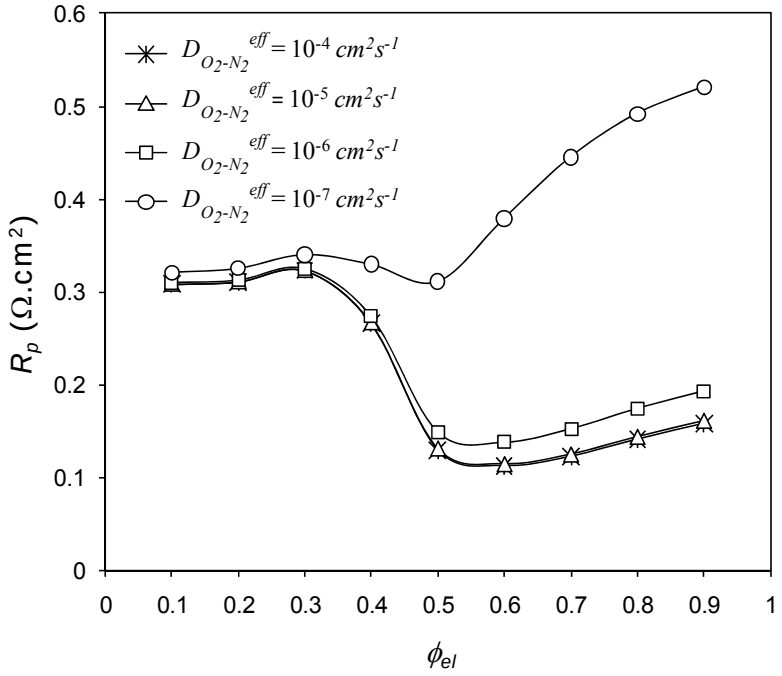

Figure 3.6 Parametric study of the effect of diffusion coefficient on the overall polarization resistance of the electrode.

Fig. 3.6 and 3.7 show a parametric study of the effect of diffusion coefficient and the conductivity of ion conductor on the performance of the electrode. Decreasing the diffusion coefficient which could be a result of decreasing porosity, can result in diffusion controlled process. According to the model

increasing the volume fraction of electronic conductor pushes the electrochemical reaction sites towards the electrolyte, far from the air channel. This in turn increases the diffusion resistance and for small values of diffusion coefficient as it is shown in Fig. 3.6 concentration polarization resistance outweighs the increase in the length of active line or decrease in activation polarization resistance. Fig. 3.7 is a parametric study on the effect of conductivity of ion conductor in the cathode. Since the conductivity of ion conducting media is usually very low, change in the conductivity has pronounced effect on the performance of the electrode.

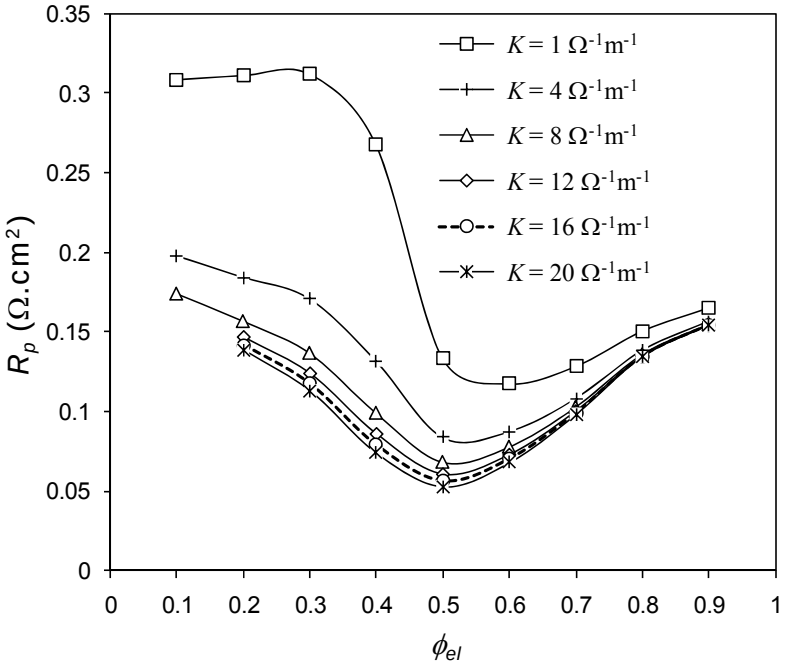

Figure 3.7 Parametric study of the effect of the conductivity of ionic conductor on the overall polarization resistance of the electrode

This change in conductivity can be applied through changing the geometric features like particle size and porosity or variations in operating conditions like temperature. For high values of conductivity the minimum of polarization resistance shifts exactly to 50 vol.% of each component and the shape of the curve becomes more symmetric just like active area or active length curve of Fig. 3.4. The reason is that increasing the conductivity decreases the ohmic resistance and thereby activation polarization determines the whole trend of the polarization

resistance curve. Activation polarization is in its minimum when the active area meets maximum point or when the composition is 50 vol.%. A slight increase in polarization resistance with increasing the LSM volume fraction in the first stages is due to the fact that by increasing LSM composition in the first stages we are just introducing some small isolated patches of LSM into YSZ which decreases the conductivity of YSZ media hence increasing the polarization resistance. Same observation is reported for conductivity by Sunde [23].

3.5 Conclusion

In this chapter a novel continuous 2D model based on random packing of electronic and ionic particles and then transformation of geometry to continuous form has been proposed. The model of transport processes based on this geometrical approach and finite element method shows very good agreement with the other observed experimental and simulation data. This framework offers its own values and advantages, since in this model every single reaction point can be identified; it gives a better image of composite electrode performance. Due to its detailed view to the electrode structure, the model can be used to study the reaction kinetics of electrode reaction.

This work needs to be extended to three dimensional space to give more practical and realistic image of the processes happening inside the composite electrodes. Percolation behaviour and especially percolation threshold is much different for three dimensional packing than two dimensional one and hence polarization and conductivity behaviour of the electrode modeled in three dimensions is expected to be different from those presented in this chapter. A vivid example is L_{TPB} and polarization curve for different compositions of the cell. While experimental and simulation data based on percolation and continuous medium theory show a wide maximum for L_{TPB} around medium compositions, Fig. 3.4 showed that there is sharp and sudden maximum for L_{TPB} at 50 vol.% LSM. In other words, Fig. 3.4 is consistent with other experimental and simulation results in a sense that maximum L_{TPB} for composite of particles of the

same size occurs at 50 vol.% percents of electron and ion conductor particles, but is not completely aligned with other data since it shows enormous improvement in L_{TPB} going from 40 vol.% LSM to 50 vol.%. This difference as said before is the result of different percolation threshold behaviour of two and three dimensional structures. The extra degree of freedom offered in a 3D geometry can alter the topological structure of the TPB significantly. Using this framework, we can also investigate the effectiveness of several alternate structured or patterned topologies to assess the most promising patterns.

References

[1] A. Barbucci, R. Bozzo, G. Cerisola, and P. Costamagna, Electrochim. Acta 47 (2002) 2183.

[2] J. H. Choi, J. H. Jang, and S. M. Oh, Electrochim. Acta 46 (2001) 867.

[3] E. Perry Murray and S. A. Barnett, Solid State Ionics 143 (2001) 265.

[4] M. J. L. Ostergard, C. Clausen, C. Bagger, and M. Mogensen, Electrochim. Acta 40 (1995) 1971.

[5] A. Hammouche, E. J. L. Schouler, and M. Henault, Solid State Ionics 28-30 (1988) 1205.

[6] M. J. L. Ostergard and M. Mogensen, Electrochim. Acta 38 (1993) 2015.

[7] H. Kamata, A. Hosaka, J. Mizusaki, and H. Tagawa, Solid State Ionics 106 (1998) 237.

[8] T. Kenjo and M. Nishiya, Solid State Ionics 57 (1992) 295.

[9] J. Kim, G. Kim, J. Moon, Y. Park, W. Lee, K. Kobayashi, M. Nagai, and C. Kim, Solid State Ionics 143 (2001) 379.

[10] P. Costamagna, P. Costa, and V. Antonucci, Electrochim. Acta 43 (1998) 375.

[11] S. H. Chan and Z. T. Xia, J. Electrochem. Soc. 148 (2001) A388.

[12] S. H. Chan, X. J. Chen, and K. A. Khor, J. Electrochem. Soc. 151 (2004) A164.

[13] X. J. Chen, S. H. Chan, and K. A. Khor, Electrochim. Acta 49 (2004) 1851.

[14] S. Sunde, J. Electrochem. Soc. 143 (1996) 1930.

[15] S. H. Chan, K. A. Khor, and Z. T. Xia, J. Power Sources 93 (2001) 130.

[16] B. Kenney and K. Karan, Solid State Ionics, 178 (2007) 297.

[17] F. Zhao, T. J. Armstrong, and A. V. Virkar, J. Electrochem. Soc. 150 (2003) A249.

[18] R. Taylor and R. Krishna, Multicomponent mass transfer, Wiley Series in Chemical Engineering, New York, 1993.

[19] E. L. Cussler, Diffusion : mass transfer in fluid systems, Cambridge University Press, New York, 1997.

[20] J. R. Ferguson, J. M. Fiard, and R. Herbin, J. Power Sources 58 (1996) 109.

[21] V. A. C. Haanappel, J. Mertens, D. Rutenbeck, C. Tropartz, W. Herzhof, D. Sebold, and F. Tietz, J. Power Sources 141 (2005) 216.

[22] M. Juhl, S. Primdahl, C. Manon, and M. Mogensen, J. Power Sources 61 (1996) 173.

[23] S. Sunde, J. Electroceram. 5 (2000) 153.

Chapter 4

Three-Dimensional Geometrical Modeling

4.1 Introduction

This chapter deals with three dimensional microstructure simulation of SOFC composite electrodes and it is the continuation of the previous chapter which was on two dimensional microstructure simulation of SOFC electrodes [1]. The extra degree of freedom afforded by the third dimension can create path ways in space for the triple phase lines that are not possible in two dimensions. Hence this is an important step in the evolution of microstructure models that captures the complexity of composite electrodes in a realistic manner.

4.2 A Brief Reminder of Background

Random nature of structure of composite electrodes suggests that a random packing of electron and ion conductor particles will be able to model the behavior of electrode. Structured packing of particles where electron and ion conductor particles are randomly distributed is used by few researchers [1-4], while others use random packing of particles [5-7]. Although porous electrode models discussed in chapter 2 based on percolation theory are capable of being extended to three dimensional models, most of the work done in that framework was

carried on in one dimension along the electrode depth [8]. This simplification which is imposed mostly to decrease computational load, in fact does not have major impact on the results and is reasonable simplification without sacrificing the accuracy. The reason for this can be found in the intrinsic assumptions for those models. The medium of the electrode is assumed to be homogeneous in the amount of active sites and the electrolyte surface as well as current collector is assumed to have the same potential. Random packing models on the other hand need at least two dimensions to represent the particles. Furthermore, their capability in predicting real world behavior of electrodes is very limited for 2D simulation as shown in chapter 3 [1]. This is because the average coordination number of particles in 2D is less than 3D case, resulting in different percolation behavior. Therefore simulations based on random packing models need to be conducted in three dimensions to obtain more realistic results.

Although results of all simulations based on random packing of particles show that there is a sharp decrease in electrode conductivity near percolation threshold, the onset of the variations differs for different works depending on the structure that's been chosen for the packing. While Sunde observed a sudden increase in electrode conductivity and decrease in polarization resistance for a simple cubic lattice structure of composite electrode near volume fraction of 0.3 [2,5], Abel *et al.* applied the same resistor network model for a face-centered cubic (fcc) lattice showing that the onset of rapid rise in electrode admittance occurs at volume fractions very close to 0.2 [9]. The reason for this difference lies in different coordination number of the particles (6 and 12 respectively) which results in different percolation thresholds of about 0.312 and 0.199 for simple cubic and fcc lattices [10,11]. Studies showed that relative magnitude of electrode, electrolyte and reaction resistance are very important parameters in deciding the composition and thickness of the electrodes [5,6,9] and for the realistic experimental values of these parameters it is very important to optimize the geometry of electrode to obtain maximum triple phase boundary line for electrochemical reaction.

4.3 Development of the Model

The current study is continuation of previous chapter and part of thee effort to understand the effect of geometry and microstructure on the performance of SOFC electrodes [1]. Random structure of SOFC composite electrodes was built in 2D first by creating random packing of YSZ and LSM particles and then transforming the structure into a continuous geometry and then solving for relevant transport phenomena as well as electrochemical reaction. This chapter deals with more realistic case of 3D simulation of the effect of geometry on the performance of composite electrodes.

The structure of composite electrode is simulated by completely random packing of spheres of different size using collision detection and location optimization open source program developed in department of computer science of the University of North Carolina in 1995 by Gottschalk *et al*. It is based on releasing particles one by one in a container and finding contact points with other particles and the walls of the container and then moving the particle to find most mechanically stable location in the packing. Starting with a layer of ion conductor at one end of electrode, the electrode is built by placing particles next to the previously formed layers and finding a stable close position of contact. The composition of the electrode i.e. the volume fraction of each constituent is controlled during the formation process based on the relative amounts and ratio of particle sizes. A layer of electron conductor at the top acts as a net-like current collector for electrode assembly. Fig. 4.1 shows a composite electrode created in this manner. After creating the packing, to obtain a certain degree of overlap between particles the sintering behavior of particles is simply modeled by enlarging the size of the particles. Sunde argued that the length of triple phase boundary resulting from the contact between an ion conductor and an electron conductor particles of the same radius r is almost three times the radius, or: $l_{TPB}/r \approx 3$ [2]. For particles of the same size this ratio corresponds to almost 10% increase in particle size for two touching spheres and therefore 10% enlargement of particle size was used for all simulations. Packing density before sintering

depends on the ratio of d_{io} to d_{el} and the maximum packing density of about 60% was observed for particles of the same size, which is less than the packing density that would be obtained if it was face centered or body centered cubic lattice (74.05% and 67.98% respectively) and more than 52.33% for simple cubic lattice.

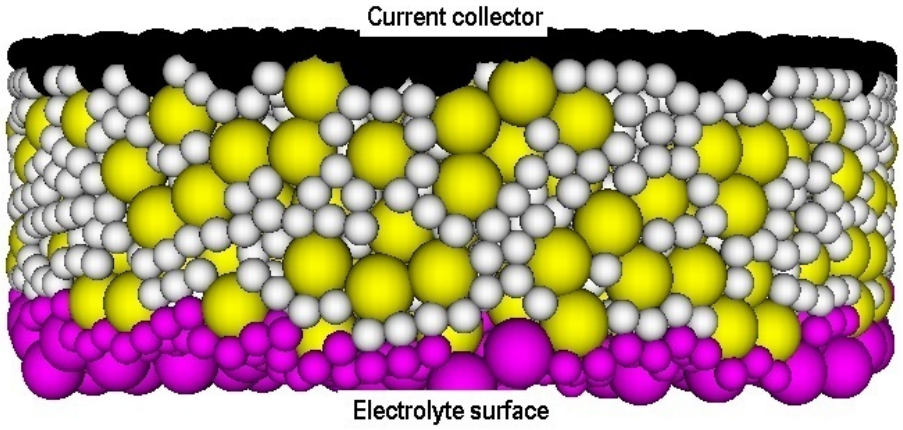

Figure 4.1 Composite electrode created in the computer. White particles are electron conductors while yellow particles represent ion conductors. Bottom layer is electrolyte surface made of ion conductors while top layer is totally electron conductor and acts as current collector.

Porosity of the final composite electrode after resizing the particles was also calculated. This was done by subtracting overlapping volumes from the solid volume giving the possibility for two or three sphere to overlap [12,13]. The packing density thus obtained was between about 74-77% corresponding to porosity of 23-26% depending on the ratio d_{el}/d_{io}. The porosity was increased artificially by introducing some random particles as pores and then deleting them, to about 30% [14,15] to make sure that mass transport resistant can be ignored.

Electrochemical reaction on a single site inside a composite electrode requires the transfer of electrons, ions and gas phase species to or from the reaction site which gives rise to the concept of triple phase boundary discussed in previous chapters. Considering the importance of TPB on the performance of SOFC electrode and direct effect of increasing L_{TPB} on decreasing electrode losses [16], most of the current work is devoted to the investigation of this effect. After creating the packing of particles with two types of electron and ion conductor spheres, each particle starts to search for its neighbors (object oriented design)

and therefore the role of each particle in the electrode is specified. Some of the particles are electrochemically active and therefore there is TPB on one or few sites of those particles. Some of them only conduct electrons or ions while some others are completely isolated from the chain of same type particles and represent a loss for the electrode. L_{TPB} is calculated separately for each contact point considering the fact that for random packing of particles the degree of overlap and hence L_{TPB} might be different for different contact points.

4.4 Results and Discussion

4.4.1 Domain Size

Electrode under study is a circular disk which might have different thicknesses to investigate the effect of thickness on the performance. Sunde used an electrode with square cross section having 20 particles in each side and then used cyclic boundary condition [2,5,6]. Although the cyclic boundary condition implies an infinite electrode size, it does not reflect the random behavior of the packing. For small samples, especially when the electrode is thick, the results of simulation do not reflect the reality and usually L_{TPB} is underestimated. Besides that, more disperse and sometimes misleading results are obtained for different random structures of the same size when the diameter of the sample disk is small. Note that in reality thickness of the electrode is very small compared to the diameter but such an electrode is impossible to create by simulation and therefore minimum reliable sizes must be selected. Fig. 4.2 shows the results of the dispersion study to determine the minimum acceptable diameter of the sample electrode disk so that the rest of the simulations could be performed based on this size. Simulation for each electrode sample has been performed 1000 times and the results of coefficient of variance are reported. As shown in this figure, point 1 corresponding to an electrode sample of 10 μm in diameter and having only about 100 electron or ion conductor particles in each layer represents more disperse L_{TPB} results. For bigger samples the coefficient of variance decreases, demonstrating more reliability for the data obtained from a single run. Calculations show that

while the probability of getting values of L_{TPB} from a single run being 3% off the population mean is less than 40% for sample represented by point 1, this probability is more than 98% for sample 6 and beyond. Therefore for the rest of this work the diameter of the container to create the packing of ion and electron conductors is chosen in a way that it contains more than 700 particles in each layer parallel to current collector.

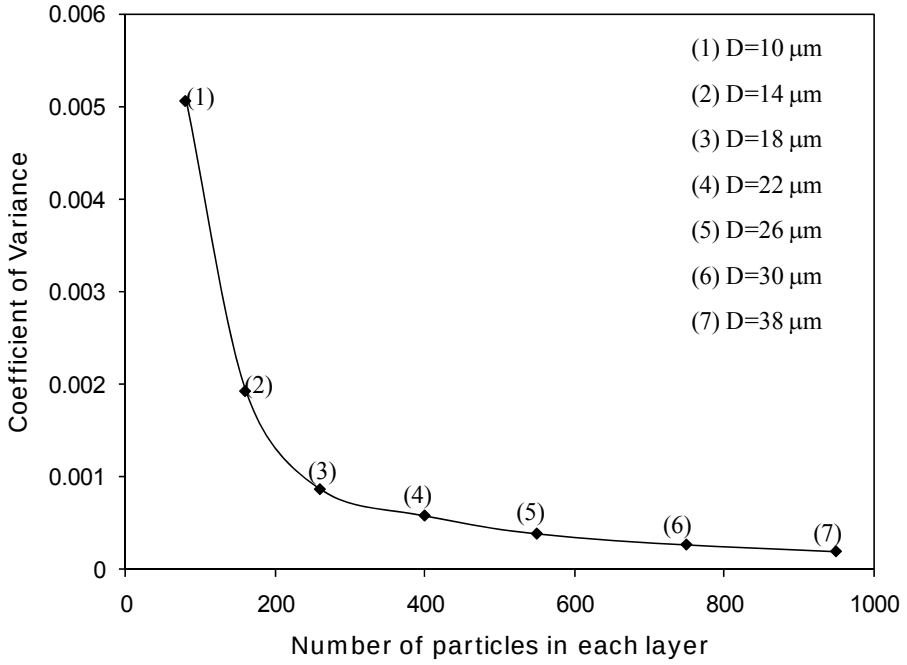

Figure 4.2 Coefficient of variance in L_{TPB} calculations for different electrode sizes. Each standard deviation point corresponds to population of 1000 computer simulations of random packing, $r_{el} = r_{io} = 1\ \mu m$.

4.4.2 Effect of Particle Size

Effect of particle size on the performance of composite electrodes has been investigated both theoretically [4,17,18] and experimentally [19,20]. Jiang *et al*. examined the effect of NiO particle size on the performance of the anode and observed much lower polarization resistance of less than 1 $\Omega.cm^2$ for average particle size of 2.9 μm compared to much higher values of more than 4 $\Omega.cm^2$ for average particle size of 10 μm [21]. Higher interfacial area between LSM and YSZ particles was observed by Song *et al.* for samples of electrode with finer

LSM particles and for high enough sintering temperatures they observed lower polarization resistance for finer sample [19]. While lower polarization resistance can directly be attributed to higher L_{TPB} [16] all these observation can be cleared in the light of percolation theory and coordination number in random packing of particles. For random packing of particles of the same size, L_{TPB} is inversely proportional to the square of particles size while active interfacial area, A_{TPB} is inversely proportional to particle size [8] or:

$$L_{TPB} \propto \frac{1}{r_p^2}$$
$$A_{TPB} \propto \frac{1}{r_p} \qquad (4.1)$$

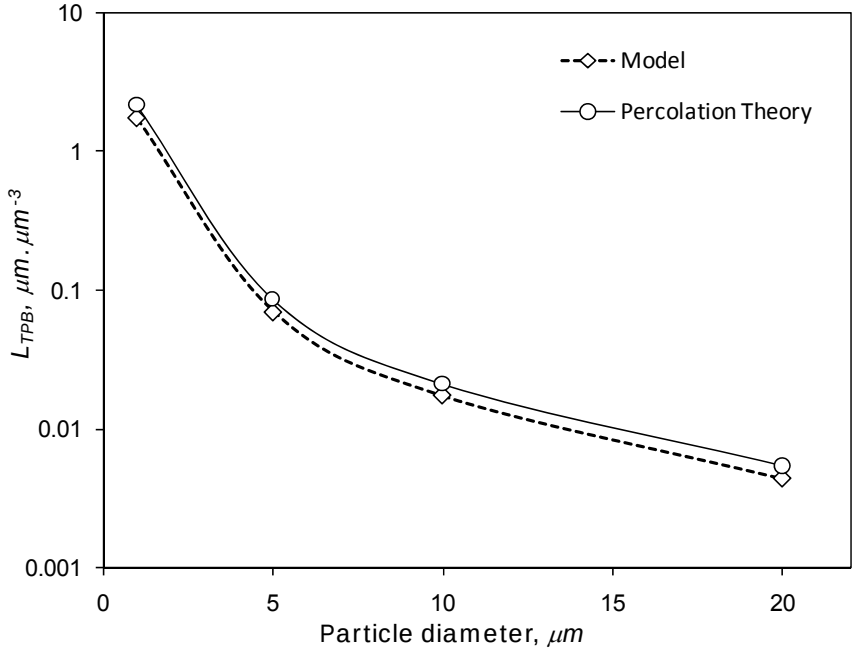

Figure 4.3 Comparison of model results and percolation theory for dependence of L_{TPB} on the diameter of particles, $r_{el} = r_{io} = 1\ \mu m$ and $\phi_{el} = \phi_{io} = 0.5$.

Figs. 4.3 and 4.4 show the results of electrochemically active L_{TPB} and A_{TPB} obtained from the random packing of particles of the same size. Continuous curves indicate the predictions of percolation theory [8]. As it can be seen there is a very good agreement between the simulation by the current model and predictions of percolation theory. Although small particles are favored to create

large L_{TPB}, very fine electrode particle size will create excessive mass transfer resistance and tends to increase concentration overpotential and therefore an optimum value of particle size must be taken. This optimum value depends on fuel cell operating parameters and especially electrode thickness [18,22].

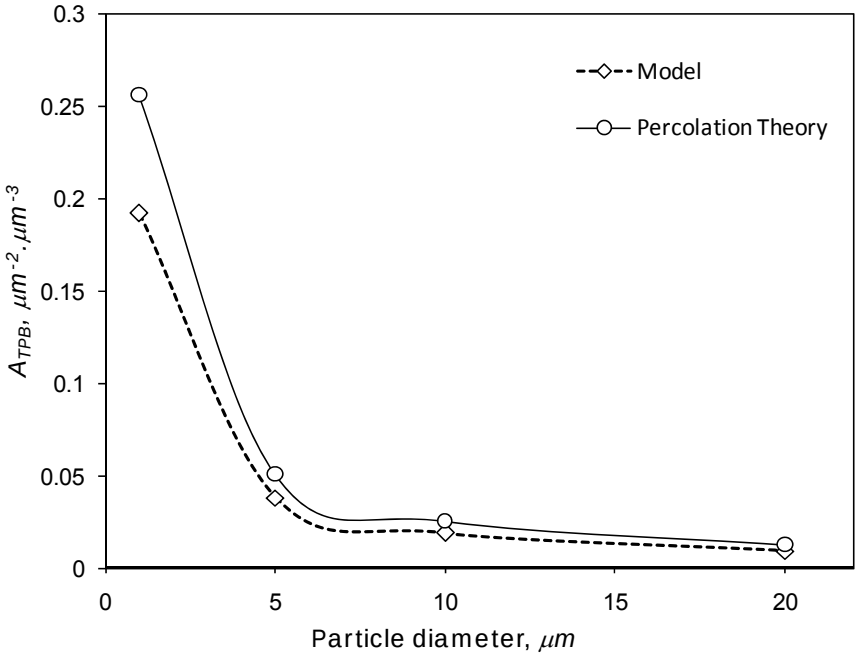

Figure 4.4 Comparison of model results and percolation theory for dependence of A_{TPB} on the diameter of particles, $r_{el} = r_{io} = 1\ \mu m$ and $\phi_{el} = \phi_{io} = 0.5$.

4.4.3 Location of Active Sites

One of the important results of the assumptions made on models based on porous electrode and percolation theory [8] is that electrochemically active sites are homogenously dispersed within the electrode. It was shown however, in the previous chapter that this is not true especially when the volume fraction of electron and ion conductor particles is not at optimal value [1]. This conclusion is further proved by looking at Figure 4.5 which shows the density of active sites along the electrode depth starting at electrolyte surface (X/L=0) and ending at current collector (X/L=1). Number of active sites per particle is the average number of electrochemically active contacts that a particle has with its neighbors. For particles of the same size only when $\phi_{el} = \phi_{io}$, the distribution of active sites is

completely homogeneous. This homogeneity also holds as long as ϕ_{io} and ϕ_{el} values fall between 40% and 60% excluding the end points. For particle concentrations which do not fall in the above mentioned range, higher active sites densities tend to occur at either ends of the electrode.

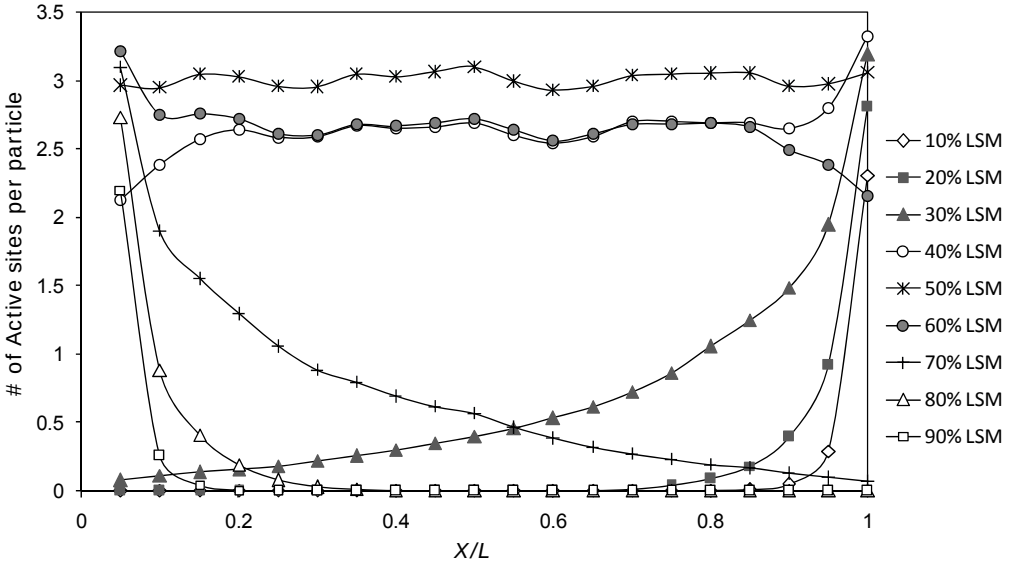

Figure 4.5 Concentration of active sites along the depth of electrode for different volume fractions of electron and ion conductors in presence of CCL layer at the top.

As it can be seen even for ϕ_{el} equal to 30% which roughly corresponds to percolation threshold of the packing, most of the active site occurs at the surface of the electrode while for ϕ_{el} =70% higher active site densities will be observed at electrolyte surface. Although the total amount of active sites is the same in both compositions, in case of ϕ_{el} =70% there will be more active sites available in close vicinity of electrolyte which is favoured as the rate of the reaction tends to be higher close to electrolyte surface and was shown in chapter 3 [1,23]. Therefore active sites will be better utilized when they are close to electrolyte surface. This finding leads to very important practical guideline in preparing SOFC composite electrodes. Applying optimum calculated composition to real electrodes is impossible giving the fact that particles have different size and always come with size distribution. Also sintering condition may change the effective size of particles and therefore alter optimum composition. Therefore with applying

theoretically calculated optimum proportions to starting powders, one may end up with an electrode with ϕ_{el} higher or lower than desired. This finding suggests that selecting a starting powder concentration (ϕ_{el}) which tends to be few percent higher than calculated optimum value can guarantee maximum possible efficient active area and therefore it is always safer to overestimate the amount of electron conductor to be used in electrode mixture.

4.4.4 Effect of Current Collector Layer

Results in Fig. 4.5 are obtained for the case of electrode covered at the top with a current collector layer (CCL) which is pure LSM (cathode) or Ni (anode). Effect of CCL in enhancing the performance of SOFC electrodes has been investigated experimentally [24,25] and theoretically [15,26]. This improvement in performance has been attributed to enhanced mass transfer and electric connectivity brought by CCL [25].

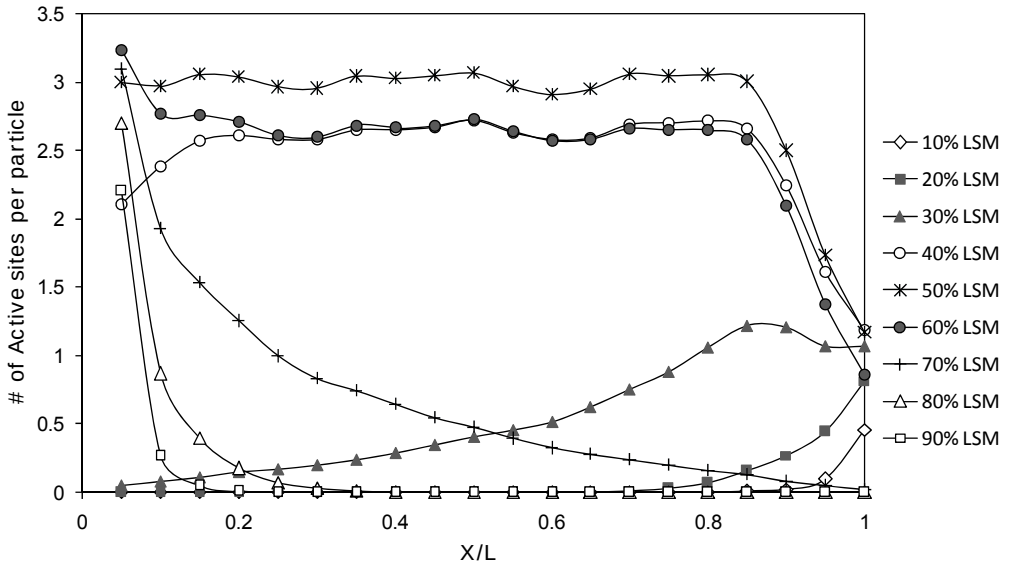

Figure 4.6 Concentration of active sites along the depth of electrode for different volume fractions of electron and ion conductors without CCL layer at the top.

Although abovementioned arguments are valid conclusions, simulation results of current work shown in Fig. 4.6 reveal other reason why CCL can improve the

performance. Fig. 4.6 demonstrates the results of the same simulation as in Fig. 4.5 but for the case where there is no CCL layer made of LSM or Ni. Current collector in this case is a simple electron conductor incapable of conducting electrochemical reaction at triple phase boundary. There is an appreciable amount of active sites lost in regions close to X/L=1. More far is the composition from optimum value of 50%, more loss is observed as a result of eliminating CCL. Best case scenario (ϕ_{el}=50%), 4% of active sites will be lost by eliminating CCL. Therefore covering the electrode with a layer of CCL will have noticeable effect on electrode performance in the form of decreasing polarization resistance.

4.4.5 Effect of Electrode Thickness

Combined effect of electrode composition and thickness are shown in Figs. 4.7, 4.8 and 4.9. Fig. 4.7 shows that for electron and ion conductor particles of the same size, maximum triple phase boundary length is obtained when $\phi_{el} = \phi_{io} = 0.5$. It also shows how the performance of electrode improves with increased L_{TPB} by increasing the thickness of the electrode.

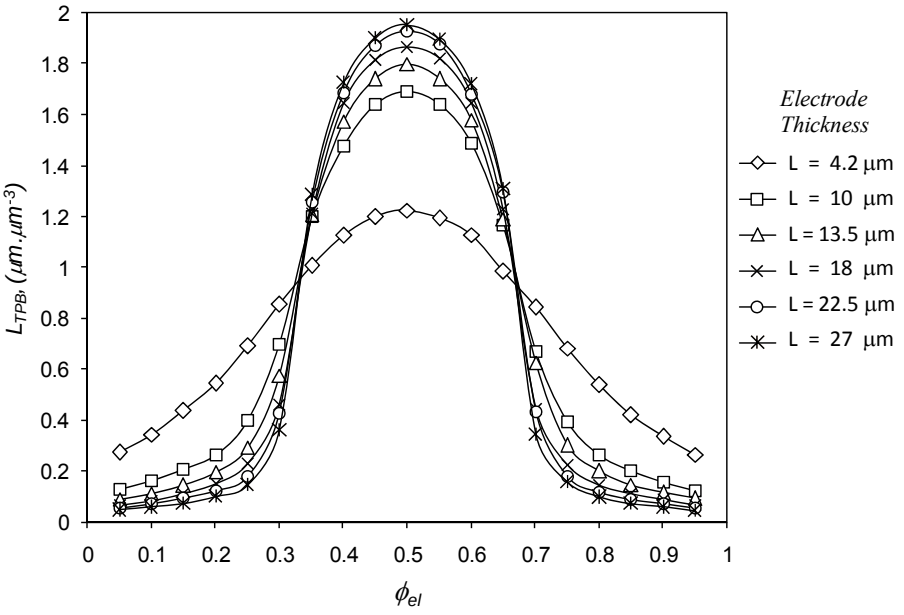

Figure 4.7 The effect of thickness is considerable at low thicknesses but levels off for higher thicknesses suggesting that there should be optimum value for the thickness taking reaction and mass transfer into account.

Ruud *et al.* showed that for a cathode made up of LSM and YSZ, the resistance of the electrode decreased by increasing the thickness up to some thickness and then remained constant [27]. This thickness at which the resistance levels off depends on particles size [28] as well as composition and conductivities of electronic and ionic phases. The results of Ruud *et al.* are justified from geometrical point of view by inspecting Figs. 4.7 and 4.8.

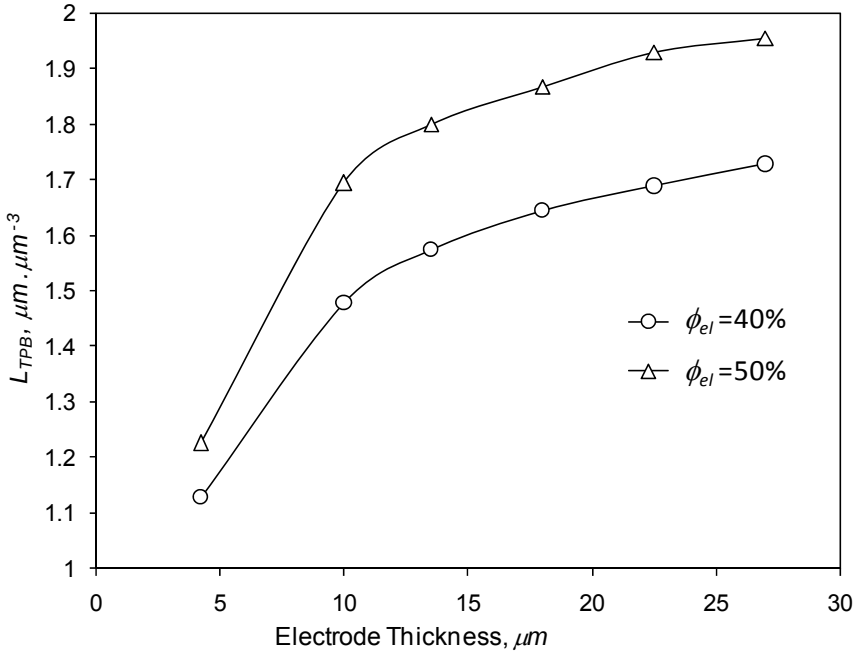

Figure 4.8 Effect of electrode thickness on L_{PBL} of the electrode for electrode composed of particles of the same size.

At low electrode thicknesses the rate at which L_{TPB} increases by increasing thickness is high and it levels off at higher thicknesses and we do not expect much improvement in amount of L_{TPB} for very thick electrodes. Juhl *et al.* reported the same phenomena in their experimental works [29] but the 'critical thickness' in case of their experiments was much lower of about 10 μm which could be the result of presence of relatively thick cathode current collector layer and lower porosity resulting in difficult mass transfer. Although the triple phase boundary length does not change beyond some thicknesses, polarization resistance of the electrode may further increase due to mass transfer and diffusion limitations for high current densities [18]. Fig. 4.9 shows how the volume percent of isolated

particles change with electrode composition. At very low concentrations of electron conductor in the electrode, the reaction frontier is at the surface of the electrode and practically bulk of the electrode is made of ion conductors while most of the electron conductor particles at the surface are active which results in very low amount of isolated particles. As ϕ_{el} increases more and more electron conductor particle is introduced to a medium mostly occupied by ion conductors and hence loose connection to their base and therefore amount of isolated clusters increases. This increase continues until the concentration reaches percolation threshold and beyond that most of the isolated electron conductors connect together to form percolating chains and hence volume fraction of isolated clusters drops rapidly.

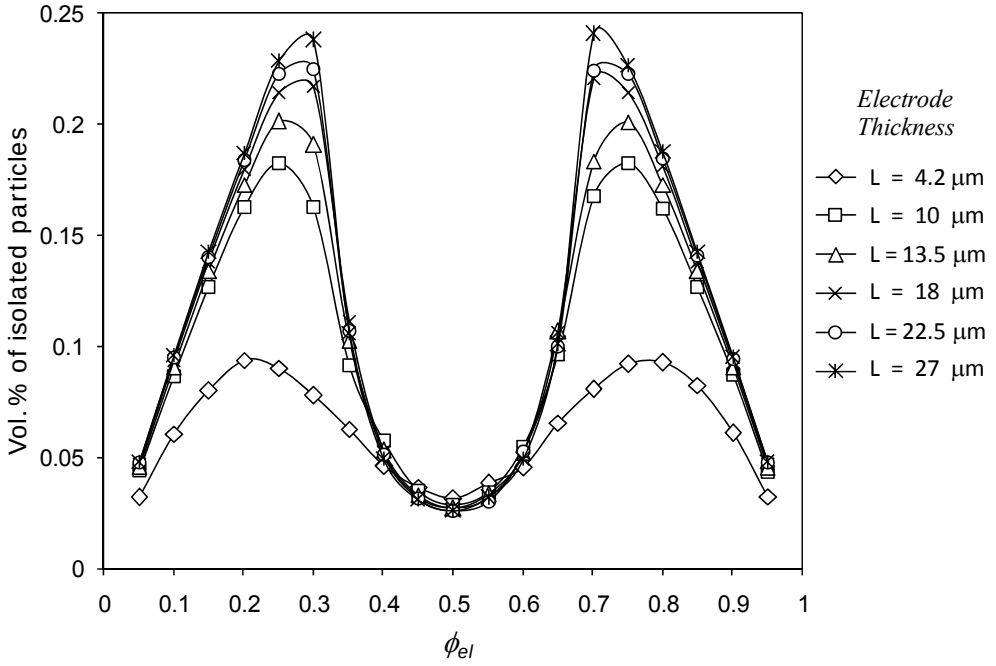

Figure 4.9 Effect of the electrode thickness on amount of isolated clusters inside the electrode. $d_{el} = d_{io} = 1\ \mu m$.

4.4.6 Effect of Particle Size Ratio

Effect of particle size ratio on triple phase boundary length is shown in Fig. 4.10. While for electron and ion conductor particles of the same size maximum triple phase boundary length occurs at $\phi_{el} = \phi_{io} = 0.5$, for d_{el}/d_{io} ratios above unity

the maximum L_{TPB} tends to occur at higher ϕ_{el} values and for size ratios less than unity L_{TPB} maximizes at lower ϕ_{el} values. These results are comparable with the results obtained through models based on percolation theory [8,18,28]. It is important to mention that although size ratios d_{el}/d_{io} = 2 and d_{el}/d_{io} = 0.5 result in almost the same optimum triple phase boundary length; the second case is more favoured from overall polarization point of view. Ionic conductivities of typical ion conductors like YSZ is very small compared to electron conductivity of electron conductors and hence having more conduction path for ions by increasing volume fraction of ion conductor (lower ϕ_{el}) will decrease the polarization resistance, resulting in better cell performance.

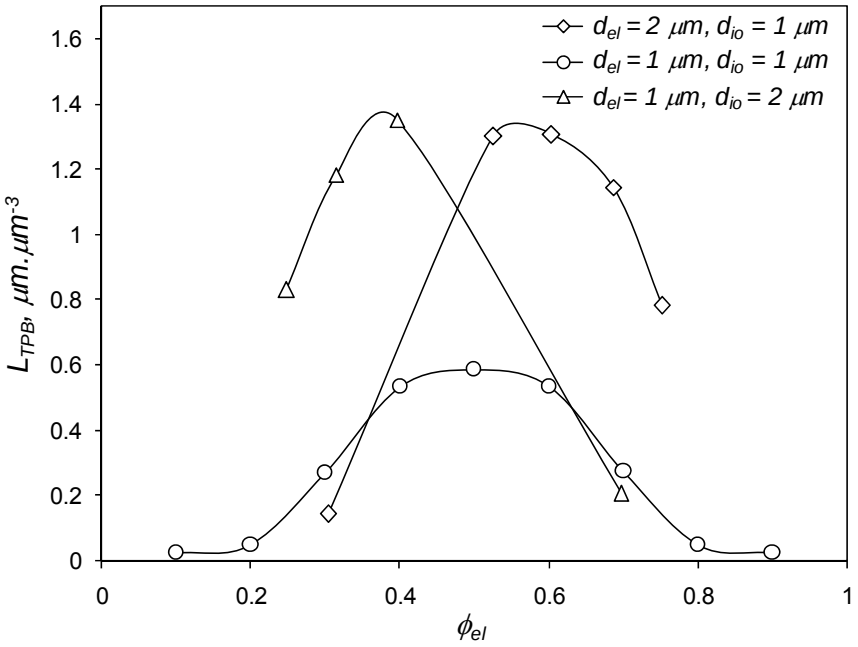

Figure 4-10 Dependence of TPBL and volume fraction of ion conductor particles for different values of particle size ratio. Average electrode thickness is 30 μm.

4.5 Concluding Remarks

In the this chapter we have developed a three-dimensional model to investigate the microstructure of solid oxide fuel cell electrodes and its characterization in terms of triple phase boundary length. While models based on percolation theory

ignore the inhomogeneous nature of composite electrode structure and most of the models based on random packing fail to capture the real randomness of the electrode structure or only consider the case of electron and ion conductor particles of the same size, in this work we have built a realistic geometrical model of the micro structure with as few assumptions as possible. Future work in the next chapter will involve simulation of the electrochemical and ohmic behavior of the electrode.

References

[1] A. Abbaspour, K. Nandakumar, J. Luo, and K. T. Chuang, J. Power Sources 161 (2006) 965.

[2] S. Sunde, J. Electrochem. Soc. 142 (1995) L50.

[3] D. G. Han and G. M. Choi, Solid State Ionics, 106 (1998) 71.

[4] Y. Ji, K. Yuan, and J. N. Chung, J. Power Sources, 165 (2007) 774.

[5] S. Sunde, J. Electrochem. Soc. 143 (1996) 1123.

[6] S. Sunde, J. Electrochem. Soc. 143 (1996) 1930.

[7] L. C. R. Schneider, C. L. Martin, Y. Bultel, D. Bouvard, and E. Siebert, Electrochim. Acta, 52 (2006) 314.

[8] P. Costamagna, P. Costa, and V. Antonucci, Electrochim. Acta 43 (1998) 375.

[9] J. Abel, A. A. Kornyshev, and W. Lehnert, J. Electrochem. Soc. 144 (1997) 4253.

[10] H. G. Ballesteros, L. A. Fernandez, V. Martin-Mayor, A. M. Sudupe, G. Parisi, and J. J. Ruiz-Lorenzo, J. Phys. A: Math. Gen. 32 (1999) 1.

[11] C. D. Lorenz and R. M. Ziff, J. Phys. A: Math. Gen. 31 (1998) 8147.

[12] K. D. Gibson and H. Scheraga, J. Phys. Chem. 91 (1987) 4121.

[13] K. D. Gibson and H. A. Scheraga, Mol. Phys. 62 (1987) 1247.

[14] S. H. Chan, K. A. Khor, and Z. T. Xia, J. Power Sources 93 (2001) 130.

[15] B. Kenney and K. Karan, Solid State Ionics, 178 (2007) 297.

[16] H. Fukunaga, M. Ihara, K. Sakaki, and K. Yamada, Solid State Ionics, 86-88 (1996) 1179.

[17] K. Sasaki, J. -P. Wurth, R. Gschwend, M. Godickemeier, and L. J. Gauckler, J. Electrochem. Soc. 143 (1996) 530.

[18] S. H. Chan, X. J. Chen, and K. A. Khor, J. Electrochem. Soc. 151 (2004) A164.

[19] H. Song, W. Kim, S. Hyun, and J. Moon, J. Electroceram. 17 (2006) 759.

[20] H. J. Cho and G. M. Choi, J. Power Sources, 176 (2008) 96.

[21] S. P. Jiang, P. J. Callus, and S. P. S. Badwal, Solid State Ionics 132 (2000) 1.

[22] M. Ni, M. K. H. Leung, and D. Y. C. Leung, J. Power Sources, 168 (2007) 369.

[23] S. H. Chan and Z. T. Xia, J. Electrochem. Soc. 148 (2001) A388.

[24] F. Zhao and A. V. Virkar, J. Power Sources, 141 (2005) 79.

[25] V. A. C. Haanappel, J. Mertens, D. Rutenbeck, C. Tropartz, W. Herzhof, D. Sebold, and F. Tietz, J. Power Sources 141 (2005) 216.

[26] D. H. Jeon, J. H. Nam, and C. Kim, J. Electrochem. Soc. 153 (2006) A406.

[27] J. A. Ruud, T. Striker, V. Midha, B. N. Ramamurthi, A. L. Linsebigler, and D. J. Fogelman, Ceram. Eng. Sci. Proc. 25 (2004) 251.

[28] X. J. Chen, S. H. Chan, and K. A. Khor, Electrochim. Acta 49 (2004) 1851.

[29] M. Juhl, S. Primdahl, C. Manon, and M. Mogensen, J. Power Sources 61 (1996) 173.

Chapter 5:

Three-Dimensional Random Resistor-Network

5.1 Introduction

Due to the composite nature of the electrode, formation of TPB inside the bulk of electrode and the overall performance of SOFC is influenced by various geometrical factors as well as electrochemical properties of materials forming the electrode and transport characteristics of the media [1-9]. That is why the optimization of electrode structure and material is very important and many studies are being conducted to develop an electrode structure which maximizes electrode performance and minimizes losses [10-15]. Due to the structural complexity of the electrode and the role of different phenomena on the overall performance, detailed simulation of electrode performance is computationally very expensive.

Early attempts to model SOFC electrodes were mostly based on percolation theory and Monte-carlo simulations [1,7,16-18]. Despite the ability of these models in predicting the composite electrode performance, they must be used inside percolation threshold and they underestimate the amount of TPB. This is because these models ignore TPBs made between short chains of electron and ion

conductors that do not go all the way from one end of the electrode (current collector) to the other end (electrolyte)[16].

With the development of fast computers, more detailed and computationally demanding models have recently been considered. These models are based on two or three dimensional packing of particles as electron or ion conductors [9,11,13,19-21]. Our first work [11] was a 2D model of circles to simulate the distribution of TPBs inside the electrode and revealed that the electrode structure is not homogeneous for electrochemical reactions. The effect of LSM and YSZ conductivities and mass transfer coefficient on overall polarization resistance was studied and it was shown that while for low ionic resistance, all TPBs inside the electrode have almost the equal amount of contribution to current generation, for high ionic resistance TPB locations near electrolyte are more favoured and current generation near current collector is small. The second work [9] was a more realistic case of 3D electrode simulation. The effect of LSM and YSZ volume percentages, particle size, and particle size ratio and electrode thickness was studied on the amount and distribution inside the electrode.

Schneider *et al.* [19,20] used a 3D packing of mono-sized particles and the resistor-network model to model the performance of SOFC electrodes. In their analysis however; linear form of Butler-Volmer equation was considered to account for charge-transfer process at TPB. This simplification limits the validity of the results to low current densities. Unlike this group, Koyama *et al.* used distribution of particle size in their packing but they averaged properties over transverse sections parallel to the electrolyte [13]. Sintering is usually accounted by enlarging particles to create a certain degree of overlap between adjacent particles [9,13,19]. Kenney *et al.* performed a geometrical assessment of TPB length, contact area and pore size for random packing of particles [21]. Their results showed that for porosities larger than 25%, over 99% of pores belong to percolating network which is believed to guarantee negligible mass transfer resistance [7,12].

Due to the importance of TPB length in the performance of the electrode, most of the modeling work mentioned above aimed at relating the effect of geometrical parameters on TPB length. TPB length however, is not the only important parameter [22]. Maximizing TPB guarantees that there is maximum amount of reaction sites available for charge-transfer process while overall performance depends on electrical, electrochemical and transport characteristics of electrode material [6,10,18] as well as spatial distribution of TPB [9,11].

In this chapter, random packing of particles is used to model SOFC composite electrodes. Geometrical analysis of the model has been addressed in the previous chapter [9] and this chapter focuses on electrochemical performance of the model electrode. Random resistor-network model has been used to obtain current-overpotential characteristics but unlike other models [19,20,23] the analysis is not restricted to ohmic and linear expression for charge-transfer equation and a complete analysis has been conducted.

5.2 Description of the Model

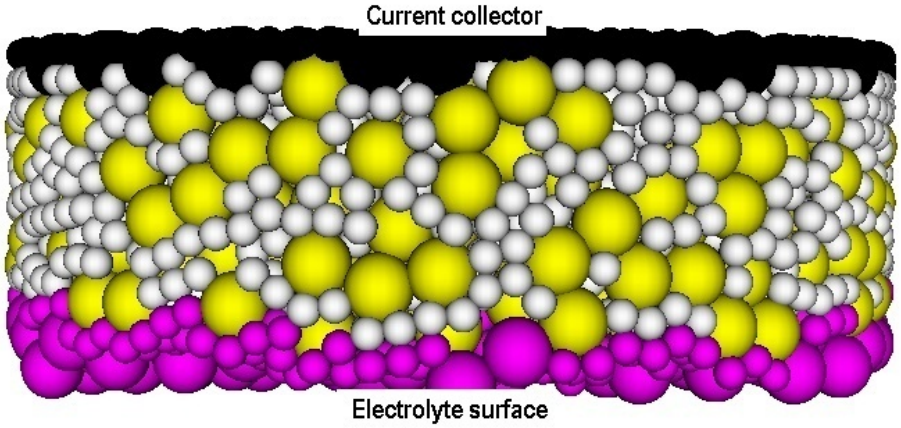

Figure 5.1 Composite electrode created in the computer. White particles are electron conductors while yellow particles represent ion conductors. Bottom layer is electrolyte surface made of ion conductors while top layer is totally electron conductor and acts as current collector.

The detailed description of the model has been given in previous chapter which deals with structural and geometrical aspects. SOFC electrode is modeled by random packing of LSM and YSZ spherical particles of different or same size.

The electrode components or spheres are added to the electrode by collision detection and location optimization and then the particles are enlarged to certain extent [16] to create enough contact area. Fig. 5.1 shows a typical model electrode. Top and bottom layers are current collector and electrolyte layer.

Void volume is calculated by subtracting the total volume of spheres after expansion from the apparent volume of the electrode considering the overlapped volume of two or three particles [24,25] as shown in Figs. 5.2a and 5.2b. It is very unlikely that four particle have common volume of intersection. Depending on size ratio r_{io}/r_{el}, porosities of 23-26 % were obtained and although these are believed to be enough to guarantee negligible mass transfer effects [7,12]; porosity was increased to 30% by introducing some void particles. Area and perimeter of intersection is also calculated and stored for each particle. Sintering theory is vague in many aspects and is too complicated and costly to implement for every single contact in this model [26] and therefore calculations of Fig. 5.2c is used to calculate contact area and perimeter. This simplification however; will slightly underestimate TPB [26,27]. Apart of being potential TPBs, contact areas will be used in resistor network model to calculate flow of electronic or ionic current from one particle to another one.

Random resistor network model as shown in Fig. 5.3 is used to simulate electron and ion conduction as well as charge-transfer process. Electron and ion transport inside LSM and YSZ is considered to be ohmic. Bond resistance, R_b (R_{el} or R_{io} in Fig. 5.3) is calculated using the approximation of Carslaw and Jaeger [28] for heat transfer:

$$R_b = R_{b,c}\frac{\pi}{4}\left(\frac{r_c}{r_p}\right)^{-1} \tag{5.1}$$

Where r_c and r_p refer to contact radius and particle radius and $R_{b,c}$ is the electric resistance of equivalent cylinder from the center of the particle to contact point:

$$R_{b,c} = \frac{l}{kA_c} \tag{5.2}$$

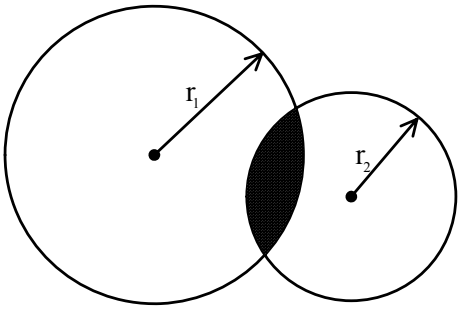

a) Overlap between two particles

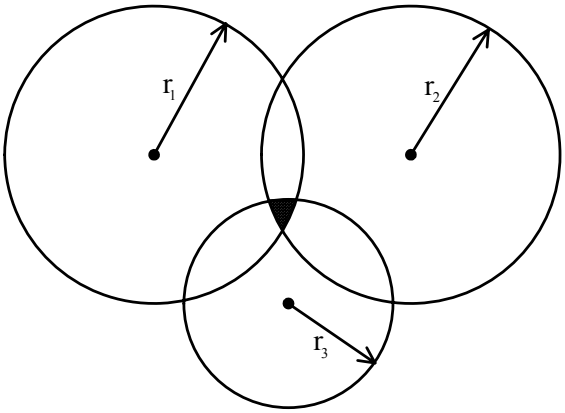

b) Overlap between three particles

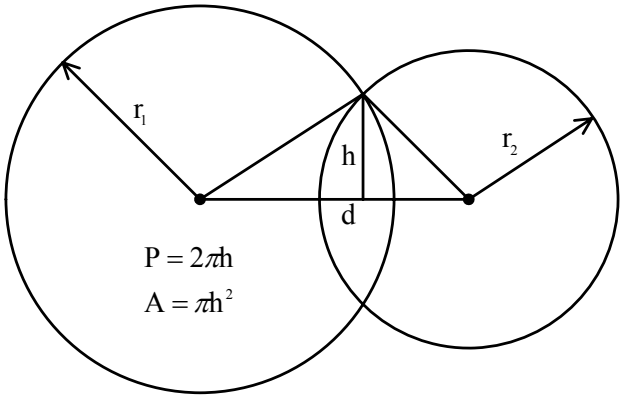

c) Calculation of contact area and perimeter

Figure 5.2 Volume of intersection between: (a) two particles and (b) three particles. (c) Calculation of L_{TPB} and interfacial area between contacting particles

In this equation l is the perpendicular distance from center of the particle to contact point, k is electronic or ionic conductivity of LSM or YSZ and A_c is contact area. Argento *et al.* [29] argued that coefficient in Eq. 5.1 is 0.899 for r_c/r_p less than approximately 0.33. Since r_c/r_p for our modeling is typically 0.4-0.5, Eq. 5.1 was used. Contact resistance between same particles or R_c was set to zero in

the current analysis due to lack of experimental information, but the model is capable of incorporating those effects.

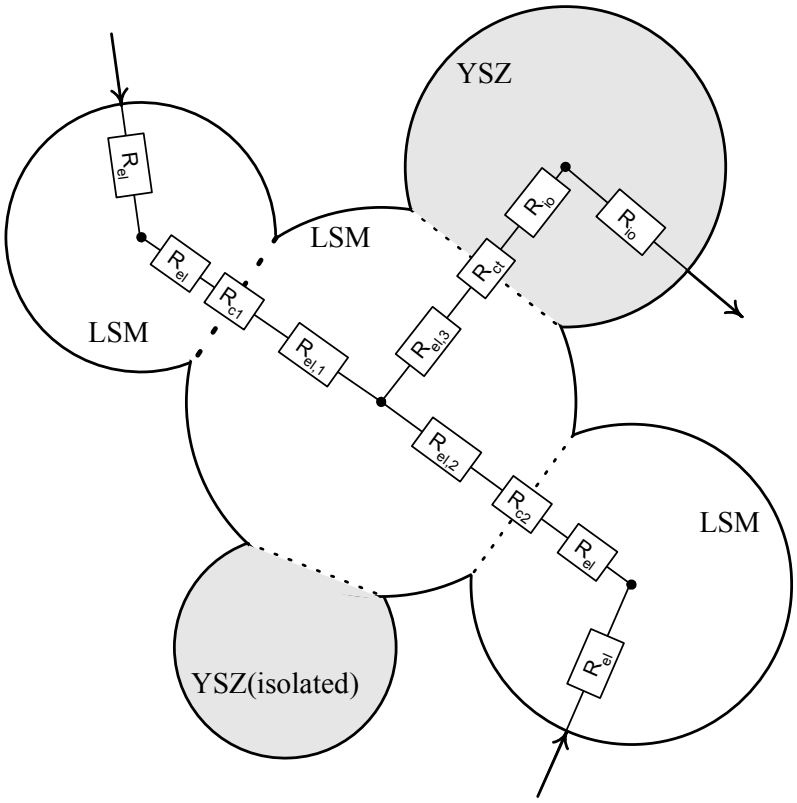

Figure 5.3 Development of random resistor network model for the electrode Composite electrode created in the computer.

Electrochemical reactions that take place on TPB inside the cathode (denoted by nonlinear resistor R_{ct} in Fig. 5.3) are expressed by the general form of Butler-Volmer equation:

$$i = i_0\left[\frac{C_O}{C_O^*}e^{-\alpha f\eta} - e^{(1-\alpha)f\eta}\right] \tag{5.3}$$

Where i_0 is exchange current density, η is overpotential and C_o/C_o^* indicates the mass transfer effect which is set equal to unity (negligible diffusion resistance) due to the existence of enough porosity in the electrode structure. R_{ct} is calculated implicitly using Newton's method as will be explained later in this chapter. Numerical values of i_0 and other constants used in this simulation are shown in Table 5.1.

Table 5.1 Values of constants

Parameter	Value	Unit	Reference
ρ_{el}	190	Ω.μm	[7]
ρ_{io}	10^5	Ω.μm	[7]
i_0	2000	$A.m^{-2}$	[7]
T	1073	K	-
ε	30 %		-

Unless the particle is isolated, for each particle in the packing a potential at the particle center is assigned as well as a potential for each contact point. The number of these contact potentials varies for each particle depending on its coordination number. There is also a current associated with each contact point. Isolated particles are completely ignored in electrochemical calculations but they are considered in porosity calculations. Ohm's law and conservation of current governs current flow within particles. For i^{th} particle:

$$\sum_{j=1}^{n} I_{ij} = 0 \tag{5.4}$$

$$V_{i0} - V_{ij} = I_{ij} R_{ij} \quad , \quad j = 1 \ldots n \tag{5.5}$$

Where n is the coordination number of the i^{th} particle. Potentials at two sides of a contact point between particles of the same type are set equal, implying that contact resistance is assumed to be zero. Potentials at two sides of TPB are related using the charge-transfer equation (Eq. 5.3). For a particle with coordination number equal to 6, there will be 13 unknowns and 13 linear and nonlinear equations. These equations include potential at the center of each particle, potentials at contact points and currents flowing from each contact points. A random packing of 20,000 particles thus represents a problem of roughly about 260,000 unknowns. Because each equation has at most 3 unknowns (two potentials and one current), using dense matrix storage is inefficient if not impossible and therefore sparse matrix storage was used to store coefficients. "Coordinate" type of storage format was used to represent the dense matrix of coefficients in the form of sparse matrix. Coordinate storage format needs a vector to represent column numbers of nonzero elements; another vector for row

numbers and a third vector for their value. This transformation reduced the memory storage requirement for system of equations from enormous amount of more than 500 GB to less than 15 MB. System of linear and nonlinear equations was then solved using Newton's algorithm. Since there are nonlinear equations involved in a random manner, computation process is complex. Matrix of semi-coefficients is formed for those unknowns involved in linear equations Eq. 5.4 and Eq. 5.5 and for nonlinear parts a tag was placed so that the code knows the space is involved in a nonlinear equation. Coefficients belonging to linear equations directly make the corresponding members of the Jacobian matrix, J(x). For all nonlinear members, Jacobian is calculated using Butler-Volmer equation. To save memory and speed up the solution process Gaussian elimination method with partial pivoting was used in MATLAB to calculate perturbation vector $\Delta x = [J(x)]^{-1} f(x)$, where $J(x)$ is the Jacobian matrix and $f(x)$ is the vector of linear and nonlinear equations.

5.3. Results and Discussion

5.3.1 Dispersion Studies

Packing of LSM, YSZ and void spherical particles was produced by collision detection and location optimization to produce model disk shaped electrode. Each particle is treated as an independent object with all characteristics and capabilities (properties and methods in object oriented design terms). Electrode diameter (D), thickness (L) and composition (ϕ) were set during packing generation. Experimentally electrode diameter has no effect on the performance and it is just a matter of size and capacity of the cell. The reason is that even for very small samples the ratio L/D is so small that wall effects are negligible. In modeling however; it is very difficult, if not impossible, to model electrode with close to real L/D ratios and that is why most of the researchers in this area take a small diameter electrode and impose cyclic boundary conditions at the wall [18,19] implying infinite diameter. This usually underestimates L_{TPB} especially for thick

samples. Furthermore, due to random nature of the packing, L_{TPB} results calculated for small electrodes are more disperse giving same set of inputs; which questions the reliability of modeling. Due to computational limitations however; it is necessary to find a minimum reliable size of the electrode for the modeling purpose. Fig. 5.4 shows series of modeling done for various electrode size and same input parameters.

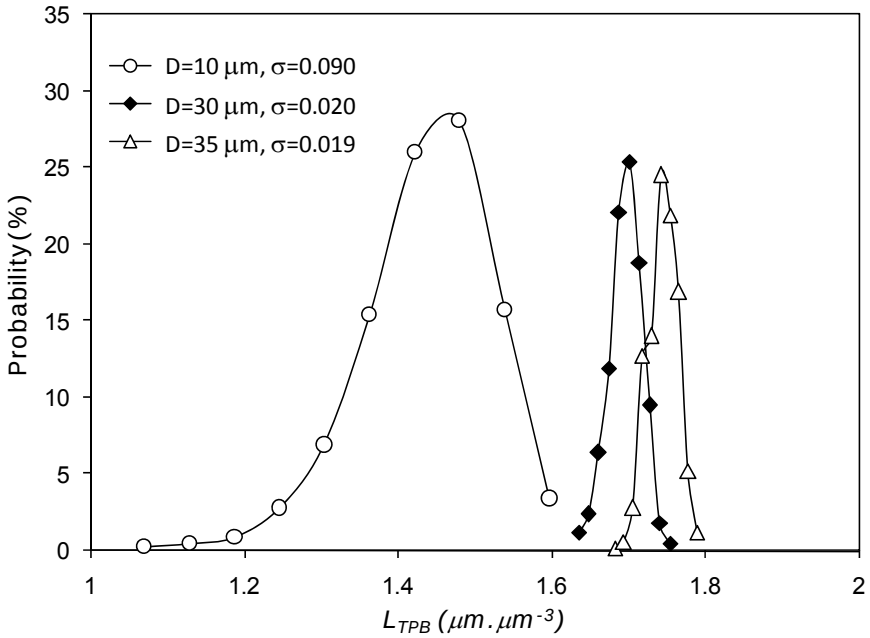

Figure 5.4 Distribution of L_{TPB} results for various electrode sizes having a population of 1000 simulation for each size. Particles are 1 μm in size and electrode thickness is 15 μm.

As it can be seen, increasing the diameter of the electrode results in less disperse data for L_{TPB} and slight increase in mean L_{TPB}. For D=30 μm and beyond, standard deviation of the results are very small and difference in mean L_{TPB} values become negligible. The reason for this observation is that at when the diameter of the electrode is increased the wall effects become negligible and more particles have the chance to be part of a percolating cluster which in turn results in higher calculated L_{TPB} and improved distribution. D=30 μm corresponds to almost 700 particles of r=1μm in one layer and therefore for all experiments, the diameter of the electrode was chosen such that the bottom most layer contained a minimum of

700 particles. Calculated values were all averaged over random execution of simulation with the same input parameters and therefore contain randomization errors shown by error bars in some curves indicating standard deviation of randomized data. These errors however are very small and are maximized in the vicinity of percolation threshold (Figs. 5.5a and 5.5b). Error bars are omitted on most of the curves to avoid undue noise and confusion.

5.3.2 Coordination Numbers and Contiguity

Many studies have been conducted recently on the identification of parameters affecting TPB length and on the measurement of L_{TPB} both experimentally [8,30] and from modeling point of view [31,32]. Wilson *et al.* [8] used dual beam FIB-SEM to scan different phases inside SOFC anode and by analyzing the data a value of 4.28×10^{6} $m.cm^{-3}$ was found for L_{TPB}. They showed in their analysis short unconnected segments that belong to isolated clusters. Isolated clusters are those LSM or NiO particles not connected to current collector or YSZ particles not connected to electrolyte. Fig. 5.5a shows how the amount of isolated particles varies inside the cathode and how L_{TPB} maximizes when both LSM and YSZ isolated particles are at their minimum. At low volume fractions of LSM, nearly all YSZ particles are connected but TPB is limited to electrode surface where most of LSM particles are in direct contact with the current collector and hence L_{TPB} is very small. This is the case for compositions with high LSM contents in which electrochemical reaction is confined to electrolyte surface only. This has been demonstrated by two dimensional CFD modeling of electrode in chapter 3 of the current work [11].

Lee *et al.* [33] studied contiguity of different phases and interfacial area showing that Ni-YSZ interfacial area as well as contiguity reach their maximum at NiO:YSZ volume ratios of almost 50%. Contiguity as well as Active LSZ-YSZ interfacial area is directly related to the effective coordination number of particles inside the electrode and for models based on percolation theory coordination number is a key parameter in calculating abovementioned values [1]. Average coordination number in a close packing of mono size particles is believed to be

6.0 [34] and Scott *et al.* [35] obtained a maximum packing density of 0.6366 for close packing of hard spheres.

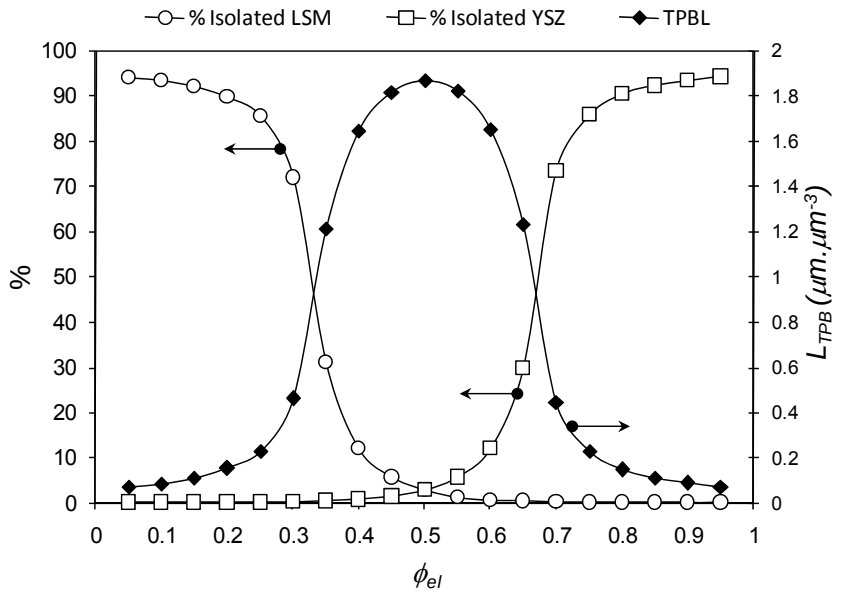

Figure 5.5a Variation of amount of isolated particles and length of TPB with electrode composition for particle size ratio equal to unity.

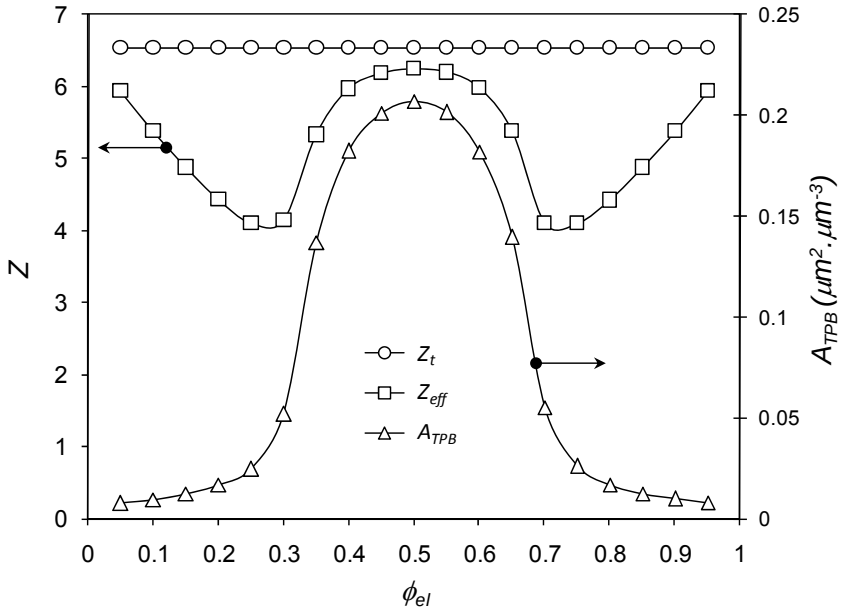

Figure 5.5b Variation of total and effective coordination number and TPB area with electrode composition for particle size ratio of unity.

Fig. 5.5b shows variation of total (Z) and effective (Z_{eff}) coordination number along with active interfacial area for different electrode compositions. Packing density and coordination number right after the packing and before sintering are 60% and 5.01. If sintering or particle enlargement was done, coordination number would have reached to about 7.15 with packing density of about 74.8%. This packing density must be decreased to 70% by voiding some random particles before enlargement. The resulting average coordination number is 6.53, slightly above the value which is usually used in electrode models [1,6].

As it can be seen, Z_{eff} (obtained by excluding isolated particles from the packing) maximizes in two ends and in equal volume fractions. At low LSM compositions, high coordination number corresponds to $Z_{io\text{-}io}$ between YSZ particles and hence this region shows low overall conductivity while at high LSM compositions Z is mostly ascribed to $Z_{el\text{-}el}$ of LSM particles. around 50% volume fraction represents a region where each particle has nearly 3 active sites [9].

5.3.3 Total and Ohmic Resistances

Fig. 5.6 shows the effect of composition on overall polarization resistance, R_p. Even though L_{TPB} is maximum at ϕ_{el}=50% implying maximum available reaction sites and hence minimum charge-transfer resistance; overall polarization ratio is minimized at compositions around ϕ_{el}=40%. The reason for this difference can be found in the difference between electronic resistance of LSM and ionic resistance of YSZ. Typical resistivity for LSM and YSZ reported in the literature are $\rho_{LSM} \approx 190 \Omega.\mu m$ and $\rho_{YSZ} \approx 10^5\ \Omega.\mu m$ respectively [7]. Having ionic resistance of more than 500 times the electronic resistance of LSM, resistance to flow of ions in YSZ phase is more than the resistance to electronic flow in LSM phase. This observation can be better described by inspecting Fig. 5.5a and 5.5b and by considering equation 5.2. Replacing $\rho = 1/k$ in equation 5.2:

$$R_{b,c} = \frac{\rho l}{A_c} \tag{5.6}$$

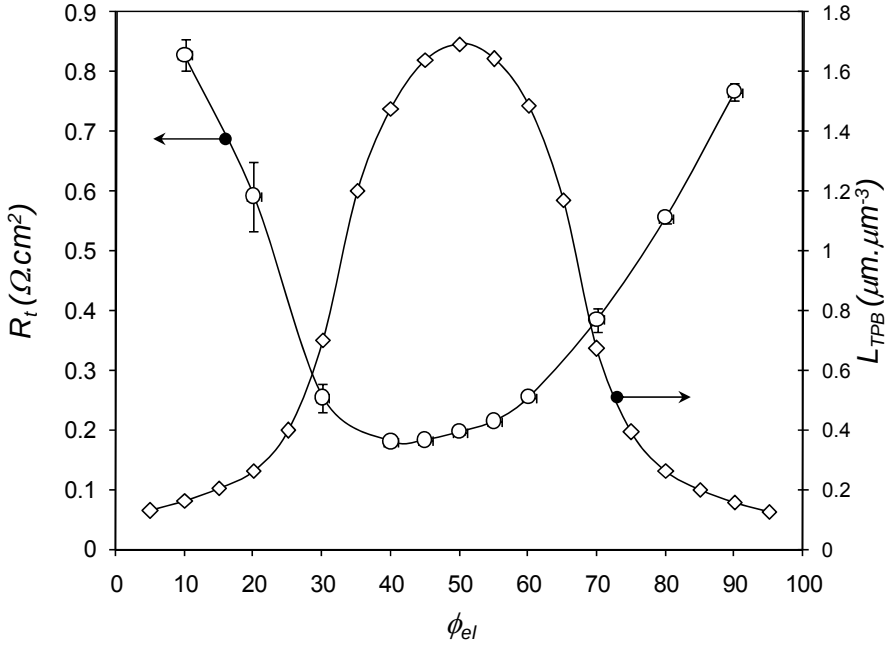

Figure 5.6 Relationship between polarization resistance and L_{TPB} and their dependence on electrode composition.

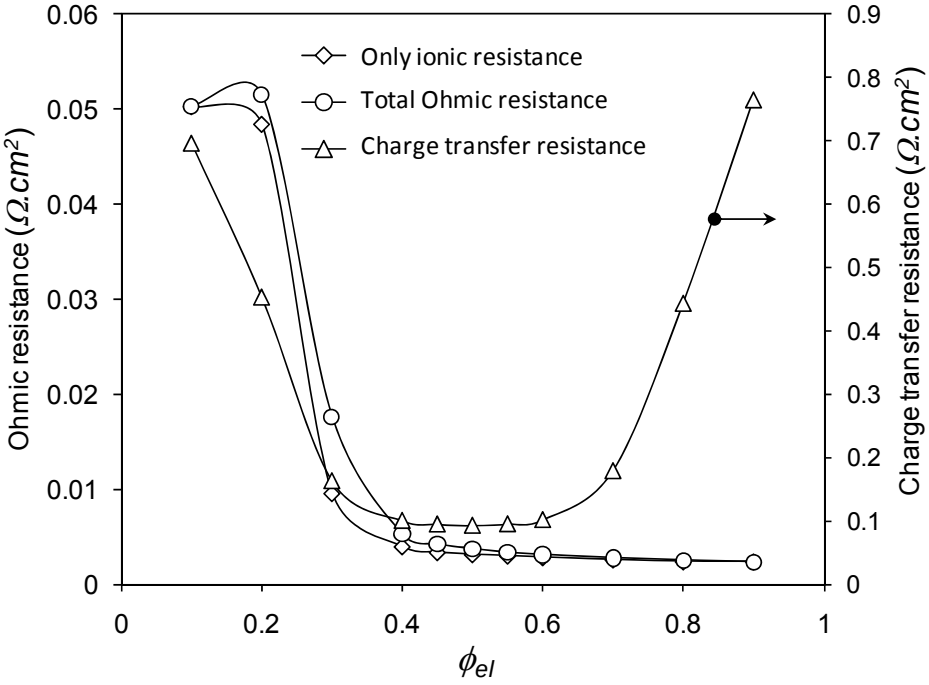

Figure 5.7 Dependence of ohmic and charge-transfer resistance to electrode composition

At low LSM compositions, percentage of isolated YSZ particles is almost zero (Fig. 5.5a) and high Z values can be assigned to contact between YSZ particles ($Z_{io\text{-}io}$). Higher number of contact points results in larger contact area (A_c) and hence lower ohmic resistance (Eq. 5.6). As it can be seen in Fig. 5.7, ohmic resistance of LSM can be ignored compared to ionic resistance of YSZ and total ohmic resistance can be assigned to YSZ phase. Ohmic resistance of the electrode is obtained by putting R_{ct} equal to zero at TPBs [18,36] which in this model translates to choosing exchange current densities large enough to ensure zero R_{ct}. Fig. 5.7 also shows that charge-transfer polarization is symmetric around minimum at 50% volume fraction and follows the trend of L_{TPB} in Fig. 5.5 or 5.6. Sunde [36] used Monte-Carlo simulation and observed similar results for slightly different geometries. Costamagna *et al.* [2] observed minimum polarization resistance below 40% at around 35% of electron conductor particles. This difference however; can be assigned to different particle sizes utilized in the experiments. In the previous chapter it was shown that how different particle sizes for electron and ion conductor can affect TPB.

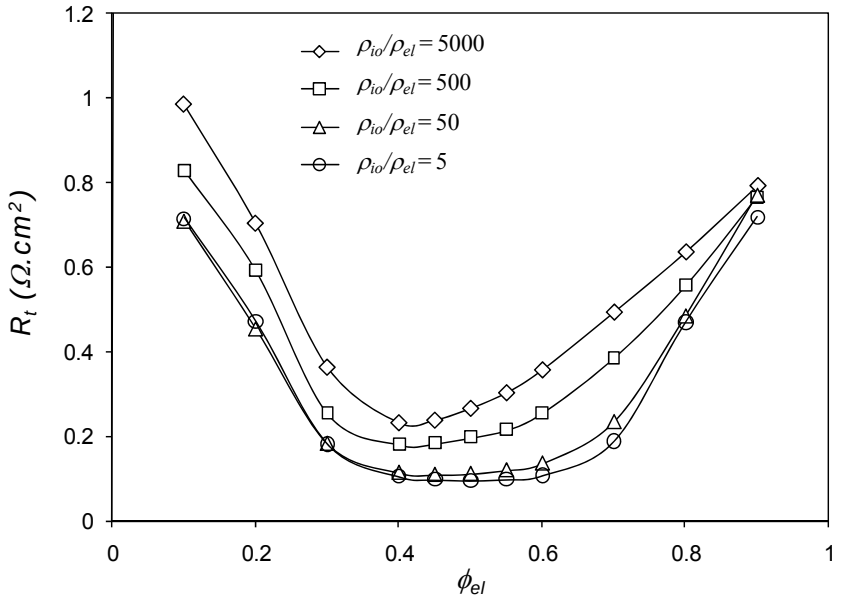

Figure 5.8 Parametric study of the relative amount of ionic and electronic resistances. ρ_{el} is kept at fixed amount of 190 $\Omega.\mu m$ while ρ_{io} has changed to obtain different ratios.

Fig. 5.8 is a parametric study of the effect of electron and ion conductor resistances on total polarization resistances of an electrode. As it can be seen lower ionic resistance gives the curve more symmetric shape with minimum at 50%. This means that when the ohmic resistance of ion conductor media is low, total polarization resistance follows the trend dictated by charge-transfer process which is directly affected by availability of TPB. At higher ionic resistances (higher ρ_{io}/ρ_{el} ratio) however, the minimum of the polarization curve tends to lean towards compositions less than 50% depending on ρ_{io}/ρ_{el} ratio. ρ_{io}/ρ_{el}=500 represents typical case of LSM and YSZ used in the current fuel cell research.

5.3.4 Effect of Electrode Thickness

Another interesting observation is the effect of electrode thickness on the performance of electrode. Length of TPB increases with electrode thickness but the rate of increase declines and beyond a certain thickness there will be no gain in TPB with increased thickness [9]. Work of Chan *et al.* [6,37] based on percolation theory showed that polarization resistance decreases rapidly with increasing thickness and then remains constant after certain thickness. This thickness at which polarization resistance levels off depends on particle size as well as conductivity of material, type of the reaction and mass transfer characteristics of electrode media. For example Xia and co-workers in two different studies reported two different thicknesses of 50 μm and 10 μm [6,37,38]. Fig. 5.9a and b show the results for the effect of thickness obtained by the model. As it is shown in Fig. 5.9a, polarization resistance drops very fast when the thickness changes from 5 μm to 10 μm but beyond that thickness there is a very small improvement in the performance of electrode. Fig. 5.9b shows the results for only one electrode composition (ϕ_{el}=40%, ϕ_{io}=60%). For thicknesses of about 15 μm and above there is no gain in terms of reduction in polarization resistance with increasing the thickness. Furthermore depending on the microstructure of the electrode, increasing the thickness may result in excess mass transfer resistance and tend to increase the overall polarization resistance, a phenomena which is shown by experimental work of Sasaki *et al.* [39].

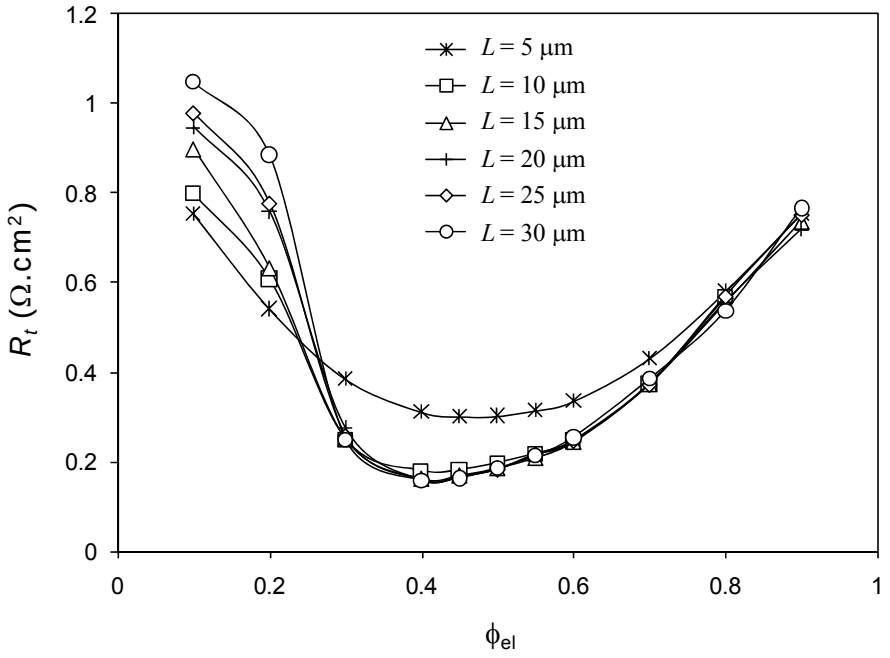

Figure 5.9a Variation of polarization resistance with electrode composition for different thicknesses of the electrode.

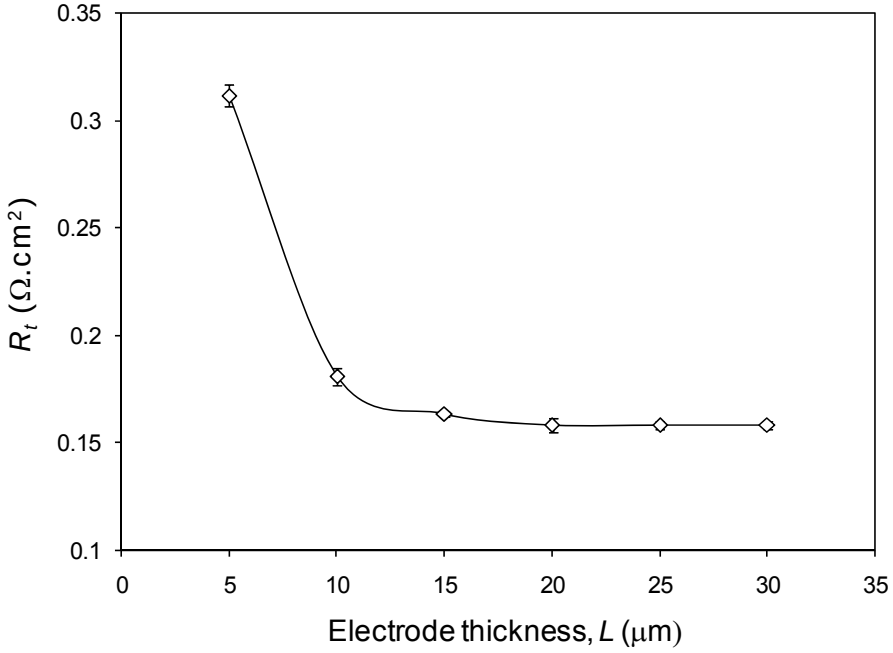

Figure 5.9b Effect of electrode thickness on polarization resistance of the electrode.

5.3.5 Exchange Current Density

Fig. 5.10 is a parametric study of the effect of exchange current density on polarization resistance of cathode. It is clear that decreasing exchange current density will increase polarization resistance, because a major part of polarization resistance comes from the charge-transfer process on TPB. Interesting point however, is the shape of curves as i_0 is increased.

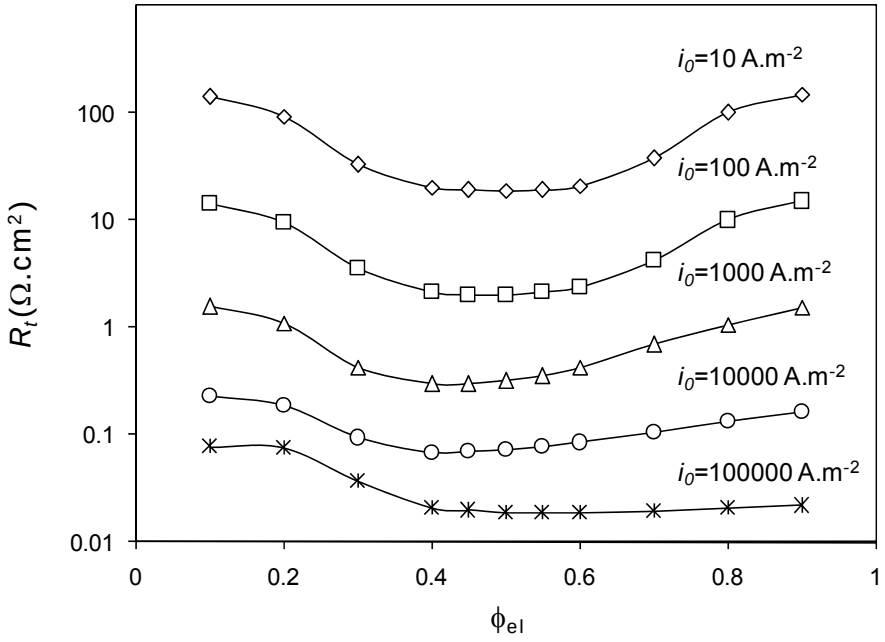

Figure 5.10 Parametric study of the effect of exchange current density on polarization resistance of electrode. Note how the shape of curves changes by increasing exchange current density.

At low exchange current densities, since resistance from charge-transfer process is dominant, the effect of ohmic resistance of LSM and YSZ can be ignored on overall polarization resistance curve and hence curve follows a path dictated by electrochemical reaction which in turn is determined by TPB. Therefore just like L_{TPB} curve on Fig. 5.5, polarization curve is symmetric with minimum point at 50% LSM and YSZ volume fraction. At high exchange current densities however, ohmic effects dominate and polarization resistance curve tends to follow ohmic path by having minimum around 40% LSM volume fraction and

very small slope for volume fractions above 40% which resembles ohmic resistance curves in Fig. 5.7.

5.3.6 Particle Size Ratio

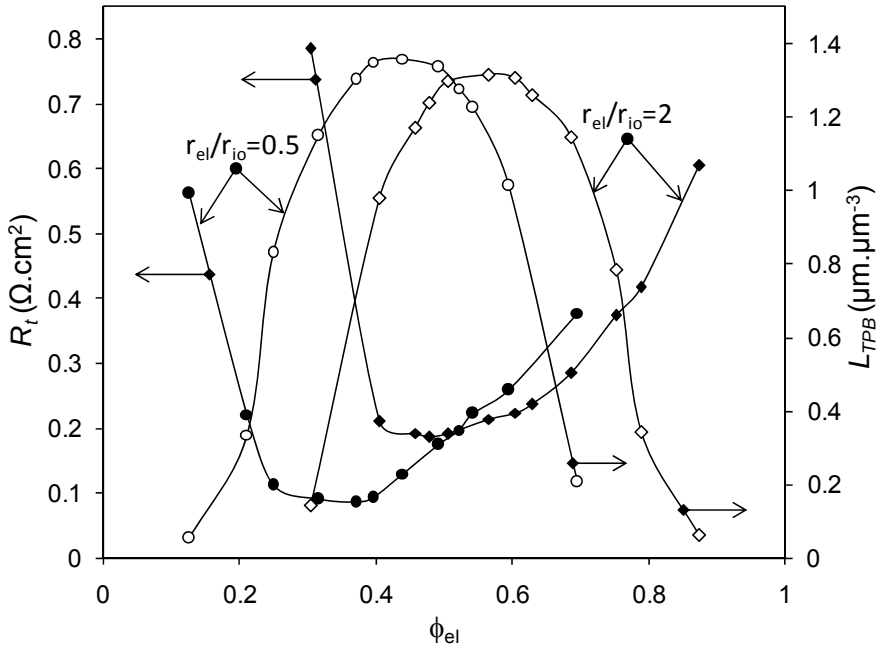

Figure 5.11 Effect of particle size ratio on polarization and L_{TPB}.

Fig. 5.11 shows the effect of particle size ratio of LSM and YSZ on total polarization and L_{TPB}. It was shown elsewhere that maximum L_{TPB} moves to higher ϕ_{el} values with increasing r_{el}/r_{io} [9,12]. This can be seen by comparing L_{TPB} curve of Fig. 5.6 with Fig. 5.11. As it can be seen, while for particles of the same size minimum polarization is observed at ϕ_{el}=40%, it is slightly more than 40% for r_{el}/r_{io} more than unity and less than 40% for r_{el}/r_{io} less than unity. This observation has been proven by experiment [18]. Close inspection of Fig. 5.11 also reveals that although r_{el}/r_{io}=0.5 and r_{el}/r_{io}=2 produce the same amount of L_{TPB} in the electrode; the former is more beneficial in a sense that it produces lower polarization. This means that it is always better from electrochemical point of view to choose electron conductor particles smaller than ion conductors provided that an appropriate amount of ϕ_{el} can be applied based on Fig. 5.11. This analysis

however, does not include material stability and thermal compatibility issues which might instruct otherwise for electrode composition.

5.4. Concluding Remarks

Although the model assumes a simple spherical shape for particles in composite solid oxide fuel cell electrodes, its ability in creating random structures with controlled porosities and with particles of different size, makes the model very useful in predicting experimental data. Furthermore it creates a detailed framework so that simple measurements can be related to less accessible microstructure and different behaviors can be interpreted and justified. In addition, object oriented design of the code made it very efficient, user friendly and easy to understand while making modifications and changes very straightforward. In contrast with similar works in the area, the model uses general Butler-Volmer equation (Eq. 5.3) rather than just opting to simplified linear form. This makes the analysis more reliable [7] but at the same time increases the computation load.

References

[1] P. Costamagna, P. Costa, and V. Antonucci, Electrochim. Acta 43 (1998) 375.

[2] P. Costamagna, M. Panizza, G. Cerisola, and A. Barbucci, Electrochim. Acta 47 (2002) 1079.

[3] M. J. L. Ostergard, C. Clausen, C. Bagger, and M. Mogensen, Electrochim. Acta 40 (1995) 1971.

[4] D. G. Han and G. M. Choi, Solid State Ionics, 106 (1998) 71.

[5] A. V. Virkar, J. Chen, C. W. Tanner, and J. Kim, Solid State Ionics 131 (2000) 189.

[6] S. H. Chan, X. J. Chen, and K. A. Khor, J. Electrochem. Soc. 151 (2004) A164.

[7] S. H. Chan, K. A. Khor, and Z. T. Xia, J. Power Sources 93 (2001) 130.

[8] J. R. Wilson, W. Kobsiriphat, R. Mendoza, H. Chen, J. M. Hiller, D. J. Miller, K. Thornton, P. W. Voorhees, S. B. Adler, and S. A. Barnett, Nat. Mater. 5 (2006) 541.

[9] A. Ali, X. Wen, K. Nandakumar, J. Luo, and K. T. Chuang, J. Power Sources 185 (2008) 961.

[10] Y. Ji, K. Yuan, and J. N. Chung, J. Power Sources, 165 (2007) 774.

[11] A. Abbaspour, K. Nandakumar, J. Luo, and K. T. Chuang, J. Power Sources 161 (2006) 965.

[12] B. Kenney and K. Karan, Solid State Ionics, 178 (2007) 297.

[13] M. Koyama, H. Tsuboi, N. Hatakeyama, A. Endou, H. Takaba, M. Kubo, C. A. Del Carpio, and A. Miyamoto, ECS Trans. 7 (2007) 2057.

[14] H. Fukunaga, M. Ihara, K. Sakaki, and K. Yamada, Solid State Ionics 86-88 (1996) 1179.

[15] H. Fukunaga, M. Ishino, and K. Yamada, Electrochem. Solid-State Lett. 10 (2007) B16.

[16] S. Sunde, J. Electrochem. Soc. 142 (1995) L50.

[17] A. M. Svensson, S. Sunde, and K. Nisancioglu, Solid State Ionics 86-88 (1996) 1211.

[18] S. Sunde, J. Electroceram. 5 (2000) 153.

[19] L. C. R. Schneider, C. L. Martin, Y. Bultel, D. Bouvard, and E. Siebert, Electrochim. Acta, 52 (2006) 314.

[20] L. C. R. Schneider, C. L. Martin, Y. Bultel, L. Dessemond, and D. Bouvard, Electrochim. Acta, 52 (2007) 3190.

[21] B. Kenney, M. Valdmanis, C. Baker, J. G. Pharoah, and K. Karan, J. Power Sources 189 (2009) 1051.

[22] J. H. Nam and D. H. Jeon, Electrochim. Acta 51 (2006) 3446.

[23] D. H. Jeon, J. H. Nam, and C. Kim, J. Power Sources 139 (2005) 21.

[24] K. D. Gibson and H. A. Scheraga, Mol. Phys. 62 (1987) 1247.

[25] K. D. Gibson and H. Scheraga, J. Phys. Chem. 91 (1987) 4121.

[26] R. L. Coble, J. Amer. Ceram. Soc. 41 (1958) 55.

[27] C. L. Martin, L. C. R. Schneider, L. Olmos, and D. Bouvard, Scr. Mater. 55 (2006) 425.

[28] H. S. Carslaw and J. C. Jaeger, Conduction of Heat in Solids, Oxford University Press, New York, 1959.

[29] C. Argento and D. Bouvard, Int. J. Heat Mass Tran. 39 (1996) 1343.

[30] J. R. Wilson and S. A. Barnett, Electrochem. Solid-State Lett. 11 (2008) B181.

[31] V. M. Janardhanan, V. Heuveline, and O. Deutschmann, J. Power Sources 178 (2008) 368.

[32] W. Zhu, D. Ding, and C. Xia, Electrochem. Solid-State Lett. 11 (2008) B83.

[33] J. -H. Lee, H. Moon, H. -W. Lee, J. Kim, J. -D. Kim, and K. -H. Yoon, Solid State Ionics 148 (2002) 15.

[34] D. Bouvard and F. F. Lange, Acta Metall. Mater. 39 (1991) 3083.

[35] G. D. Scott and D. M. Kilgour, J. Phys. D 2 (1969) 863.

[36] S. Sunde, J. Electrochem. Soc. 143 (1996) 1930.

[37] X. J. Chen, S. H. Chan, and K. A. Khor, Electrochim. Acta 49 (2004) 1851.

[38] Z. T. Xia, S. H. Chan, and K. A. Khor, Electrochem. Solid-State Lett. 7 (2004) A63.

[39] K. Sasaki, J. Wurth, R. Gschwend, M. Godickemeier, and L. J. Gauckler, J. Electrochem. Soc. 143 (1996) 530.

Chapter 6:

General Discussion, Validation, and Recommendations

6.1 Introduction

Although the results of the model obtained in the previous chapters confirm the experimental data in the trend and magnitude, the main goal of chapters 3 through 5 however, was to introduce the model and show its capability to simulate real SOFC electrodes. Detailed arguments of chapter 2 in introducing and comparing electrode models, showed the merits of the model compared to other models practiced in the field. Since this model is based on real nature of the electrode which is a random mix of electron and ion conductor particles, it can better describe the random behaviour of composite electrodes and inhomogeneous nature of charge-transfer processes occurring within the electrode structure.

6.2 The Nature of Experimental Data

Random nature of the electrode packing requires us to repeat the experiment few times and average the results to get an answer which is statistically significant within acceptable degree of confidence [1]. This problem however, can be alleviated and practically even eliminated by employing big samples as discussed

before [1]. It should be mentioned however that even this apparently shortcoming, is not the problem of the model but characteristics of composite electrodes which can even be observed in experimental data for different samples of the electrode made with precisely controlled condition. The examples of this highly deviant data due to electrode random structure are vast and spread all over SOFC literature. Gong *et al.* investigated the effect of electrode thickness on electrode performance and charge-transfer resistance [2]. While 70% of experimental data follow a reasonable trend also confirmed by the current model and thin film model [3], 30% of points divert from the expected trend and show either very low or very high polarization [2]. Lee *et al*. introduced even a more interesting finding. There is a decrease in electrode conductivity in going from 20 vol.% Ni anode to about 27 vol.% Ni and then conductivity increases abruptly [4]. This behaviour cannot be justified by continuous models [5-8] as they expect a gradual increase in conductivity of the electrode and furthermore Ni concentration may not fall into percolation threshold of the electrode [1]. Assuming all experimental procedure and precaution was precisely followed, current model however predicts the possibility of this observation as formation of isolated islands close to percolation threshold and sudden percolation of those islands discussed before briefly [1,9] and will be seen and explained in Fig. 6.2. For an electrode composed of only ion conductor, the overall conductivity is the effective conductivity of ion conductors. As small amounts of electron conductors are added, due to their small amount the new particles most probably do not contribute to the conductivity but get lost inside the big ocean of ion conductors and form isolated islands. These isolated islands not only do not improve the conductivity but also further hinder the ocean flow by narrowing the flow passage and making straits and hence the conductivity decreases. Muecke *et al*. report conductivity data for different electrode composition which in some cases is more than 300% different for different samples of the same composition [10] which can again be described in the light of randomness of the electrode structure. This discussion is only valid assuming that experimental condition is completely

controlled and all conditions are identical which is expected from any experimental work.

6.3 Comparison with Experimental Findings

6.3.1 Randomness of the Electrode Structure

As it was discussed extensively in chapter 2, this model effectively captures the random nature of composite electrode structure. Although the simple regular spherical shape of electron and ion conductor particles may contrast completely shapeless structure of real composite electrodes, the results of the model showed that it captures the main characteristics of the electrode behaviour. As it was discussed in chapters 4 and 5, the random nature of the packing requires us to repeat the experiment few times to get the results which are statistically credible. Although big enough electrode samples tend to give close to identical results in terms of L_{TPB}, this difference in data among samples can be seen even in real experiments with sample dimensions far bigger than simulation samples. The data are more scattered when electrode composition is around outer boundaries of percolation threshold as shown in Fig. 6.1.

Fig. 6.1 shows coefficient of variance (variance of data divided by average) for a sample electrode with different volumetric compositions. Each data point corresponds to coefficient of variance of 100 random execution of electrode at the same composition and presents coefficient of variance for geometric properties such as L_{TPB} and A_{TPB}. Coefficient of variance for electrochemical data such as polarization is slightly different (with the same trend) as polarization not only depends on the quantity of TPBs but also on the location of TPBs as it was reviewed on chapter 3. Dispersion is maximum around 30 vol. % and 70 vol. % of electron conductor as at this point a slight change in structure may make a fruitful bridge and bring a big isolated island into electrochemical utilization which otherwise will be wasted. Dispersion is also low at both ends of the curve as at these points amount of either electron conductor or ion conductor is so low that in practice only electrode or electrolyte surface contributes to L_{TPB} and therefore

tends to stay constant over different runs of program. Tables 6.1 and 6.2 show 15 program runs randomly selected from the abovementioned 100 runs respectively for 30 vol. % and 50 vol. % electron conductor demonstrating the difference in numerical values for different program execution. Although for most of the results of this thesis, each data point indicates an averaging over about 100 identical runs, statistical analysis showed that only few runs can give satisfactory results with a very narrow confidence interval [1].

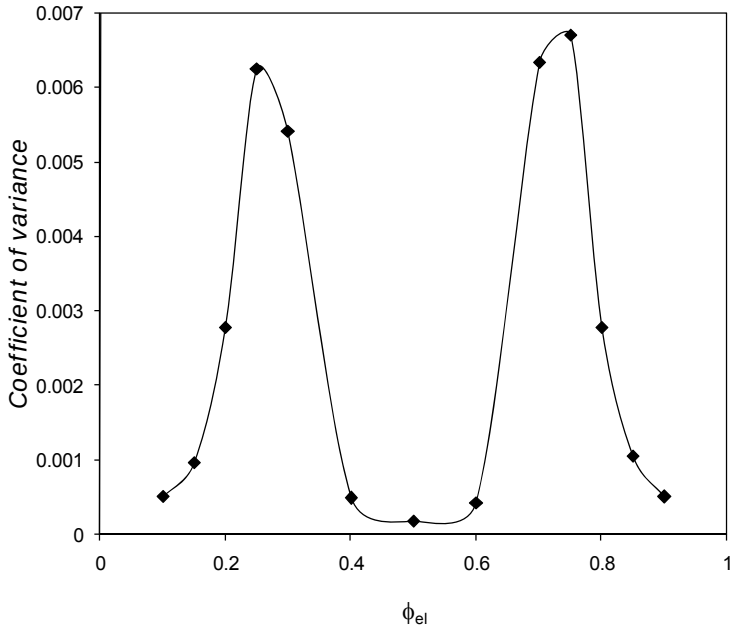

Figure 6.1 Coefficient of variance in data (L_{TPB} for example) from a sample electrode running in different compositions.

6.3.2 Conductivity and Composition

Effect of conductivity on electrode performance has been considered in experimental literature by few groups [10-18]. The details of the dependence of conductivity on electrode thickness have been discussed in chapter 2. The general trend in conductivity change in going from low percentages of electron conductor to higher values is an almost constant value followed by abrupt increase in conductivity at percolation threshold and then following a slightly increasing trend. The sudden increase resembles the transition from conductivity of ion conductor to conductivity of electron conductor.

Table 6.1 Random program runs chosen from 100 random packing to calculate geometrical properties of packing when $\phi_{el} = 0.30$.

#	ϕ_{el}	L_{TPB} ($\mu m.\mu m^{-3}$)	A_{TPB} ($\mu m^2.\mu m^{-3}$)	ε	ϕ_{ap}	$\phi_{a,LSM}$	$\phi_{a,YSZ}$	ϕ_{ip}
40	0.3002	0.7544	0.0750	0.2941	0.4988	0.4812	0.5064	0.1556
25	0.3002	0.9104	0.0905	0.2941	0.5979	0.5883	0.6021	0.1239
46	0.3002	0.9468	0.0941	0.2941	0.6132	0.6110	0.6141	0.1166
98	0.3002	0.9773	0.0972	0.2941	0.6347	0.6173	0.6422	0.1147
6	0.3002	0.9863	0.0982	0.2941	0.6443	0.6475	0.6429	0.1058
84	0.3002	1.0005	0.0996	0.2941	0.6515	0.6538	0.6505	0.1051
22	0.3002	1.0491	0.1045	0.2941	0.6721	0.6765	0.6702	0.0969
71	0.3002	1.0130	0.1006	0.2941	0.6545	0.6612	0.6517	0.1017
70	0.3002	0.9224	0.0918	0.2941	0.6000	0.5849	0.6065	0.1248
19	0.3002	0.9263	0.0920	0.2941	0.5956	0.6036	0.5921	0.1193
85	0.3002	1.0049	0.0999	0.2941	0.6453	0.6560	0.6407	0.1034
16	0.3002	1.0242	0.1019	0.2941	0.6583	0.6714	0.6527	0.0993
12	0.3002	0.8719	0.0868	0.2941	0.5706	0.5683	0.5716	0.1308
30	0.3002	0.8669	0.0863	0.2941	0.5658	0.5689	0.5645	0.1297
99	0.3002	1.0911	0.1085	0.2941	0.7067	0.7272	0.6979	0.0821

#	$\phi_{i,LSM}$	$\phi_{i,YSZ}$	Z	Z_{eff}	$Z_{LSM\text{-}LSM}$	$Z_{YSZ\text{-}YSZ}$	$Z_{LSM\text{-}YSZ}$	$Z_{YSZ\text{-}LSM}$
40	0.5177	0.0002	6.9484	5.1321	1.2568	4.8068	2.1207	1.0779
25	0.4112	0.0007	6.9484	5.4921	1.5251	4.7953	2.6093	1.2792
46	0.3884	0.0000	6.9484	5.5694	1.5718	4.7912	2.7158	1.3280
98	0.3821	0.0000	6.9484	5.6109	1.5439	4.7819	2.8081	1.3691
6	0.3514	0.0005	6.9484	5.7019	1.7107	4.8205	2.8633	1.3652
84	0.3462	0.0017	6.9484	5.6920	1.6583	4.7899	2.8872	1.3937
22	0.3229	0.0000	6.9484	5.7798	1.7062	4.7743	3.0501	1.4446
71	0.3383	0.0002	6.9484	5.7345	1.7022	4.7951	2.9351	1.4101
70	0.4146	0.0005	6.9484	5.4778	1.4567	4.7802	2.6338	1.2926
19	0.3964	0.0005	6.9484	5.5303	1.5541	4.7909	2.6731	1.2982
85	0.3434	0.0005	6.9484	5.7137	1.6976	4.7897	2.9129	1.3972
16	0.3286	0.0010	6.9484	5.7521	1.7181	4.7931	2.9522	1.4231
12	0.4305	0.0022	6.9484	5.4099	1.4852	4.8029	2.4806	1.2264
30	0.4300	0.0010	6.9484	5.4101	1.4755	4.8158	2.4818	1.2174
99	0.2728	0.0002	6.9484	5.9465	1.8833	4.8178	3.1800	1.5076

Table 6.2 Random program runs chosen from 100 random packing to calculate geometrical properties of packing when $\phi_{el} = 0.50$.

#	ϕ_{el}	L_{TPB} ($\mu m.\mu m^{-3}$)	A_{TPB} ($\mu m^2.\mu m^{-3}$)	ε	ϕ_{ap}	$\phi_{a,LSM}$	$\phi_{a,YSZ}$	ϕ_{ip}
63	0.5	1.7624	0.1753	0.2930	0.9573	0.9593	0.9552	0.0255
21	0.5	1.7628	0.1755	0.2930	0.9638	0.9634	0.9641	0.0176
17	0.5	1.8034	0.1794	0.2930	0.9668	0.9648	0.9689	0.0164
37	0.5	1.8035	0.1797	0.2930	0.9732	0.9740	0.9723	0.0130
86	0.5	1.7791	0.1770	0.2930	0.9658	0.9696	0.9621	0.0176
31	0.5	1.7798	0.1772	0.2930	0.9655	0.9644	0.9665	0.0161
91	0.5	1.7807	0.1772	0.2930	0.9636	0.9665	0.9607	0.0183
26	0.5	1.7822	0.1773	0.2930	0.9672	0.9706	0.9638	0.0176
74	0.5	1.7831	0.1776	0.2930	0.9663	0.9631	0.9696	0.0166
12	0.5	1.7831	0.1772	0.2930	0.9655	0.9658	0.9651	0.0171
57	0.5	1.7837	0.1776	0.2930	0.9627	0.9624	0.9631	0.0188
13	0.5	1.7847	0.1777	0.2930	0.9646	0.9655	0.9638	0.0161
38	0.5	1.7856	0.1777	0.2930	0.9679	0.9692	0.9665	0.0176
97	0.5	1.7856	0.1778	0.2930	0.9684	0.9692	0.9675	0.0181
45	0.5	1.7862	0.1781	0.2930	0.9685	0.9699	0.9672	0.0164

#	$\phi_{i,LSM}$	$\phi_{i,YSZ}$	Z	Z_{eff}	$Z_{LSM\text{-}LSM}$	$Z_{YSZ\text{-}YSZ}$	$Z_{LSM\text{-}YSZ}$	$Z_{YSZ\text{-}LSM}$
63	0.0202	0.0308	6.9484	6.6569	3.4325	3.3860	3.2557	3.2397
21	0.0157	0.0195	6.9484	6.7463	3.4790	3.5255	3.2444	3.2438
17	0.0229	0.0099	6.9484	6.7557	3.4209	3.4506	3.3159	3.3241
37	0.0120	0.0140	6.9484	6.7978	3.4674	3.5009	3.3156	3.3118
86	0.0150	0.0202	6.9484	6.7385	3.4663	3.4557	3.2848	3.2701
31	0.0137	0.0185	6.9484	6.7619	3.4927	3.4821	3.2762	3.2728
91	0.0157	0.0209	6.9484	6.7333	3.4540	3.4561	3.2800	3.2766
26	0.0174	0.0178	6.9484	6.7373	3.4328	3.4738	3.2862	3.2817
74	0.0188	0.0144	6.9484	6.7528	3.4821	3.4749	3.2797	3.2691
12	0.0161	0.0181	6.9484	6.7419	3.4557	3.4527	3.2882	3.2872
57	0.0215	0.0161	6.9484	6.7263	3.4352	3.4615	3.2797	3.2762
13	0.0147	0.0174	6.9484	6.7583	3.4940	3.4612	3.2786	3.2827
38	0.0202	0.0150	6.9484	6.7434	3.4390	3.4721	3.2916	3.2841
97	0.0164	0.0198	6.9484	6.7403	3.4571	3.4591	3.2831	3.2814
45	0.0144	0.0185	6.9484	6.7484	3.4793	3.4547	3.2903	3.2725

The data reported by Kim *et al*. [13] however is not consistent with all other experimental data in a sense that it does not show rapid jump in conductivity around percolation threshold. It is possible that in obtaining those data, authors failed to separate resistance posed by the presence of electrolyte.

Fig. 6.2 shows results of conductivity of Ni-YSZ anode with composition along with experimental data from Dees *et al.* [11] for electrodes manufactured with two different starting powders of YSZ. The particle size in the model is taken equal to 0.1 μm according to Dees *et al.* for *Zirkar* powder [11]. The conductivities for pure Ni and YSZ are taken equal to 2×10^4 $S.cm^{-1}$ and 0.1 $S.cm^{-1}$ according to Sunde [19]. Overpotential applied does not have any effect on conductivity data and same method explained in Fig. 5.7 of chapter 5 is employed to calculate electrode conductivity.

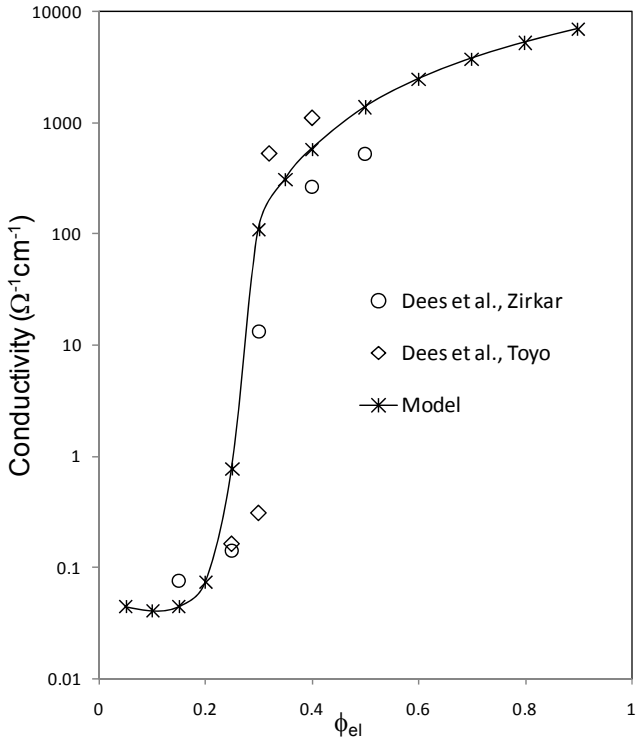

Figure 6.2 Effect of composition on the conductivity of electrode compared with observations of Dees *et al.* [11] for Ni-YSZ anode.

As it can be seen from the Figure, the model describes experimental data very closely proving that it captures the conductivity behaviour of composite

electrodes. Although not clear in experimental data, the model shows a slight decrease in conductivity with increasing Ni volume fraction at values below 20%. This effect as discussed before cannot be captured with continuous models and is the result of increasing isolated agglomerates of Ni which connect rapidly at above 20%.

6.3.3 Polarization and Composition

As discussed in chapter 2, experimental data show a strong dependence of polarization resistance on the composition of the electrode [13,16,20,21]. In chapter 4 and 5 it was shown that for an electrode composed of particles of the same size, the maximum L_{TPB} and A_{TPB} is achieved when volume percentage of electron and ion conductors are the same. This is shown in Fig. 6.3 for a cathode composed of LSM and YSZ particles of same size of 1 μm diameter.

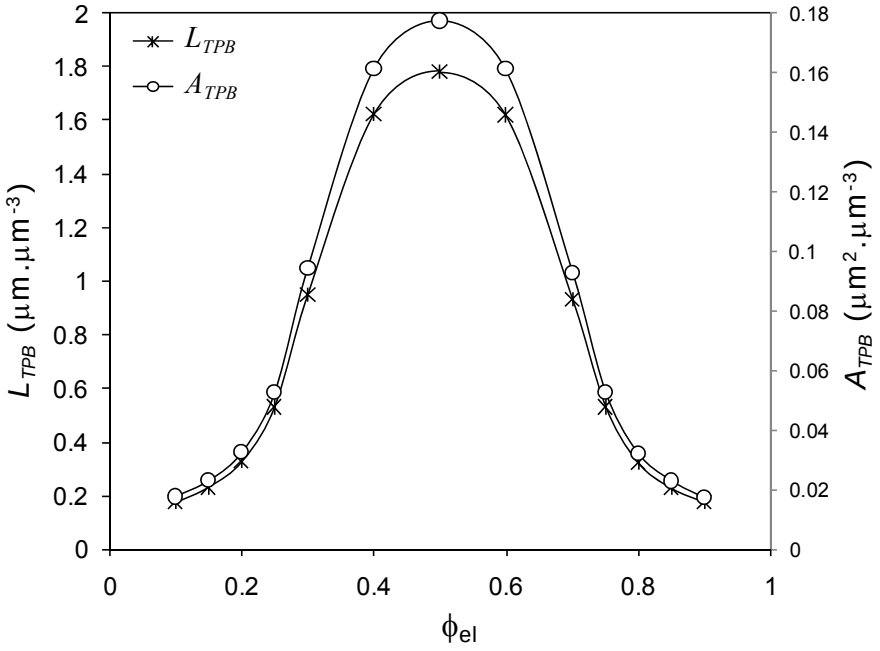

Figure 6.3 Effect of composition on L_{TPB} and A_{TPB}.

Since electrochemical reaction in composite electrodes is assumed to take place in triple phase boundaries, polarization resistance which in the current model stands for charge-transfer resistance follows the trend of L_{TPB} in opposite

direction and hence it is almost symmetrical as L_{TPB} and A_{TPB} curves with composition are. Fig. 6.4 shows values of polarization resistance calculated by the model along with experimental data from Kenjo *et al.* [20]. Although applied overpotential is not clear in the text, a potential of 50 mv is applied in this case. However, due to linearity of charge-transfer equation at low overpotentials the data are valid even if experimentally applied potentials are slightly different. As it can be seen, the model reasonably follows experimental data which poses a wide range minimum at intermediate compositions. Looking at experimental data, it seems that polarization resistance reported for ϕ_{el}=0.4 is a bit high compared to adjacent data points. The higher experimental polarization data compared to the model predictions maybe ascribed to mass transfer resistance which although is believed not to be important [7,22], it exists in small amounts.

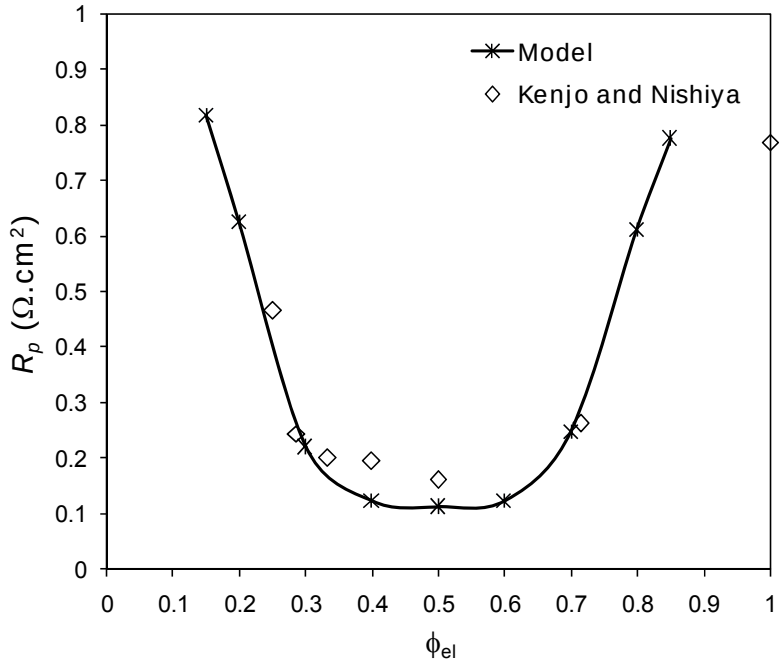

Figure 6.4 Polarization resistance of composite cathode shows a broad minimum at intermediate compositions which is in good agreement with experimental observations of Kenjo and Nishiya [20].

The experimental data point for a simple electrode (ϕ_{el}=1) suggests a very low value compared to other experimental data and compared specially to the model suggestion. Although the practically and structural stability of this type of

electrode is highly questioned, low resistance maybe ascribed to thinner electrode in this case which causes the elimination of diffusion resistance.

Despite the fact that charge-transfer polarization curve is almost symmetrical following the footsteps of L_{TPB} or A_{TPB}, Total polarization resistance curve is not symmetric and as it is shown in chapter 5 depends on relative resistivity of LSM and YSZ with a minimum falling around ϕ_{el}=0.4 for typical values.

6.3.4 Effect of Size Ratio

There is no consistent experimental data on the effect of particle size ratio on the performance of fuel cell. Few authors are found to investigate this effect on electrode performance [16,19,24-26]. The results are sometimes seemed to be contradicting. Lee *et al*. compared two composite Ni-YSZ anode structures, one with different size Ni and YSZ particles and the other with particles milled to the same size [24]. They concluded that composite made by particles of the same size showed better electrochemical performance compared to the one composed of different size particles. They blamed poor Ni contiguity due to large Ni particles [24]. Camaratta and Wachsman on the other hand performed experiments of cathodes for different particle sizes and concluded that electrodes composed of different electronic and ionic conductor size exhibit better performance compared to those composed of same size particles [16]. Although contradicting at first glance, it must be kept in mind that two experiments are conducted for two different electrodes with completely different material. Thermal and sintering behaviour of Ni and YSZ are totally different with $Bi_2Ru_2O_7$ (BRO7) and $Er_{0.4}Bi_{1.6}O_3$ (ESB20) and these are not the factors fully understood and covered in the current model. Furthermore particle size ratio used in the work of Lee *et al*. [24]is about 60 (d_{NiO}=12.5 μm, d_{YSZ}=0.21 μm) which is huge compared to ratio of about 1.6 or 0.56 (d_{el}=1.31 μm, d_{io}=0.81 μm or d_{el}=0.73 μm, d_{io}=1.31 μm) used in the work or Camaratta and Wachsman [16]. Another point is that Lee *et al*. compared this electrode with a composite of same particles of size 3 μm. It is clear that the former will exhibit much larger concentration polarization due to the

presence of fine 0.21 μm YSZ particles and although their conclusion is acceptable, the results seem to be influenced more by the difference in concentration polarization than particle size ratio only.

The results of Camaratta and Wachman however, are more aligned with the predictions of the current model [16]. While they have not done independent experiments demonstrating the effect of composition of polarization for different particle size ratio, they showed that for mixture composed of same volume of electron and ion conductors (50/50), electrodes made by different size electron and ion conductor show better performance compared to the electrodes made by the same size particles. They further showed that when there is size difference in effect, the electrode with smaller d_{el}/d_{io} is more beneficial. Ostergard *et al*. also showed that mixture of fine and coarse LSM and YSZ particles perform better compared to electrode composed of only fine particles.

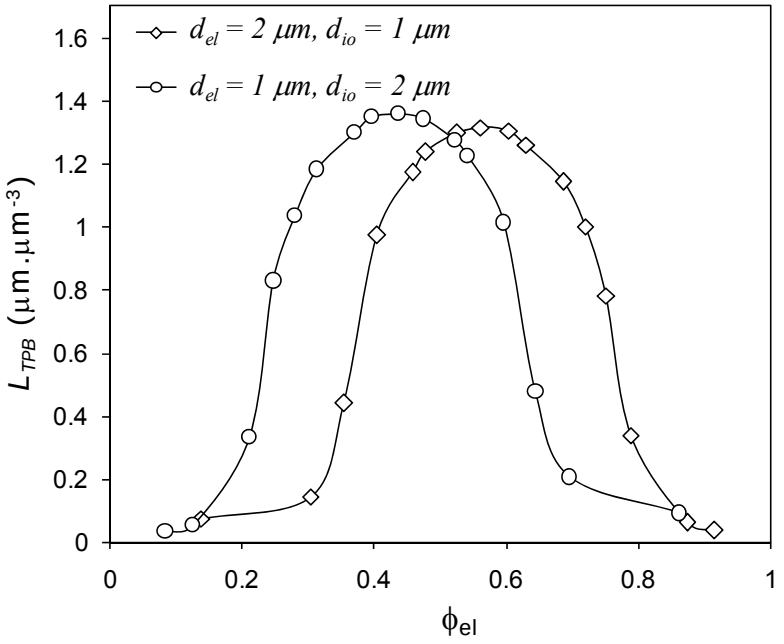

Figure 6.5 Effect of particle size ratio on L_{TPB} of a composite electrode. Maximum amount of L_{TPB} shifts towards higher ϕ_{el} values as d_{el}/d_{io} increases. There is a slight improvement in maximum L_{TPB} for lower d_{el}/d_{io} values.

Fig. 6.5 above shows the effect of particle size ratio on active triple phase boundary of a composite electrode. Comparing to Fig. 6.3, it is obvious that

maximum L_{TPB} has shifted to the left or right side of ϕ_{el}=0.5 depending on the ratio d_{el}/d_{io}. This suggests that percolation threshold must have shifted accordingly. In Fig. 6.6, polarization resistance is plotted against electrode composition for two cases of d_{el}/d_{io} =2 and d_{el}/d_{io} =0.5.

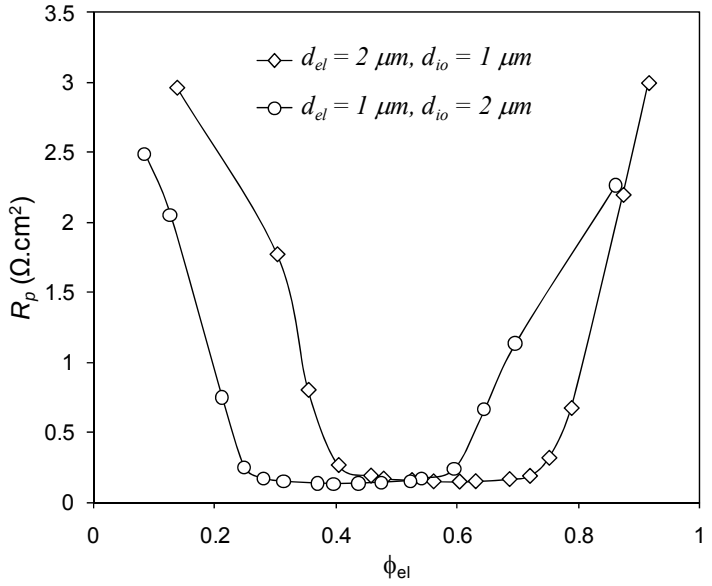

Figure 6.6 Effect of particle size ratio on polarization resistance. Minimum R_P shifts towards higher ϕ_{el} values as d_{el}/d_{io} increases.

Minimum polarization resistance is slightly less for d_{el}/d_{io} =0.5. The difference is more obvious looking at Fig. 6.6 which shows a higher maximum L_{TPB} for d_{el}/d_{io} =0.5. While this difference is small and seems trivial, it is not the best practical lesson which can be learnt from these graphs. What is clear is that, one should not expect best performance at intermediate compositions of the electrode while the particle size ratios deviate largely from unity. Although the polarization curve has a wide and flat minimum implying that the polarization resistance is not a strong function of composition around intermediate compositions, one should know that the results are presented only for d_{el}/d_{io} =0.5 and d_{el}/d_{io} =2 and for lower or higher ratios the difference is more dramatic. Furthermore by inspecting total polarization resistance curves given in Fig. 5.11 it is clear that overall electrode resistance does not have a wide minimum and choosing 50/50 volume percentage for composite of d_{el}/d_{io}=0.5 may pose an overall resistance twice the one that would have obtained if the composition was 30% of LSM.

There is some published simulation work on the percolation threshold and conductivity behaviour of composites as it is important issue in composite material design [27-31]. It is noted that size ratio of conductive and isolating phase has appreciable effect on percolation behaviour of composite and lower percolation threshold can be obtained for conducting phase if the size of conducting phase is smaller than isolating phase, i.e. d_{el}/d_{io} <1. Model proposed by Kusy [28] and Millaris and Turner [32] assumed that ratio d_{el}/d_{io} is much smaller than unity. This basically means that conductive particles with their massive numbers form a conductive layer around the isolating particles which might be desirable form conduction point of view but not for the case of SOFC electrodes which continuity of both phases is equally important. If ratio d_{el}/d_{io} is not too far from the unity, a satisfactory contiguity of both electron and ion conductor particles can be obtained which is crucial to have a high performance composite electrode of solid oxide fuel cell.

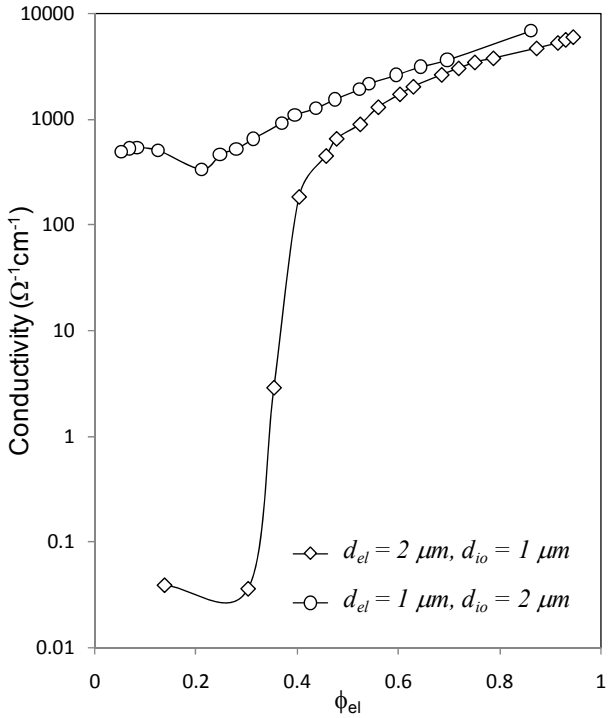

Figure 6.7 Effect of particle size ratio on polarization resistance. Minimum R_P shifts towards higher ϕ_{el} values as d_{el}/d_{io} increases.

Fig. 6.7 shows the effect of particle size ratio on the conductivity of Ni-YSZ composite electrode. Comparing this figure with Fig. 6.2 which models Ni-YSZ electrode composed of particles of the same size, it is evident that the location of the sudden jump in conductivity has shifted from about ϕ_{el}=0.25 to about ϕ_{el}=0.38 for d_{el}/d_{io} = 2.0 which is a remarkable shift. This observation is consistent with the previously mentioned observations which suggest there should be a shift in percolation threshold towards higher electron conductor volume fractions as d_{el}/d_{io} increases [27-31].

For values of d_{el}/d_{io} less than unity, the trend is a bit different. While one can see the shift of minimum towards ϕ_{el} values of less than 0.2, the minimum conductivity is very high compared to the other case and the case with particles of the same size and never reaches the low conductivity of YSZ in the composition range considered here. It is an interesting observation and again in agreement with previous research [27-31] and can be justified qualitatively as follows. Given the size ratio $r = d_{el}/d_{io}$ between electron and ion conductor particles and assuming that the composite has a volume fraction of ϕ_{el} of electron conductor, the number fraction, ϕ_n of the electron conductor particles can be obtained following a simple mathematics:

$$\phi_n = \frac{\phi_{el}}{\phi_{el}(1-r^3)+r^3}, \qquad r = \frac{d_{el}}{d_{io}} \tag{6.1}$$

For simplicity of comparison, table 6.3 below provides a numerical representation of the above equation for different values of ϕ_{el} and r:

As it can be seen in the table above for r = 0.5 very small amount of ϕ_{el} produces large number of electron conductor particles which are smaller in size. While ϕ_{el} = 0.05 causes ϕ_n = 0.05 for r = 1, it produces $\phi_n \approx 0.30$ when the ratio is r = 0.5. This huge number of electron conductor particles for very low volume percentage guarantees enough percolated electron conductor particles to keep conductivity well above low conductivity of ion conductor particles. At very low ϕ_{el} values conductivity decreases as expected. First maximum of the conductivity

curve demonstrate the optimum local balance between percolation of electron conductor particles and ion conductor particles above which point conductivity decreases slightly and increases as expected and below which conductivity decreases due to loss of percolated electron conductor chains. It should however kept in mind that although slight difference in electron and ion conductor particle size will benefit the electrode and improve the performance as seen in before, very large or small ratios will cause aggregation of one phase and will tend to decrease triple phase boundary and hence the performance of the electrode.

Table 6.3 Number fraction of electron conductor particles as function of volume fraction and size ratio $r = d_{el}/d_{io}$.

ϕ_{el} (%)	ϕ_n (%)				
	r = 0.1	r = 0.5	r = 1	r = 2	r = 10
1	90.992	7.477	1.0	0.126	0.001
2	95.329	14.035	2.0	0.254	0.002
3	96.868	19.835	3.0	0.385	0.003
4	97.656	25.000	4.0	0.518	0.004
5	98.135	29.630	5.0	0.654	0.005
10	99.108	47.059	10.0	1.370	0.011
15	99.437	58.537	15.0	2.158	0.018
20	99.602	66.667	20.0	3.030	0.025
25	99.701	72.727	25.0	4.000	0.033
30	99.767	77.419	30.0	5.085	0.043
40	99.850	84.211	40.0	7.692	0.067
50	99.900	88.889	50.0	11.111	0.100

6.3.5 Effect of Electrode Thickness

As it was shown before L_{TPB} increases with electrode thickness with declining rate so that after some thickness there is no gain in L_{TPB} [1]. It was shown in chapter 5 that total polarization resistance also drops rapidly with increasing thickness and then levels off. Fig. 5.9b suggests a thickness of about 15 μm for the cathode under the study. Thickness of 10 μm was obtained by the same other people based on continuum porous electrode model [33,34].

Fig. 6.8 is a comparison of the model predictions with experimental observations of Juhl *et al*. [35] and Kenjo and Nishiya [20]. The experimental

data are obtained for different electrode thickness ranges and as it can be seen the model shows a good agreement with both data sets. In converting data of Kenjo and Nishiya [20] to electrode thickness an average electrode density of 5000 kg/m^3 has been used [36] and overpotential applied was 50 mv. Polarization resistance drops sharply with increasing thickness initially and then almost levels off. There is a continuous and slight decrease in polarization resistance with thickness reflecting the increasing trend of L_{TPB} with thickness shown in Fig. 4.5a of chapter 4. Note that polarization resistance represents only charge-transfer resistance as mass transfer resistance is ignored in the current model.

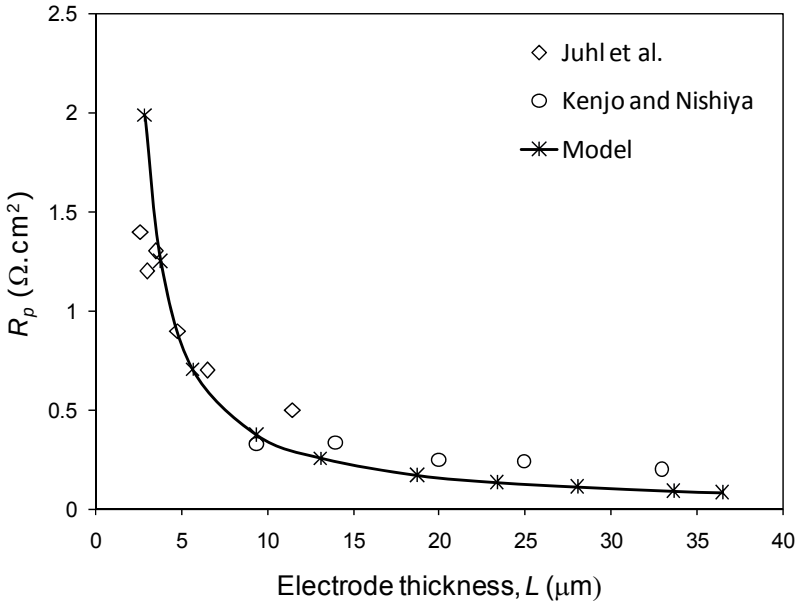

Figure 6.8 Effect of electrode thickness on polarization resistance of composite cathode composed of LSM and YSZ. Experimental data of Juhl *et al*. [35] and Kenjo and Nishiya [20] for different thickness ranges show a good agreement with model predictions.

The difference in Fig. 6.8 and 5.9b is that Fig. 5.9b is obtained for overall resistance of the electrode including polarization and ohmic resistance while Fig. 6.8 represents charge-transfer polarization resistance. That is why in Fig. 5.9b further decrease in resistance is not observed beyond thickness of about 20 μm and rather there is a slight increase. That is because with increased electrode thickness, the effect of increased L_{TPB} is countered by increased ohmic resistance and the overall effect is an increase in resistance. At high thicknesses as can be

seen in Fig. 6.8 predictions of the model is consistent lower than experimental observations. Since both model data and experimental data are obtained under no ohmic resistance, higher values of resistances in experimental observations can only be ascribed to mass transfer polarization resistance which comes to play in thicker electrodes while ignored by the model. Comparing this figure and Fig. 5.9b and taking into account the effects of mass transfer resistances, an optimum thickness of electrode can be realized below which charge-transfer polarization resistances are dominant and above which mass transfer and ohmic resistances grow. Sasaki *et al*. [37] observed this optimum thickness for LSM-YSZ cathode to be about 25 μm. At low current densities the minimum is wide while it gets more distinguished and unique for higher current densities across the electrode. This is true since at high current densities, mass transfer resistance is more dominant and grows rapidly with thickness.

6.4 Summary of the Model

The model presented in this thesis, with reasonable simplifications, is a direct translation of real random structure of solid oxide composite electrodes. The available experimental data can be described qualitatively and quantitatively with the current model while more specific experiments are needed to prove the merits of the model in approaching real performance characteristics of composite electrodes and suggesting useful guidelines towards design of electrodes. The work modeled for the first time a more realistic geometrical and electrochemical view of composite electrode based on totally random packing of particles and examined the effect of particle size difference among electron and ion conductor particles. Although in some cases based on discrete random packing of particles, the models have been claimed to handle particles of different size, the authors are unaware of any random packing modeling data revealing the effect of size ratio between electron and ion conductor particles. The work of Kenney *et al*. however, is an exception which is being conducted independently parallel to this work and so far has revealed only geometrical implications that particles of different size have on composite electrode structure [38]. Those features are covered in the

chapter 4 of the current work [1]. Furthermore, in spite previous attempts which employed a linear form of charge-transfer equation [39-42], this model used complete nonlinear Butler-Volmer equation and solved nonlinear system of equations.

6.5 Recommendations for Design

Based on the observations from the model, the following recommendations can be made to design and manufacture composite electrodes with higher performance and lower losses:

- Optimum composition of the electrode for particles of the same size depends on relative conductivity of electron and ion conductors. In the typical cases of Ni or LSM for electron conductor in anodes or cathodes and LSM for ion conductor or as electrolyte, best overall performance was observed for ϕ_{el} = 40% (Fig. 5.6). Values of ϕ_{el} higher than 50% and less than 35% should be avoided.
- Having different size of electron and ion conductor particles is beneficial as long as electron conducting particles are smaller and the ratio d_{io}/d_{el} is not too high. Although very high d_{io}/d_{el} ratios will improve electrode conductivity, L_{TPB} will decrease due to isolation of large and low populated ion conductor particles. d_{io}/d_{el} ratio of more than 4 is not recommended. Care should be applied in choosing optimum composition when d_{io}/d_{el} ratio above unity exits. The higher the d_{io}/d_{el} , the lower optimum ϕ_{el} is required.
- Optimum thickness seems to fall around 20 μm. The optimum thickness curve has a wide base if mass transfer polarization is negligible and thicknesses up to 40 μm can be chosen with confidence of having close to optimum performance. If the mass transfer is believed to have appreciable effect or the particle size is too small, values higher than 20 μm are not recommended as the active sites deep inside the electrode will starve and performance will drop.

- Applying a very thin current collector layer (CCL) of electro-catalyst is recommended as it decreases polarization resistance by increasing L_{TPB}. In the model cathode it was shown that applying a layer of LSM increased L_{TPB} by about 4%.

Also as general observations, it was shown that decreasing ohmic resistance of electron conductor particles and the electrochemical activity of electro-catalyst has direct influence on the performance of the electrode by lowering the polarization resistance.

6.6 Suggestions for Future Work

Although the developed model gives good understanding of composite electrode structure and performance, it lacks one of the characteristics of real electrodes which contribute to loss of performance in composite electrodes. Although mass transfer resistance is believed to be negligible in the presence of enough porosity as discussed in previous chapters, there are practical situations where either thickness is high or porosity is low and particles are very small and mass transfer becomes an issue. A complete model however should address the problem of diffusion inside the pores of electrode. The concept of producing continuous structure from random packing in two dimensions discussed in chapter 3 was able to incorporate mass transfer equations into the model. Further work is required to apply this or similar concept into three dimensions.

As it was discussed in chapter 2, impedance spectra of composite electrodes depend on the microstructure of the electrode. Impedance spectrum gives precious information about the performance and effectiveness of the electrode and can identify design and manufacture problems. Deriving impedance spectra for random electrode structures produced in the model can therefore make another tool to analyse and evaluate electrode structure.

References

[1] A. Ali, X. Wen, K. Nandakumar, J. Luo, and K. T. Chuang, J. Power Sources 185 (2008) 961.

[2] W. Gong, S. Gopalan, and U. Pal, J. Mater. Eng. Perform. 13 (2004) 274.

[3] S. Srinivasan and H. D. Hurwitz, Electrochim. Acta 12 (1967) 495.

[4] J. -H. Lee, H. Moon, H. -W. Lee, J. Kim, J. -D. Kim, and K. -H. Yoon, Solid State Ionics 148 (2002) 15.

[5] P. Costamagna, P. Costa, and V. Antonucci, Electrochim. Acta 43 (1998) 375.

[6] P. Costamagna, P. Costa, and E. Arato, Electrochim. Acta 43 (1998) 967.

[7] S. H. Chan, K. A. Khor, and Z. T. Xia, J. Power Sources 93 (2001) 130.

[8] S. H. Chan and Z. T. Xia, J. Electrochem. Soc. 148 (2001) A388.

[9] A. Abbaspour, K. Nandakumar, J. Luo, and K. T. Chuang, J. Power Sources 161 (2006) 965.

[10] U. P. Muecke, S. Graf, U. Rhyner, and L. J. Gauckler, Acta Mater. 56 (2008) 677.

[11] D. W. Dees, T. D. Claar, T. E. Easler, D. C. Fee, and F. C. Mrazek, J. Electrochem. Soc. 134 (1987) 2141.

[12] V. Dusastre and J. A. Kilner, Solid State Ionics 126 (1999) 163.

[13] J. Kim, G. Kim, J. Moon, Y. Park, W. Lee, K. Kobayashi, M. Nagai, and C. Kim, Solid State Ionics 143 (2001) 379.

[14] R. M. C. Clemmer and S. F. Corbin, Solid State Ionics 166 (2004) 251.

[15] Y. Yin, W. Zhu, C. Xia, and G. Meng, J. Power Sources 132 (2004) 36.

[16] M. Camaratta and E. Wachsman, J. Electrochem. Soc. 155 (2008) B135.

[17] B. H. Kwak, H. K. Youn, and J. S. Chung, J. Power Sources 185 (2008) 633.

[18] R. M. C. Clemmer and S. F. Corbin, Solid State Ionics 180 (2009) 721.

[19] S. Sunde, J. Electroceram. 5 (2000) 153.

[20] T. Kenjo and M. Nishiya, Solid State Ionics 57 (1992) 295.

[21] J. Kim, G. Kim, J. Moon, H. Lee, K. Lee, and C. Kim, Solid State Ionics 133 (2000) 67.

[22] B. Kenney and K. Karan, Solid State Ionics, 178 (2007) 297.

[23] S. H. Chan and Z. T. Xia, J. Appl. Electrochem. 32 (2002) 339.

[24] C. Lee, C. Lee, H. Lee, and S. M. Oh, Solid State Ionics 98 (1997) 39.

[25] T. Suzuki, Z. Hasan, Y. Funahashi, T. Yamaguchi, Y. Fujishiro, and M. Awano, Science 325 (2009) 852.

[26] M. J. L. Ostergard, C. Clausen, C. Bagger, and M. Mogensen, Electrochim. Acta 40 (1995) 1971.

[27] F. Bueche, J. Appl. Phys. 43 (1972) 4837.

[28] R. P. Kusy, J. Appl. Phys. 48 (1977) 5301.

[29] A. Kubovy, J. Phys. D 19 (1986) 2171.

[30] W. J. Kim, M. Taya, K. Yamada, and N. Kamiya, J. Appl. Phys. 83 (1998) 2593.

[31] M. Rottereau, J. C. Gimel, T. Nicolai, and D. Durand, Eur. Phys. J. E 11 (2003) 61.

[32] A. Malliaris and D. T. Turner, J. Appl. Phys. 42 (1971) 614.

[33] S. H. Chan, X. J. Chen, and K. A. Khor, J. Electrochem. Soc. 151 (2004) A164.

[34] X. J. Chen, S. H. Chan, and K. A. Khor, Electrochim. Acta 49 (2004) 1851.

[35] M. Juhl, S. Primdahl, C. Manon, and M. Mogensen, J. Power Sources 61 (1996) 173.

[36] S. Ahmed, C. McPheeters, and R. Kumar., J. Electrochem. Soc. 138 (1996) 2712.

[37] K. Sasaki, J. Wurth, R. Gschwend, M. Godickemeier, and L. J. Gauckler, J. Electrochem. Soc. 143 (1996) 530.

[38] B. Kenney, M. Valdmanis, C. Baker, J. G. Pharoah, and K. Karan, J. Power Sources 189 (2009) 1051.

[39] S. Sunde, J. Electrochem. Soc. 143 (1996) 1930.

[40] S. Sunde, J. Electrochem. Soc. 142 (1995) L50.

[41] L. C. R. Schneider, C. L. Martin, Y. Bultel, D. Bouvard, and E. Siebert, Electrochim. Acta, 52 (2006) 314.

[42] J. Deseure, Y. Bultel, L. C. R. Schneider, L. Dessemond, and C. Martin, J. Electrochem. Soc. 154 (2007) B1012.